LASER CLADDING WITH POWDER

effect of some machining parameters
on clad properties

Marcel Schneider

De promotiecommissie is als volgt samengesteld:

Voorzitter en secretaris:

Prof.dr.ir. H.J. Grootenboer	(Universiteit Twente)

Promotor:

Prof.dr. L.H.J.F. Beckmann	(Universiteit Twente)

Assistent-promotor:

Dr.ir. J. Meijer	(Universiteit Twente)

Leden:

Prof.dr. W. Wei	(Universiteit Twente)
Prof.dr.ir. J.-P.G. Kruth	(KU Leuven)
Prof.dr.ir. J.B. Jonker	(Universiteit Twente)

title:	Laser cladding Ph.D. Thesis University of Twente, Enschede, The Netherlands March 1998
author:	M.F. Schneider
ISBN:	90 365 1098 8
subject headings:	laser cladding

printed by: Print Partners Ipskamp, Enschede

LASER CLADDING WITH POWDER

effect of some machining parameters on clad properties

PROEFSCHRIFT

ter verkrijging van
de graad van doctor aan de Universiteit Twente,
op gezag van de rector magnificus,
prof.dr. F.A. van Vught,
volgens besluit van het College voor Promoties
in het openbaar te verdedigen
op donderdag 19 maart 1998 te 15.00 uur.

door

Marcel Fredrik Schneider

geboren op 19 juli 1968
te Haarlem

Dit proefschrift is goedgekeurd door de promotor:

prof.dr. L.H.J.F. Beckmann

en de assistent-promotor:

dr.ir. J. Meijer

Summary

Laser cladding is performed to improve the surface properties of metallic machine parts locally. A cladding material with the desired properties is fused onto a substrate by means of a laser beam. The mixing between the two materials must be as small as possible to utilise the properties of the coating material most effectively. By improving a technical surface locally with a dedicated material, one can use an ordinary cheap base material for the surface that is not being exposed to high loads.
Laser cladding is considered as a strategic technique, since it can yield surface layers that, compared to other hard facing techniques, have superior properties in terms of pureness, homogeneity, hardness, bonding and microstructure. Hence, it was decided to introduce this technique in the Dutch industry.

The project consisted of three parts. One part covered the achievement and enhancement of insight in phenomena that occur in laser cladding. The second part involved the development of tools that facilitate the use of laser cladding. The third part consisted of the development of practical applications. Some aspects of this project are discussed in this thesis.

This thesis is directed to laser cladding with powder and a CO_2 laser as heat source. The laser beam intensity profile turned out to be an important pa-

rameter in laser cladding. A numerical model was developed that allows the prediction of the surface temperature distribution that is attained with an arbitrarily shaped intensity profile. Input parameters for this model are laser machining parameters and properties of the laser beam, as well as material properties and the absorption of laser energy at the surface. The thermal material properties and the absorptivity were derived from experiments.
An analysis that was performed with this model on several 'standard' laser beam intensity profiles, showed that an oblong laser spot with a homogeneous energy distribution in the direction perpendicular to the direction of motion yield the most uniform temperature distribution. That property is useful for laser cladding, because such a temperature distribution results in uniform material properties along the track width. Especially for the cladding of larger areas, this is a very useful feature.
Another reason for the use of integrators is the achievement of a laser spot with well defined dimensions and an energy distribution that is independent of the applied laser source. This is essential for an effective transfer of cladding results from one laser system to another.
Therefore, such a line integrator has been developed. The required homogeneous energy distribution was achieved.

Experiments performed on laser cladding with preplaced powder proved that this method is suitable for obtaining single clad tracks. The powder is mixed with a chemical binder to form a paste which is spread over the substrate.
The temperature on the interface between coating material and substrate is a very important parameter in laser cladding. If this interface temperature remains too low, wetting of the substrate by the liquid clad material is limited. In that case, irregularly shaped tracks with a lot of cracks, porosity and a poor bonding, are produced. However, if too high interface temperatures are reached, severe melting of the substrate occurs. The high degree of mixing between elements of the cladding material and the substrate can deteriorate the clad properties.
Some melting of the base material is required to attain a strong fusion bond. In the applied material combination, a cobalt base powder applied on a hot working steel, a relatively large dilution of 15 % proved to be the most effective for achieving clad layers with a good hardness and a perfect bonding. It is possible to reduce this dilution, but as a consequence the hardness is reduced as well.
The preheating of the substrate to 100-200 °C reduces the cooling rates. This reduces the residual stress and enhances the wetting and the bonding. Temperatures of 300 °C and above are not applicable, because of evaporation of the

chemical binder. Without a binder the powder is being blown away by the shielding gas.
The preplaced powder method is not suitable for the cladding of larger areas by making several adjacent partly overlapping tracks. Cracking of the cladded areas could not be prevented with the applied material combination. More seriously is the occurrence of a severe degree of dilution, that is inevitable. Since the newly produced track contracts during cooling, the bare substrate area directly next to it is molten when performing the next laser scan.

Laser cladding with powder injection did result in good quality clad areas without severe dilution. Powder particles are injected into the laser generated melt pool. These particles are heated during their flight through the laser beam. Melting occurs only when they enter the melt pool. The supplied material enlarges the melt and forms a layer on the surface. Compared to the preplaced powder method, the melt depth is easier to control and porosity is less likely to occur.
The particles form a cloud that attenuates the laser beam. In the applied configuration, the measured attenuation by a cloud consisting of particles Stellite 6 was less than 5 %. The attenuated laser power heats the powder particles. This heating was described in a physical analytical model. Most important parameters for the heating of a particle are the particle size, the powder velocity and the laser power.
If the powder is heated to such an extent that a metal vapour is formed, a plasma can be formed. This plasma effectively absorbs all laser radiation and stops the process. A plasma can only be formed over a certain critical powder density level (~ $2 \cdot 10^6$ W/cm^2). In the applied configuration, this level is reached in the focal area only. Plasma formation could be prevented by exchanging the initially applied lens with one with a larger focal length. This increased the beam waist in the focal region. Hence, the critical power density level could was not exceeded anymore.

The applicability of laser cladding was shown successfully with the development of several industrial applications.

Samenvatting

Lasercladden wordt toegepast om de oppervlakte-eigenschappen van metalen machine-onderdelen plaatselijk te verbeteren. Het cladmateriaal wordt met behulp van een laser als warmtebron opgelast op het basismateriaal. Daarbij is het essentieel de vermenging tussen het cladmateriaal en het basismateriaal zoveel mogelijk te berperken om zodoende de eigenschappen van het cladmateriaal optimaal te benutten, terwijl toch een sterke smelthechting wordt verkregen. Door alleen ter plaatse van de optredende belasting een cladlaag aan te brengen en verder te volstaan met een eenvoudig basismateriaal, kan een aanzienlijke besparing op materiaalkosten worden bereikt.
De eigenschappen van laser gecladde lagen zijn bijzonder goed in vergelijking met andere technieken die harde deklagen opleveren: een zeer goede hechting, een fijnkorrelige microstructuur, een betere homogeniteit, een geringere mate van porositeit, een grotere hardheid en de mogelijkheid om bijzondere metastabiele fases te verkrijgen. Lasercladden wordt daarom beschouwd als een veelbelovende techniek, die voor bepaalde bedrijfstakken van strategisch belang kan zijn. Daarom werd besloten het lasercladden ook in de Nederlandse industrie te introduceren.

Het project dat daartoe werd opgezet bestond uit drie delen. Het eerste deel betrof het verkrijgen en vermeerderen van proceskennis. Het tweede deel omvatte het ontwikkelen van hulpmiddelen en gereedschappen die het toepassen van het lasercladden in de praktijk moeten vereenvoudigen. Het laatste gedeelte bestond uit het ontwikkelen van echte toepassingen. Aspecten van deze drie delen worden behandeld in dit proefschrift.

Dit proefschrift richt zich op het cladden met poeders, waarbij een CO_2 laser dient als warmtebron. Het intensiteitsprofiel van de laserbundel blijkt in belangrijke mate het cladresultaat te beïnvloeden. Er is een numeriek model ontwikkeld dat de temperatuurverdeling aan het oppervlak ten gevolge van een willekeurig gevormde intensiteitsverdeling kan berekenen. Als invoerparameters voor het model fungeren verder machine- en laserbundelparameters, (thermische) materiaalparameters en de absorptie. De waarden van de thermische materiaalparameters en de absorptie zijn experimenteel bepaald. Een analyse van enkele standaard intensiteitsprofielen met dit model toonde aan dat een zg. lijnbron, dat is een laser spot met een langwerpige homogene energieverdeling in de richting loodrecht op de bewegingsrichting de meest uniforme temperatuurverdeling over de breedte van het cladspoor geeft. Daarmee worden dan ook de meest uniforme materiaaleigenschappen verkregen. Vooral voor het cladden van vlakken, wat het aanbrengen van meerdere sporen naast elkaar vereist, is dit erg nuttig.
Een tweede reden voor het gebruik van integratoren is dat dit resulteert in een goed begrensde spot op het werkstuk met een gedefinieerde energieverdeling die onafhankelijk is van de laserbron. Dit is noodzakelijk voor een doeltreffende overdracht van cladresultaten tussen lasersystemen.
Een dergelijke lijnintegrator is daarom ontworpen en gerealiseerd. De verwachte energieverdeling bleek inderdaad gerealiseerd te worden.

Een uitgebreide serie experimenten toonde dat het cladden met vooraf aangebracht poeder een geschikte methode is voor het aanbrengen van enkelvoudige cladlagen. Het poeder wordt gemengd met een bindmiddel en daarna in de vorm van een pasta aangebracht op het substraat.
De temperatuur op de interface tussen cladlaag en substraat is bepalend voor het resultaat. Een te lage temperatuur belemmert een goede bevochtiging van het substraat door het vloeibare cladmateriaal. Daardoor ontstaan onregelmatige lagen met veel scheuren, porositeit en een slechte hechting. Bij te hoge temperaturen smelt het basismateriaal te veel en ontstaat te veel menging.

Voor een goede cladlaag is een geringe mate van insmelting in het basismateriaal noodzakelijk voor het verkrijgen van een sterke smelthechting. Bij de gebruikte materiaalcombinatie, een poeder op basis van cobalt met een warmwerkstaal, blijkt een relatief grote vermenging van ongeveer 15 % te resulteren in de beste eigenschappen: een goede hechting en een hoge hardheid over de cladlaag. Het is wel mogelijk minder vermenging te verkrijgen, maar dan neemt de hardheid af.
Voorverwarmen van het substraat tot 100 à 200 °C vermindert de afkoelsnelheden, waardoor de spanningen in de cladlaag afnemen. Voorverwarmen bevordert tevens het uitvloeigedrag en de hechting. Bij temperaturen van 300 °C of hoger verdampt echter het bindmiddel en wordt het poeder weggeblazen door het schutgas.
Het aanbrengen van meerdere sporen naast elkaar ten einde grote vlakken te cladden bleek niet succesvol met deze methode. Scheurvorming was met deze materiaalcombinatie niet te voorkomen. Bovendien is een te grote menging inherent aan het proces, doordat het substraat direkt naast een gevormd spoor bloot komt te liggen door contractie tijdens afkoeling van dit spoor en daardoor door het laserlicht wordt beschenen bij het aanbrengen van een volgend spoor.

Goede resultaten met het cladden van grotere vlakken zijn wel behaald met behulp van cladden met poederinjectie. Daarbij worden poederdeeltjes in een door de laser gevormd smeltbad geblazen. Deze deeltjes worden voorverwarmd in de laserbundel, maar worden pas in het smeltbad volledig gesmolten. Het toegevoerde materiaal vergroot het volume van het smeltbad en vormt na afkoelen een deklaag op het substraat. Door het andere procesverloop bij het cladden met poederinjectie is de insmelting in het basismateriaal is eenvoudiger te controleren dan bij de voorgeplaatst poeder methode, zijn de restspanningen lager en vermindert de aanwezigheid van porositeiten. Bovendien is het goed mogelijk grotere vlakken met cladlagen te bedekken.
De opwarming van poederdeeltjes tijdens hun vlucht door de laserbundel is gemodelleerd. De opwarming van het poeder bleek sterk afhankelijk van de deeltjesgrootte, de poedersnelheid en het laservermogen. In de gebruikte configuratie is de gemeten verzwakking van het laservermogen door een stroom van deeltjes Stelliet 6 minder dan 5 %. Het intensiteitsprofiel van de laserbundel wordt derhalve nauwelijks beïnvloed door de poederwolk.
Indien poederdeeltjes te sterk verhit worden bij hun gang door de laserbundel, kan een plasma worden gevormd. Dit plasma absorbeert de invallende straling en stopt daardoor het cladproces. Voor de vorming van een plasma is een bepaalde kritische vermogensdichtheid van ca. $2 \cdot 10^6$ W/cm^2 nodig. Het blijkt dat

deze in de gebruikte opstelling slechts in de buurt van het brandpunt wordt gerealiseerd. De vorming van een plasma kon worden voorkomen door een optiek met een langere brandpuntsafstand te kiezen, waardoor de bundeldiameter rond het brandpunt toeneemt en de kritische vermogensdichtheid niet meer overschreden kan worden.

De praktische bruikbaarheid van het lasercladden is succesvol aangetoond met de ontwikkeling van enkele industriële toepassingen.

List of symbols

A	absorptivity [-]
C	density powder cloud [kgm^{-3}]
c_p	specific heat [$Jkg^{-1}K^{-1}$]
d_c	clad depth [m]
D	dimension laser spot on workpiece in traverse direction [m]
D_{pn}	diameter powder nozzle [m]
E	specific energy ($E=P/vD$) [Jm^{-2}]
$E_{a,c,r,ra,t,0}$	particle energy (*a*: absorbed; *c*: convective loss; *r*: reflective loss; *ra*: radiative loss; *t*: transmitted; *o*: incident) [J]
f_v	volume fraction of powder particles in the powder stream [-]
g	gravitational acceleration [ms^{-2}]
H	specific enthalpy [Jkg^{-1}]
h	grid step size [mm]
h_c	clad height [m]
I	beam power density [Wm^{-2}]
k	thermal conductivity [$Wm^{-1}K^{-1}$]
l_z	distance from top of powder cloud to particle [m]
L	latent heat of fusion [Jkg^{-1}]
m	mass [kg]

m_p	powder mass flow rate [kgs^{-1}]
p	pressure [Nm^{-2}]
P	laser power [W]
P_{at}	attenuation of laser power [W]
q	power of point source [W]
q	heat source [Wm^{-3}]
R	reflectivity [-]
r_p	radius of powder particle [m]
s	distance from exit powder nozzle [m]
t	time [s]
t_c	total clad height [m]
t_i	interaction time [s]
t_{in}	instant particle enters laser beam [s]
t_{out}	instant particle leaves laser beam [s]
T	temperature [K]
T_0	initial temperature [K]
T_{max}	maximum temperature [K]
v	feed rate workpiece [ms^{-1}]
v_p	velocity powder particles [ms^{-1}]
w_c	clad width [m]
w_{of}	waist of focused laser beam [m]
x_{in}	x-position where particle enters the laser beam [m]
x_{out}	x-position where particle leaves the laser beam [m]
x,y,z	Cartesian co-ordinate system [m]
α	heat exchange coefficient to environment [Wm^{-2}K^{-1}]
α	thermal expansion coefficient [K^{-1}]
β	extinction coefficient ($\beta=\beta_0 f_v$) [m^{-1}]
Δt	time interval [s]
ΔT	temperature difference [K]
Δx	distance centre laser beam and centre powder stream [m]
θ	angle powder injection nozzle relative to the workpiece [°]
θ_p	angle of particle movement relative to the workpiece [°]
κ	thermal diffusivity [Wm^{-2}]
μ	fluid viscosity [kgs^{-1}m^{-1}]
ν	kinematic viscosity($\nu=\mu/\rho$)[m^{2}s^{-1}]
ρ	material density [kgm^{-3}]
τ	thermal time constant [s]
ϕ	half angle of divergence powder stream [°]

Contents

Chapter 1

Preface

1.1 Introduction

To improve the surface properties of metallic mechanical parts, such as the resistance against wear and corrosion, several thermal surface treatments are available; for instance, flame spraying, plasma spraying and arc welding are established techniques. Characteristic for these techniques is the application of a surface layer with the required properties on top of a cheap material without those properties. Depending on the applied technique, common problems are a combination of a poor bonding of the applied surface layer to the base material, the occurrence of porosity, the thermal distortion of the workpiece, the mixing of the surface layer with the base material and the inability of a very local treatment.

One of the techniques that overcomes these problems is laser cladding. Laser cladding has been defined as “a process which is used to fuse with a laser beam another material which has different metallurgical properties on a substrate, whereby only a very thin layer of the substrate has to be melted in order to achieve metallurgical bonding with minimal dilution of added material and substrate in order to maintain the original properties of the coating material” [Komvopoulos, 1990].

Laser cladding has established itself in practice. Well known applications include the improvement of the wear resistance of diesel engine exhaust valves, the enhancement of the corrosion resistance of gas turbine blades and the repair of dies and inserts. The high-quality surface layers that can be produced by laser cladding only, make it a strategic technique.
The importance of this technique was also recognised by the Dutch Ministry of Economic Affairs. As the laser cladding technique was virtually unknown in the local industry, they sponsored a project that should introduce this technology into the Dutch industry. As the available knowledge at the start of the project was negligible, the projected started with an extensive literature research (chapter 2). This was followed by some series of experiments which contributed to a better understanding of the process and gave insight in the mechanisms that rule laser cladding. It was clear then that a successful introduction of laser cladding into industry could only be achieved by making the process less empirical and by developing industrial applications that can serve as an example. Therefore, more experiments had to be performed. Some tools had to be employed to enhance the process knowledge and to support the development of new industrial applications. These tools included mathematical tools that can describe some essential parts of the process, as well as dedicated equipment that allows an easy transfer of results between laboratories and improves the clad quality. This thesis is a result of this project.

1.2 Overview of the thesis

In chapter 2 a literature research is presented. It shows that the development of new laser cladding applications is up to now an experience based process. The lack of models contributes to the necessity to perform expensive series of experiments and feasibility tests for new applications. Nevertheless, many aspects of laser cladding are already understood and dedicated peripheral equipment has been developed.

Laser cladding consists of two essential parts:

1. melt pool formation and fusion by a moving laser beam;
2. supply of cladding material to the substrate.

Ad. 1 Characteristic for laser cladding is the conflict between the demands of achieving a good metallurgical bonding (and thus melting of the substrate) on the one hand and attaining no mixing between the coating material and the

substrate on the other hand. This means that the heat input by the laser source must be well-controlled to achieve an acceptable degree of mixing.
It also followed from the literature that the properties of produced clad layers depend strongly on the applied temperature cycle. The favourable properties of clad layers are not only the result of the pureness of the surface layer, but are also caused by the high cooling rates that occur. This so-called quenching results in the formation of favourable fine-grained microstructures or in metastable phases.
These two reasons, i.e. the control of the degree of mixing and the dependency on the temperature cycle, make it important to control the laser energy distribution and the resulting temperature distribution over the surface. In chapter 3 a numerical model is described which allows the calculation of the surface temperature distribution that is imposed by an arbitrarily shaped moving laser spot. An evaluation of the effect of several common laser beam profiles showed that a line shaped laser beam with an uniform power density distribution is best suited for the achievement of a more or less uniform temperature distribution and therewith constant clad properties over the width of the track. This conclusion is supported in the literature by several authors.
In order to cover larger areas it can be necessary to apply several adjacent tracks. This enhances the necessity to apply a laser beam with a uniform power density distribution. However, the power density distribution is a characteristic property of a laser system. Therefore, dedicated optics must be used to change the original laser power density distribution into a uniform one. A line integrator which was developed to perform that task, is demonstrated in this thesis in chapter 4. The use of integrators makes cladding results independent of the applied laser source. Therefore, results can be exchanged more easily between different laser systems. This aspect agrees well with the intended facilitation of transfer of cladding results to the Dutch industry.

Ad. 2 The second part of the process is the addition of a cladding material to the substrate. Various methods are available, but according to the literature the most common method is the application of powder. This can be done prior to the process (preplaced) or during the process (powder feeding). The effect of process parameters on clad layer properties was investigated for laser cladding with preplaced power as well as for laser cladding with powder injection. These two methods have a quite different process course. When cladding with preplaced powder, the melt pool is formed on top of the cladding material and proceeds downwards to the substrate. Only when the substrate has been melted a clad layer can be formed. However, the powder injection method starts with the

formation of a melt pool in the substrate in which cladding powder is being fed. Thus a clad layer is formed almost instantaneously. The preplaced powder results are presented in chapter 5.
In the case of laser cladding with powder injection, powder particles are transported by a gas stream and injected into the melt pool. The powder particles absorb laser energy on their way through the laser beam. Therefore, they are preheated on arrival in the melt pool. In the melt pool, they exchange heat and mix with the elements already present. The powder particles might also affect the laser power density. If this happens indeed, this effect must be incorporated in the model described in chapter 3. The interaction between powder and laser beam is studied in chapter 6.
Experiments showed that plasma formation can occur in the process area. This is a critical phenomenon, because the plasma can shield the substrate from the laser beam and thus stop the cladding. This phenomenon is discussed in chapter 6 as well.

As mentioned before, the work described in this thesis was initiated to introduce the laser cladding technology in the Dutch industry. Emphasis was put on the achievement of good quality metal clad layers on top of steel surfaces. Having gained enough insight in the process mechanisms, the final step which is necessary to convince industry to apply laser cladding themselves is the development of practical applications. Some examples of such applications that were developed in the author's laboratory are shown in chapter 7.

Chapter 2

Laser cladding: state-of-the-art

2.1 Laser cladding and other laser surface treatments

Laser cladding is one of the laser surface treatments. The positive effects of laser surface treatments are based on a change of the microstructure or the material composition of the surface layer due to a thermal cycle which is induced by a moving laser source. The process is shown schematically in figure 2.1.
The treated area is heated by absorption of energy delivered by the laser beam. The heat input due to a high power laser beam is well confined and very intense. Hence, heating rates in the surface layer are high. The heated layer is self-quenched after passing of the laser beam by diffusion of heat to the cold bulk. The high heating and cooling rates in the surface layer result in grain refinement and in the formation of metastable phases and/or altered microstructures.
Larger areas can be treated by making several adjacent tracks. Some processes require the use of a shielding gas to avoid corrosion of the treated area.

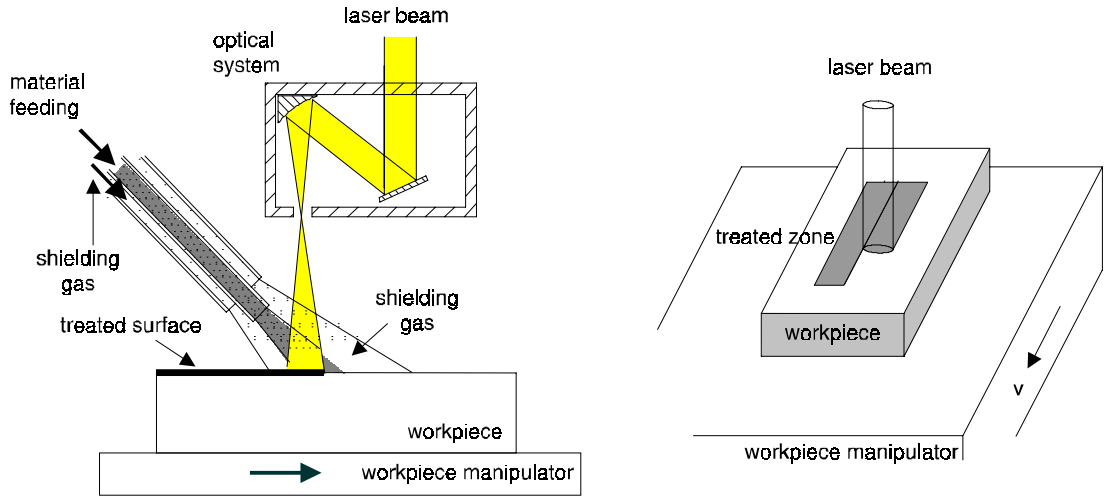

Fig. 2.1 The workpiece performs a relative movement to the laser beam. The area exposed by the laser beam is treated. Larger areas can be treated by applying several adjacent tracks.

In our research a 2 kW CO_2 laser was used as heat source. This power level can be seen as a minimum requirement for laser surface treatments. In most industrial applications the laser power is above 5 kW. This allows the treatment of larger areas in one process step. The wavelength of 10.6 µm causes significant reflection losses. At room temperature only 6-10 % of the radiation is absorbed in a solid low alloy steel surface [Grünenwald, 1996; Stern, 1990]. The absorption can be increased by using special (graphite) coatings [Dausinger, 1988]. Under cladding conditions the absorption of CO_2 radiation on a mild steel surface is considerably larger: about 30 % [Grünenwald, 1996].
Recently, Nd:YAG lasers have been developed to laser powers of several kWs, making them useful for laser surface treatments. The wavelength of 1.06 µm is more efficient: absorption on a solid steel surface is about 30 % [Stern, 1990]. Under cladding conditions the absorption increases to 60 % [Grünenwald, 1996]. Another advantage over the CO_2 laser is the possibility to transport the laser beam through optical fibres, allowing flexible beam handling systems. Taking into account both advantages, one can thus say that this laser type is very useful for future laser surface treatments.
Three groups of laser surface treatments are distinguished: those without melting, those with melting of the surface and those with melting of the surface and additional material.
The working principle of the most common laser surface treatments is summarised in figure 2.2.

The effects of laser remelting and laser transformation hardening are based on a microstructural change of the surface layer. However, it can be necessary or cheaper to apply a layer with a different composition on top of the base material if the base material itself can not be improved sufficiently.
Three laser techniques that can enhance surface properties by changing the material composition in the surface can be distinguished: laser alloying, laser dispersing and laser cladding. These techniques are shown schematically in figure 2.3.
All three methods involve the formation of a melt pool to which material is applied. Depending on the achieved degree of mixing between the added material and the base material in the surface layer, one can distinguish laser alloying and laser dispersing on the one hand, and laser cladding on the other hand. The first class is characterised by a complete mixing and/or reaction of the added elements with the base material. In contrast, laser cladding generates a surface layer that hardly contains elements of the substrate on top of the base

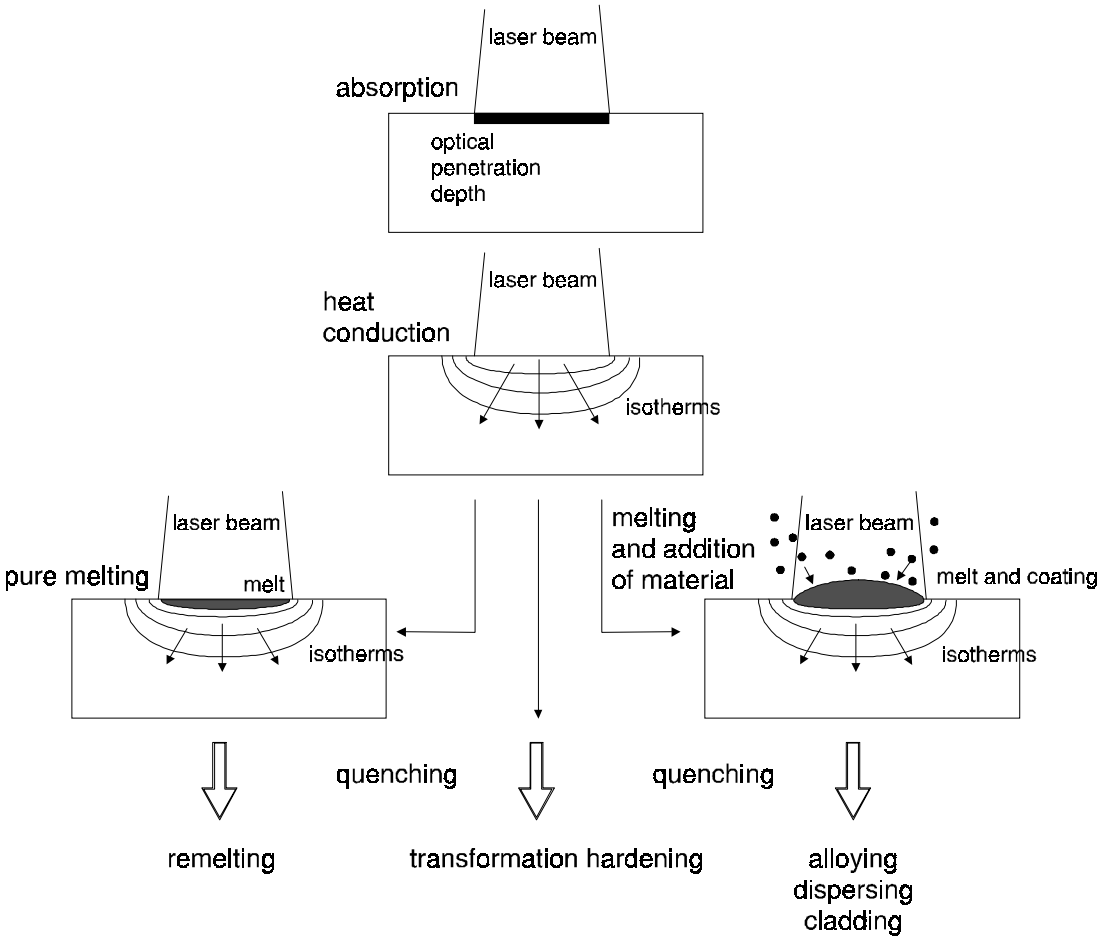

Fig. 2.2 Laser surface treatments are distinguished with respect to the surface temperature (solid phase/melt pool) and to the addition of material.

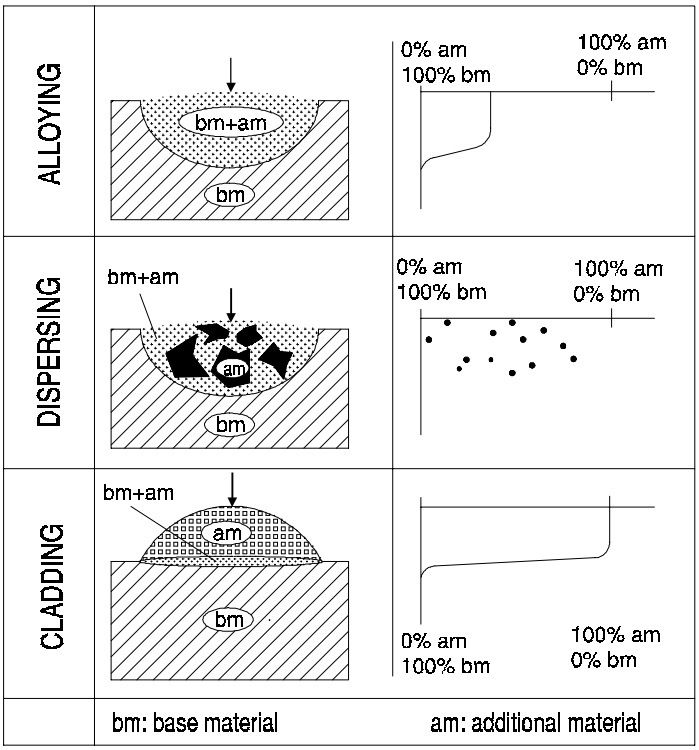

Fig. 2.3 Laser alloying, dispersing and cladding. The right part of the picture indicates the distribution of the added elements measured top-down in the centre of the track.

material. Just enough mixing is allowed to achieve a strong bonding. Hence, the properties of the produced clad layer depend entirely on the applied coating material.

2.2 Applicability of laser cladding

Laser cladding is a technique used in order to produce hard [Amende, 1990; Folkes, 1994; Lang, 1994; Lugscheider, 1990], wear resistant [Brenner, 1996; Choi, 1994; Eiholzer, 1985; Fischer, 1996; Gassmann, 1992; Liu, 1994; Nowotny, 1994; Wolf, 1995] and/or corrosion resistant [Bruck, 1987; Fellowes, 1990; Fouquet, 1993; Gasser, 1996; Lugscheider, 1994; Singh, 1987; Wang, 1993] surface layers. Laser cladding can also be applied to produce thermal barriers [Damborenea, 1993; Pei, 1995; Smurov, 1992; VandeHaar, 1988], to achieve layers suitable for application in nuclear power-stations [Corchia, 1987; Li, 1992] or to obtain surface layers that prevent stacking [Frenk, 1991]. The technique is used to produce high quality surface layers on top of new parts, to produce entire parts [Gebhardt, 1996; Haferkamp, 1995; Kreutz, 1995] and, to

refurbish and improve used parts [Flinkfeldt, 1994; König, 1994; Riabkina-Fishman, 1996].

Table 2.1 gives some examples of reported industrial applications of laser cladding. Cladding is applied on mechanical parts that are exposed to an aggressive environment: thermal cycles with high heating and cooling rates, corrosive gases, high temperatures, abrasive particles and/or cavitation erosion.

Most of these parts only require local treatment that can be performed with a single clad track. An example is the cladding of a diesel engine exhaust valve with a Stellite 6 clad layer that has a width of about 2.5 mm and a thickness of 1.0 mm. Such layers can be applied with a 2 kW CO_2 laser system.

On the other hand, the cladding of an extruder screw [Schneider, 1995; Wolf, 1995] with a 10 mm wide, 2 mm thick layer over a length of more than 3 m is an example of a non-local treatment which requires the use of a 10 kW laser. Laser cladding is not the most economic alternative for the coating of such a rather large area in terms of coverage rate or production costs. However, in this case all other techniques would fail to achieve a strong fusion bond between coating and base material, or would result in severe distortion of the screw.

For the cladding of even larger areas, very high power CO_2 lasers with a laser power of more than 20 kW are available. They can be used to produce 44 mm wide and 5.5 mm high tracks in one step [Volz, 1994].

Table 2.1 Industrial applications of laser cladding.

Source	**Part/industry**	**Material**
Rolls Royce [Macintyre, 1983]	high pressure gas turbine blade shroud	Triballoy on Nimonic
Pratt & Whitney [Eboo, 1983]	interlock	
Combustion Engineering [Eboo]	turbine blade	
	parts of off-shore drilling heads	CrC, Cr, Ni on cast iron
Fiat [Eboo, 1983]	cylinder and valve	on cast iron
GM [Eboo, 1983]	automotive parts	Stellite, Triballoy T-800
Rockwell [Eboo, 1983]	aerospace	Stellite, Colmonoy
Westinghouse [Eboo, 1983]	turbine blade	Stellite 6, Stellite SF
[Bruck, 1987]	turbine blade, plough blade	Stellite 6
[Lubbers, 1994]	diesel engine valve	Stellite 6
[Schneider,1995]	extruder screw plastic machinery	LC2.3B (Ni-base)
[Wolf, 1995]	extruder screw plastic machinery (steel 1.4541)	Al-bronze
[Haferkamp, 1994]	deep drawing tool (cast iron GGG60)	Stellite SF6

Source	Part/industry	Material
[Weerasinghe, 1987]	drainage plough blade	Stellite 6
[Amende, 1990]	leading edge steam turbine blade	Stellite 6
[Küpper, 1990]	valve in combustion engine	Triballoy T-800
[Blake, 1985]	(X45CrSi9)	
[Blake, 1985]	aircraft engine turbine blade Z-notch	
	leading edge turbine blade in industrial	Stellite 6
[Amende, 1988]	gas turbine in power plant	
[VandeHaar, 1988]	deformation tool	Stellite 6
[Bruck, 1988]	gas turbine airfoil thermal barrier	Inconel 625 + CrC
[Bruck, 1988]	valve seat	AISI 410
[Bruck, 1988]	stainless steel seal runner	Stellite 6
[Bruck, 1988]	stainless steel gate valve	Stellite; induction heating
[Ritter, 1991]	leading edge steam turbine blade	Stellite 6,F
[Wissenbach, 1991]	valves	
[Gasser, 1996]	valve in combustion engine	
	(X45CrSi9)	Stellite 21
[Gasser, 1996]	extruder screw plastic machinery	Ni-Cr-Al-Y
[Fischer, 1996]	(14CrMoV6 9)	
	moulding die (45NiCr6)	Co-Cr-W-C
[Nowotny, 1996]	exhaust valves large Diesel engines	Ti-6Al-4V + cubic BN
[Lang, 1994]	(NiCr20AlTi ~ DIN 2.4952)	Stellite 6
[Li, 1992]	camshaft	
[König, 1992]	compressor blade (Ti-6Al-4V)	Ni-Cr alloy
[Amende, 1988]	nuclear valve (AISI 304)	PWA Alloy 694
Pratt&Whitney [Duhamel, 1986]	blowing mould	
	extruder screw plastic machinery	Stellite
[Bergmann, 1994]	jet engine turbine blade notch (PWA	Stellite 6, Colmonoy 5
[Corchia, 1987]	Alloy 1455)	
	die for production of glass bottles	
	components of nuclear plants (AISI 304)	

2.3 Laser cladding versus conventional methods

Laser cladding is one of the coating techniques that are in use for improving surface properties of mechanical parts. Examples of other thermal coating methods are flame spraying, plasma spraying and arc welding. The coating that

is applied on the base material must provide the required surface properties, such as resistance against corrosion or wear. The use of a dedicated material on top of a cheap base material results in considerable material cost savings.
The coating material can be preplaced on the substrate to be covered or it can be provided to it during the process. All processes apply a heat source to melt the coating material and/or the base material. Depending on the technique, a fusion bond or an adhesive bond is achieved between the surface layer and the base material.
In general, the use of a laser beam in surface treatments offers several advantages over conventional heat sources [König, 1989; Molian, 1990; Oberländer, 1992; Webber, 1987]:

- the energy supply can be well controlled;
- very local treatment is possible;
- the total heat input is low, resulting in minimal distortion;
- the heating and cooling rates are high, resulting in a fine microstructure and/or metastable phases;
- the treatment is a non-contact process. There is no tool wear, nor act mechanical forces on the workpiece;
- the process depth is well defined.

Atamert [1989], Cai [1990], Li [1994], Monson [1990] and Oberländer [1992] describe some more advantages of laser cladding over conventional coating techniques. The combination of a controlled minimal dilution of the substrate by the coating material and nevertheless a very strong fusion bond between them, is a unique feature of laser cladding. Porosity in the coating can be prevented entirely and a homogeneous distribution of elements can be achieved.

2.4 Laser cladding methods

Two material application principles can be distinguished: The two stage (preplaced) technique and the one stage (in-situ) technique, which are both displayed in figure 2.4. These two methods are both used in practice. The coating material is predominantly supplied in the form of powder particles.

Two stage process

Several methods of laser cladding with preplaced material are in use. Examples are the melting of flame and plasma sprayed layers [Cuetos, 1993; Gasser, 1996; Juch, 1994; Li, 1992; Lugscheider, 1990; Mordike, 1994; Reichelt, 1996; Smurov, 1992], the melting of preplaced powder [Arlt, 1994; Belmondo, 1979; Bruck, 1988; Flinkfeldt, 1994; Hirose, 1995; Lugscheider, 1992; Matthews,

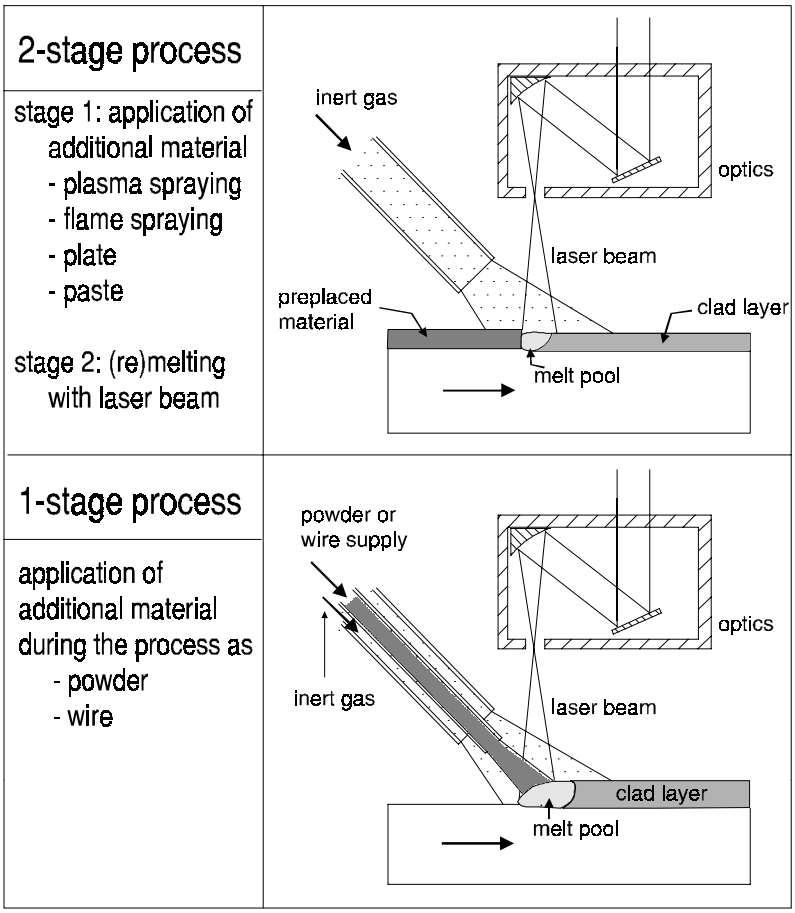

Fig. 2.4 Two stage (preplaced) and one stage (in-situ) laser cladding.

1983; Nurminen, 1985; Sakamoto, 1995] and the melting of preplaced plates or chips [Duhamel, 1986; Tosto, 1994].

Technically speaking, the cladding of flame and plasma sprayed layers is in fact remelting. This remelting may be necessary, because the properties and performance of conventionally applied coatings may be seriously degraded due to poor inter-particle bonding, considerable porosity or extensive chemical inhomogeneity [Li, 1992].

Laser cladding of plasma sprayed layers requires some special attention. The sprayed layer must have enough bonding to the substrate to prevent it from peeling off the substrate due to expansion during the second stage of the process.

Laser cladding with preplaced powder is the most common two stage cladding method. The applied powders are the same as those used in flame and plasma spraying. The powder must be mixed with a chemical binder to ensure that it

will stick to the substrate during the process; It has to be given enough structural strength to withstand forces imposed by gas flows or gravitation [Arlt, 1994]. The chemical binder evaporates during the process. This can result in some porosity in the clad layer.
The second stage of the process starts with the formation of a melt pool in the surface of the coating material. The melt pool propagates to the interface with the substrate. Continued heating ensures that the melt pool is extended to the substrate and that a strong fusion bond is achieved. The heat input must be well controlled to prevent deep melting of the substrate and the therefrom resulting severe dilution on the one hand, and to achieve a strong fusion bond on the other hand.
The two stage methods are particularly useful for parts that can be treated in one single track. It is of course possible to apply several adjacent tracks, but this will result in an increased dilution. This can be illustrated with figure 2.5. Before the first clad track is produced, the entire area is covered by the preplaced material. A part of the coating is molten by the laser beam. After passing of the beam, the molten material contracts due to surface tension. Hence, the substrate area directly next to the produced clad layer is not covered with preplaced material anymore. When the next track is made, the non covered part of the substrate is directly irradiated by the laser beam. Deeper melting of the substrate will occur in this area.

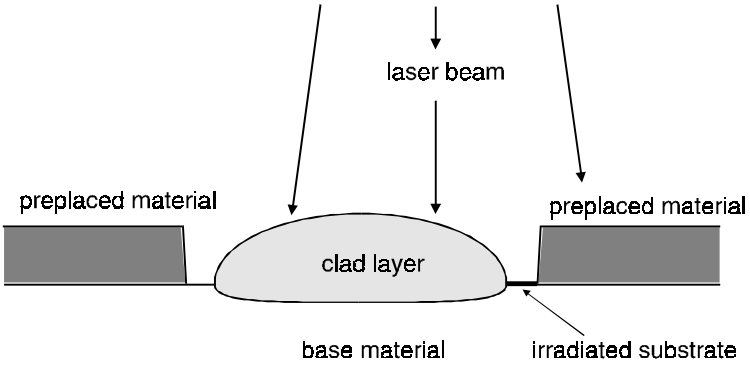

Fig. 2.5 The molten coating contracts during the solidification. Hence, the substrate next to the clad layer is exposed to the laser beam during the application of the next track.

One stage process

The one stage process starts with the formation of a melt pool in the substrate. Simultaneously, coating material is fed into this pool and melts; a strong fusion bond between coating material and substrate is achieved immediately.

The one stage process has several other advantages over the two stage process:
- larger areas which require the application of several adjacent tracks can be produced with less dilution. Contraction of the clad layers on cooling down still occurs, but because material is fed to the substrate next to the previous track no part of the substrate is irradiated unnecessarily;
- the coating thickness can be varied on-line by controlling the material feed rate;
- products with a complex geometry can be treated, because material is fed continuously to the interaction zone. Therefore, flowing out of the molten material by gravitation is not problematic anymore.

Two methods of material feeding are available: wire feeding and powder injection.

Wire feeding [Burchards, 1990; Draugelates, 1994; Hensel, 1992; Hinse-Stern, 1992; Steenbergen, 1993] can be useful for the cladding of rotationally symmetric products that can be clad in one continuous track. The positioning of the wire to the substrate is a critical aspect of the process for two reasons:
- the wire is usually in direct contact with the melt pool in the substrate. In order not to disturb that melt pool the process requires the use of an accurate wire positioning system and an accurate control of the wire feeding rate [Burchards, 1990; Steenbergen, 1993];
- the substrate is partly shielded from the laser beam by the solid wire. To allow a good quality clad layer, i.e. one with a good bonding to the substrate, flown out and a smooth surface, a ratio between beam diameter and wire diameter of at least a factor three must be used [Burchards, 1990]. The wire must be well aligned to the centre of the laser spot to ensure the formation of a symmetrical clad layer.

The wire feeding nozzle must be close to the processing area to allow an accurate feeding of the wire in the melt pool. Therefore, the machining of a curved products, concave shapes in particular, is difficult.

The use of rotating wire feeding heads allow cladding with a constant angle between wire and substrate as well as a constant angle between the injection direction and the relative movement of the substrate.

The process efficiency can be increased by the application of an induction unit to preheat the wire [Burchards, 1990; Hinse-Stern, 1992].

The injection of powder into a laser generated melt pool is a much more common method compared to wire cladding [Frenk, 1993; Grünenwald, 1992; Pelletier, 1993; Volz, 1994; Wolf, 1995]. The method is more flexible [Hensel, 1992]: it allows the on-line variation of clad dimensions and clad composition and, many more elements and alloys are available as powder then as wire.

Powder injection cladding is a more robust method than wire cladding, because there is no direct contact with the melt pool and, the laser beam can pass through the stream of powder particles instead of being obstructed by the wire.
Powder feeders can be based on various working principles. Two such principles are shown in figure 2.6. The left picture shows a feeder consisting of a powder container from which powder flows by gravity into a slot in a rotating disk. The powder is transported to a suction unit from which it is transported by a gas stream to a powder nozzle. The volumetric powder feed rate is controlled by the dimensions of the slot and the speed of the disk [Carvalho, 1995].
Another method for powder dosing is the use of a pneumatic screw feeder [Weck, 1994; Weerasinghe, 1984] (figure 2.6 right). The powder is taken from a container to the powder pick-up and transported to the powder nozzle. The powder feed rate is controlled by the rotational speed and dimensions of the screw.
A different approach to powder feeding is the application of a hopper and a combination of pneumatic and vibrational forces. A standard ultra-sonic cleaning device is suitable for delivering the vibrational forces. The powder is taken from the hopper by means of a pressure difference and transported to the processing zone [Metzbower, 1986; Macintyre, 1983].
The development of new powder feeders for laser cladding is directed to the direct control of the flow rate: control of mass flow instead of volumetric flow and instantaneous flow variations [Carvalho, 1995; Nowotny, 1996; Schiere, 1996; Weck, 1994].
The powder must be transported from the feeder to the process area. This can be done by the use of a carrier gas (argon, helium, nitrogen) or simply by gravitation. Subsequently, it is directed to the melt pool by a powder nozzle.
The powder nozzle can have several configurations. Two basic lay-outs are shown in figure 2.7. The co-axial supply of powder (figure 2.7 left) [Nowotny, 1996; Pelletier, 1994; Tucker, 1984; Vetter, 1994] can be integrated with the optical system. An advantage of a co-axial powder supply is the independence of the powder supply of the direction in which the workpiece moves. Another advantages of the co-axial powder supply are the controlled heating of the powder before it enters the melt pool and the high powder efficiency [Jouvard, 1997; Lemoine, 1994; Li, 1995; Vetter, 1994]. However, not all products can be accessed with a co-axial powder nozzle.
The lateral supply of powder (figure 2.7 right) allows the treatment of all kinds of shapes by applying dedicated powder nozzles. Basically, lateral powder nozzles are just tubes with the proper length, shape and diameter. Lensch [1996] developed a curved tubular nozzle to clad inner diameters of tubes.

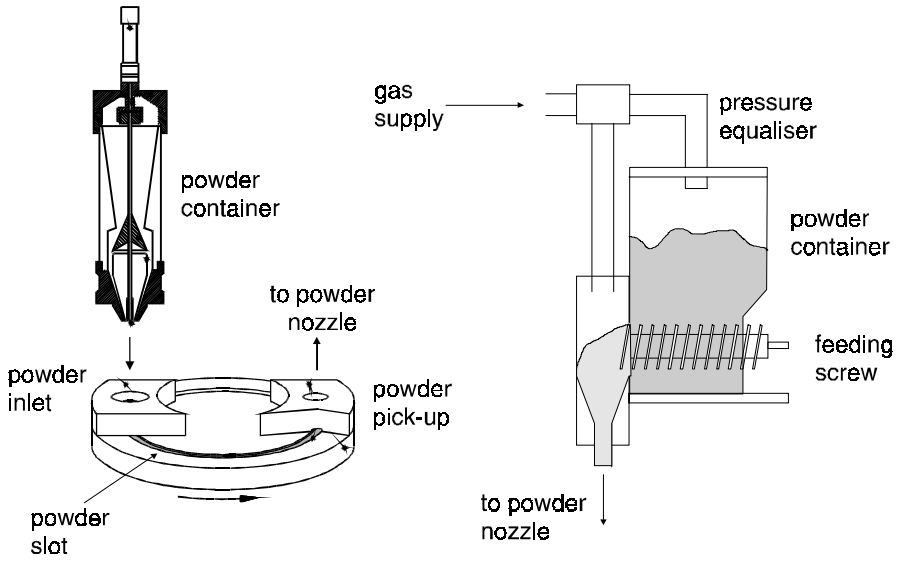

Fig. 2.6 Two powder dosing principles.

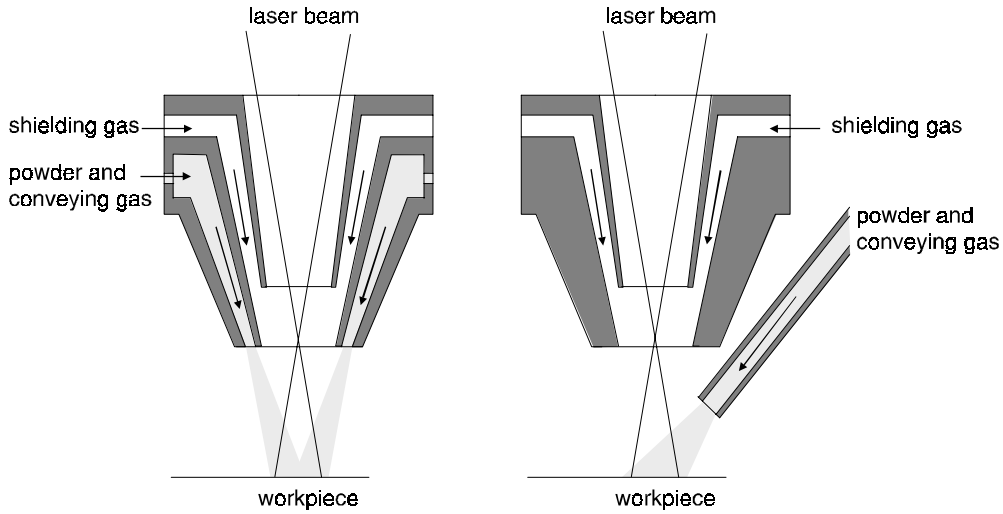

Fig. 2.7 Co-axial (left) and lateral (right) powder supply.

2.5 Clad layer properties

The properties of clad layers are classified in four groups (table 2.2).
Some of those properties may be inter-related. The wear resistance can, for instance, be affected by the hardness, the microstructure, the number of cracks and their depth and direction, the bonding between base material and substrate, etc.

Tab. 2.2 Properties of clad layers.

geometrical properties	mechanical properties	metallurgical properties	qualitative properties
clad dimensions	hardness distribution	microstructure	porosity
dilution	residual stress	dilution	cracking
roughness	wear resistance	grain size	
	tensile strength	homogeneity	
		corrosion resistance	

In practice, it is difficult to produce a clad layer which meets all requirements. Usually a balance must be found between several properties. An example is the reduction of crack formation in the clad layer by preheating the substrate. The preheating reduces the cooling rates and the resulting residual stress. Consequently, crack formation is avoided and, the hardness is reduced as well [Brenner, 1996; Eigenmann, 1995; Evers, 1993; Freitas, 1993]. Crack prevention is important, because cracks initiate corrosion fracture and reduce fatigue strength.

dilution

Laser cladding requires the achievement of a strong fusion bond between the cladding material and the substrate, which, in its turn, requires the formation of a melt pool in the substrate. It has to be noted however, that the depth of this melt must be as small as possible in order to obtain a pure surface layer which is not diluted by the base material.

The dilution of the produced clad layer by elements of the substrate is used to characterise the clad quality. It can be measured in two ways [Bruck, 1987]. The first method is based on the clad layer geometry (figure 2.8). The dilution is then defined as the ratio of the clad depth (d_c) in the substrate over the total clad height (t_c). This geometrical approach assumes an homogeneous distribution of elements over the clad cross-section.

The second method is based on an analysis of the material composition in the clad layer ('chemical' or 'volumetric' dilution). A comparison is made between the material composition of the pure coating material and the composition of the substrate is made. This method allows the determination of a variation of the dilution over the clad depth and is preferred over the geometrical approach.

In chapter 5 (laser cladding with preplaced powder) two examples are given to illustrate the effect of dilution on some coating properties. The first example shows how the measured geometrical dilution relates to the hardness distribution. The second example shows that the chemical dilution is the most useful of the two, because not all clad layers have a uniform distribution of elements.

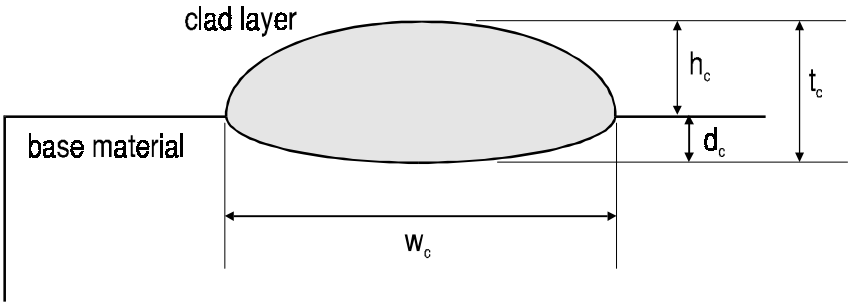

Fig. 2.8 Cross-section of a single clad layer with definition of the clad geometry: clad height (h_c), clad depth (d_c), total clad height (t_c) and clad width (w_c).

porosity

The presence of holes in the clad layer is being referred to as porosity. Porosity can be caused by several reasons. First, it may be the result of the formation of gas bubbles that are trapped in the solidifying melt pool. This phenomenon can be decreased by a vibration of the workpiece (frequency: 25 Hz; amplitude: 20 μm) [Powell, 1981]. It was observed that this 'vibro' laser cladding also reduces internal stresses and cracking.

Secondly, if solidification proceeds in different directions, some regions in the melt can be enclosed. A contraction occurs upon solidification of these enclosed regions. That contraction causes tensile stress in the layer and may even lead to the formation of holes. These two kinds of porosity are to be found in the clad layers.

Two other kinds of porosity are confined to the substrate-clad interface. The first one is caused by the presence of minor flaws, such as grease which influences the surface tension and therewith the bonding of the coating material to the substrate.

The last type of porosity appears when overlapping tracks are applied as indicated in figure 2.9. This so-called 'inter-run porosity' can occur when too much powder is supplied. This can be avoided with a width-height ratio of more than five [Steen, 1987].

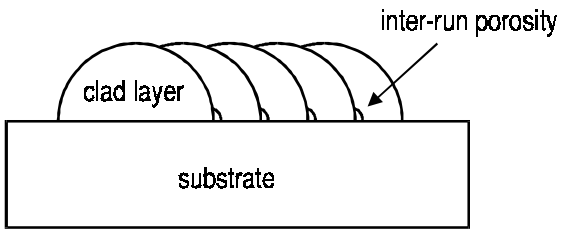

Fig. 2.9 Inter-run porosity.

Some examples of porosity which occurred in actual laser cladding experiments are given in chapter 7.

2.6 Material properties

Laser cladding is used to improve the surface properties of metallic machine parts. A wide variety of commercial metallic or ceramic powders is available. Those powders were developed for the use in plasma and flame spraying. They are also fit for use in laser cladding, because the intended functional properties are the same. In appendix 4 an extensive overview is given of combinations of powders and base materials as reported in the literature.

An essential aspect of laser cladding is the achievement of a strong fusion bond over the entire interface between the substrate and the clad layer. A good wetting between the coating material and the substrate is therefore required. Because of the poor wettability of ceramics to metals, it is very difficult to clad ceramics on top of a metal substrate [de Hosson, 1995; Lugscheider, 1994; Zhou, 1991]. The application of sandwich layers between the intended surface coating and the substrate [Cuetos, 1993; Li, 1992; Liu, 1994; Smurov, 1992] or the use of binders can be helpful [Lang, 1994; Lugscheider, 1994; Nowotny, 1994; Singh, 1987; Zhou, 1991]. Preheating may also help to enhance wetting [Ellis, 1995].

The basic requirement for a fusion welding is that the two coupling materials are soluble in each other and, there is question of a phase equilibrium between them [Li, 1992]. For most alloys this requirement poses no difficulty, but pure metals can sometimes be difficult to clad on top of each other. Aluminium and cobalt, for instance, are not soluble in each other, so there is no phase equilibrium. Phase equilibrium's exist only between aluminium and some intermetallics or between cobalt and other intermetallics. So, the only way to bond them together is to sandwich them with intermetallics.

Multi-layers can also be applied in metal-metal combinations to reduce residual stress due to repeated heat input [Frenk, 1993] and to form a functionally gra-

dient layer with a low dilution and the intended properties on top [Jasim, 1993; Sepold, 1989].
Convection is the single most important factor influencing the geometry of the pool, including pool shape and ripples. Convection is also the main mechanism for mixing added material with the substrate [Chan, 1984; Picasso, 1994]. Since the microstructure and chemical composition of the clad strongly depend on the degree of mixing and the cooling rates during solidification and consequent cooling, the parameters controlling these mechanisms are important to the laser cladding process [Komvopoulos, 1990]. Material properties that influence these mechanisms are, among others, the melting point and the thermal conductivity.
The melting point of the substrate must preferably be higher than that of the coating material. If this is not the case, then it is possible that during solidification and subsequent cooling of the clad layer, the substrate region just underneath it can be heated to a temperature over the melting point. This region will subsequently lose its strength. Under the effect of the stress of the clad above, hot tear will occur along this region [Li, 1992]. Such a situation will in any case result in porosity along the interface.
The formation of cracks in the clad layer is mainly caused by the thermal stress created by the high thermal gradient built up during the cooling stage and the difference between the thermal expansion coefficients [Frenk, 1991, 1993; Li, 1992; Pilloz, 1990; Vasauskas, 1996; Zhang, 1994; Zhou, 1991]. Especially layers that are characterised by the presence of hard and brittle particles, such as carbides, are prone to cracking [Luft, 1995]. Ceramic layers are also vulnerable to cracking, because of their limited ductility combined with the difference in thermal expansion coefficients compared with metals [VandeHaar, 1988].
Residual stresses can be reduced by a reduction of the cooling rate. This can be achieved by preheating [Brenner, 1996; Evers, 1993; Glumann, 1994; Schneider, 1993].
The different base materials can be classified into two groups. The first group contains all steels. The second group contains non-ferrous base materials, such as aluminium and titanium.

2.6.1 Powders on a steel substrate

Cobalt base powders ('Stellites')
Cobalt base superalloys ('Stellites') are very popular with regard to the improvement of the wear resistance of mechanical parts, especially in hostile environments [de Hosson, 1996]. Those powders are mixtures of cobalt and other

elements like nickel, chromium, tungsten, carbon and molybdenum. Chromium is added to form carbides and to provide strength to the cobalt matrix as well as to enhance the resistance against corrosion and oxidation. Tungsten and molybdenum have large atomic sizes and give, therefore, additional strength to the matrix. They also form hard brittle carbides. Nickel is added to increase the ductility.

The predominant carbide found in Stellites is of the chromium rich M_7C_3 (M=metal) type. These carbides (2200 Hv) are responsible for the hardness of the clad (~ 550 Hv) and for the wear resistance. In low-carbon alloys other carbides such as M_6C and $M_{23}C_6$ are abundant [de Hosson, 1996].

If the wear properties of a given cobalt-base powder mixture is not sufficient, then hard particles, such as carbides, nitrides and borides, can be added directly to this mixture [Gassmann, 1992; Glumann, 1994; Grünenwald, 1992; Nowotny, 1994; Volz, 1994]. Those hard particles usually have a high melting temperature. The flow in the melt pool must ensure that they are uniformly mixed with the other elements and become embedded in the matrix provided by the molten cobalt-base material.

Gassmann [1992] described the addition of tungsten carbide (WC/W_2C) to a Stellite powder in order to enhance the abrasive wear resistance. Tungsten carbide is distinguished by a minimal plastic deformation capacity, a low thermal expansion and a high wettability by molten metals, especially cobalt. Due to the low free formation enthalpy tungsten carbide is dissolved in the solid state by molten cobalt. The dissolution increases with the temperature of the melt and the interaction time. Depending on the carbon concentration in the melt, dissolved tungsten carbide recrystallises either to WC, or with low carbon concentrations, to W_2C or brittle phases such as Co_3W_3C and Co_6W_6C. It is therefore important to keep the temperature in the melt as low as possible. Not only results this in a low carbide dissolution, it also ensures a dense coating with lower tensile stresses.

By far the most popular commercial cobalt base powder is Stellite 6 (table 2.1). Stellite 6 can be applied on e.g. dies, inserts, valves, feeder screws in plastic machinery and turbine blades. The working temperature is limited to 500 °C. For many of the applications in table 2.1 it is possibly not the best available coating. However, it is selected mostly because its properties and clad behaviour are well known and because it has established itself in other hardfacing techniques.

Nickel base alloys

Nickel base alloys are suited for application in parts that are exposed to an aggressive atmosphere at elevated temperatures. They have a good high temperature corrosion and oxidation resistance. Nickel base alloys can also be used as a substitute for cobalt. This may be important in the future, because cobalt is a relatively rare and expansive element, whereas nickel is widely available and much cheaper.
An example of an application is the cladding of a high pressure gas turbine blade or the improvement of a feeder screw in plastic machinery [Amende, 1988].
Elements that are commonly mixed with nickel are chromium, boron, carbon, silicon and aluminium. The formation of hard borides and silicon carbide improves the wear resistance and hardness. However, a too large presence of these hard phases makes the coating very brittle [Arlt, 1994; Becker, 1991; Grünenwald, 1992; Lugscheider, 1990]. Hard particles can also be mixed with the added elements [Pelletier, 1994]. Luft [1995] describes the addition of tungsten carbides to a mixture of Ni-B-Si in order to achieve a solidified nickel rich solid solution with finely distributed Ni_3B and dissolved tungsten.
The addition of boron and silicon improves the wetting behaviour. Hence, very smooth surfaces can be achieved [Wolf, 1995].
Aluminium can be added to further increase the hardness. The hardness increase is due to the formation of intermetallic phases ($NiAl_3$ and Ni_2Al_3) [Grünenwald, 1996; Marsden, 1990] or an oxide layer (Al_2O_3).

Iron base alloys
Although the selection of an iron base alloy for improving surface properties of an iron base substrate may not be the most obvious choice, some research has been done to this subject.
It has been reported that a mixture of iron, chromium, carbon and mangane or tungsten has superior wear properties compared to Stellite 6 [Choi, 1994; Eiholzer, 1985; Komvopoulos, 1994]. The elements that are added to iron ensure the formation of carbides, contribute to the oxidation and corrosion resistance and promote the solid solution strengthening. The main carbide type found in this kind of clad layer is M_6C instead of the M_7C_3 type found in Stellite 6.
Others have reported on the application of austenitic corrosion resistant steel layers on top of ordinary low carbon steels [Fouquet, 1994; Jasim, 1989]. The corrosion resistance of those layers can be further improved by increasing the molybdenum content in it [Huang, 1995].

2.6.2 Non-ferrous substrates

2.6.2.1 Nickel base substrates

Nickel base alloys retain their mechanical properties up to high temperatures and are corrosion resistant. Therefore, they are especially useful for applications that undergo high temperature corrosion and wear, such as exhaust valves of large Diesel engines for ship propulsion or power generation [Fischer, 1996] as well as for jet engine turbine blades [Duhamel, 1986]. However, the wear properties of nickel base alloys are not very good. The resistance to wear can be improved by using cobalt base alloys which have a better wear endurance than nickel [Cooper, 1989; Duhamel, 1986; Gassmann, 1992; Macintyre, 1983], by making use of a protective oxide layer such as chromium oxide [Fellowes, 1990] and zirconium oxide [Damborenea, 1993] or by the addition of hard particles in a binder alloy [Gassmann, 1992; Jasim, 1993; Zhu, 1993]. Oxide layers are not only very hard, they also form a thermal and chemical barrier between the metal and the aggressive environment [Fellowes, 1990; Singh, 1987; VandeHaar, 1988; Vasauskas, 1996]. A problem with ceramic layers is that they often have a poor adherence to the coating. Reactive elements such as hafnium and yttrium can improve this adherence [De Damborenea, 1993; Singh, 1987; Sircar, 1989].
One of the applications of laser cladding on a nickel base substrate that has established itself in practice is the cladding of notches of jet engine turbine blades [Duhamel, 1986]. A high wear point exists at the notch between neighbouring blades forming the outer shroud of jet engine turbine stages. The material in the notch region experiences rubbing contact with the adjacent blade during engine operation. The wear resistance could be increased by the application of a cobalt based alloy (PWA alloy 694).

2.6.2.2 Aluminium and titanium base substrates

Aluminium and titanium alloys (predominantly Ti-6Al-4V) are popular materials for constructing mechanical parts in aerospace and automotive industry, because of the combination of low weight and high strength. Unfortunately, at high temperatures the mechanical properties and the wear resistance are poor. These properties can be enhanced by applying a nickel base layer [Kar, 1988; Liu, 1994; Sallamand, 1993; Sircar, 1989]. Thus the advantage of light weight is combined with a good high temperature mechanical behaviour.
Nickel, titanium and aluminium form several brittle intermetallic compounds, such as Al_3Ni, Al_3Ni_2 and AlNi. The formation of these compounds on the inter-

face leads to cracking. Suitable sandwich layers like Ni-Al bronze can prevent this [Liu, 1994].
Firmly bonded aluminium oxide layers could be obtained by cladding an aluminium alloy with a mixture of aluminium and silicon oxide [De Hosson, 1995]. In this reaction coating the following reaction occurred:

$$2Al+3/2SiO_2=Al_2O_3+3/2Si.$$

The presence of silicon in the produced oxide layer seems to be favourable for the wetting by liquid aluminium.
The hardness of an aluminium or titanium alloy can also be increased by the injection of a mixture of hard particles and an aluminium respectively titanium alloy. Especially silicon carbide and titanium carbide seem to be useful hard particles [Folkes, 1994; Hegge, 1990; Ricciardi, 1990]. Lang [1994] investigated the injection of a very hard cubic boron nitride and Ti-6Al-4V mixture on a Ti-6Al-4V compressor blade.

2.7 Effect of process parameters

The physical and process variables that affect the clad results are shown in figure 2.10 [Ollier, 1995]. In order to be able to predict cladding results, the relationships between these variables and the clad results must be known and solved simultaneously. At the moment no exact solutions are available.

2.7.1 Experimental methods

Many authors have studied the laser cladding process by means of a simple parameter variation for a fixed material combination [Komvopoulos, 1990; Kreutz, 1995; Nurminen, 1983]. This parameter variation can help to enhance the process knowledge and results in tables such as table 2.3, which shows qualitatively how clad properties are influenced by the process parameters.
Parameter variation can also yield process diagrams like the one shown in figure 2.11 [Kreutz, 1995]. This diagram indicates the clad height as a function of the powder injected per unit of length for two different feed rates and two powder densities. The clad height increases with power density and powder mass. The properties of the clad are insufficient for low and high powder feed rates originating either from dilution or lack of fusion.

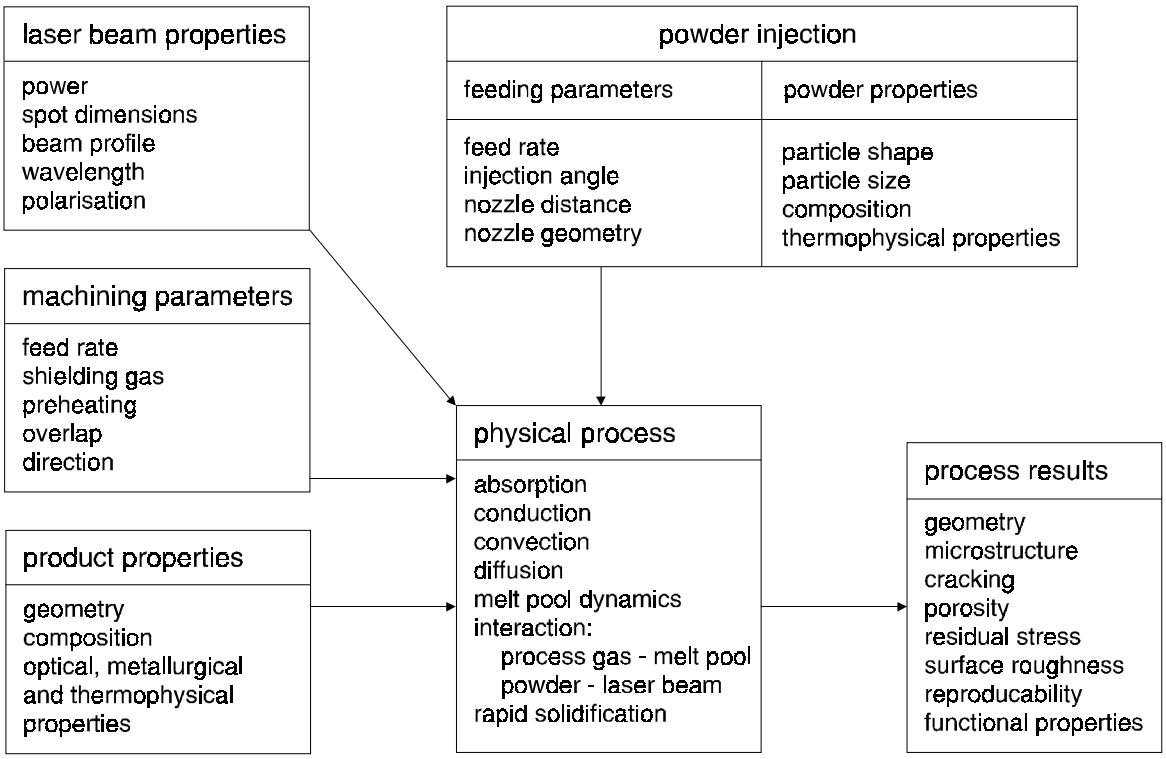

Fig. 2.10 Variables in laser cladding with powder injection [Ollier, 1995].

Tab. 2.3 Reported effects of increase of parameter values on clad layer properties (+: increase; -: reduction).

properties / parameters	clad height	melt depth	geometrical dilution	hardness/ cracking	maximum clad thickness
laser power	-	+	+	-	+
feed rate	+	-	-	+	-
quantity of coating material	+	-	-	+	+
laser spot	+	-	-	+	-

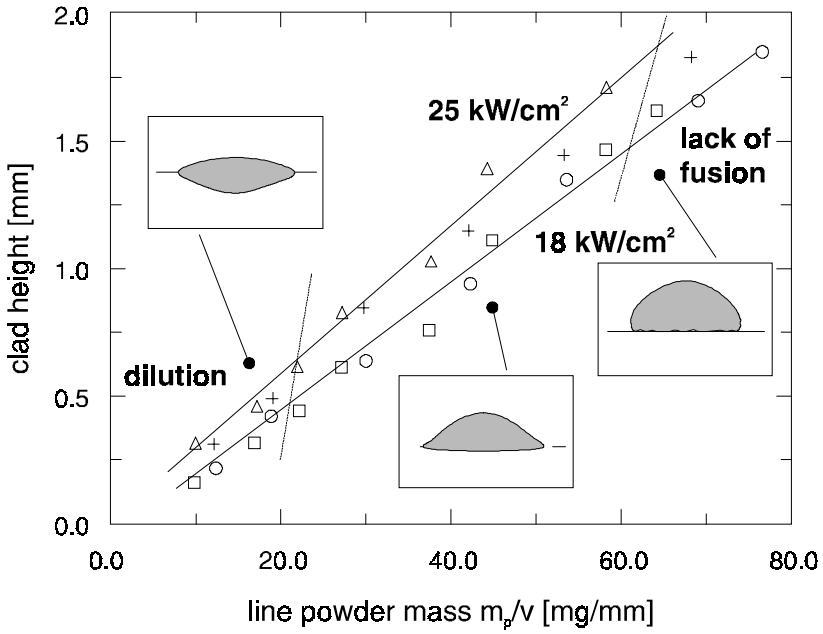

Fig. 2.11 Example of a process diagram achieved by parameter variation [Kreutz, 1995]. 25 kW/cm²: Δ: 350 mm/min, +: 300 mm/min; 18 kW/cm²: o: 350 mm/min, □: 300 mm/min. Powder: Stellite 6; Substrate: C45.

Others [Blake, 1985; Chen, 1989; Engström, 1988; Kar, 1988, 1989; Komvopoulos, 1990; Molian, 1988; Singh, 1985] relate laser cladding results to the specific energy E:

$$E = \frac{P}{v\,D} \qquad \text{Eq. 2.1}$$

where P is the laser power, v is the feed rate of the workpiece and D is the diameter of the laser spot.

The maximum coating thickness that can be applied during laser cladding depends on the specific energy [Chen, 1989; Marsden, 1990]. Below a certain level of the specific energy no fusion bond can be formed, whereas beyond another level the dilution becomes too large [Molian, 1989]. Kar [1989] and Singh [1985] suggest that a decrease of the specific energy due to an increase of the feed rate can enhance the solid solubility of alloying elements.

In this thesis it is shown that the specific energy alone is not a suitable parameter for explaining laser clad properties: the thermal cycle in the surface layer will be different for each specific parameter combination that results in a certain value of the specific energy. This opinion is shared by Ellis [1995] and is

supported by the experimental results which are presented in chapter 6. It is also supported by figure 2.12. This figure was composed by taking values of the interaction time and power density as reported in the literature for laser cladding of cobalt based powders on low alloy steels. According to this figure, all experiments are in the range of 0.5 - 15 kJ/cm^2. Average values for interaction time and powder density are respectively 0.5 s and 15 kW/cm^2.

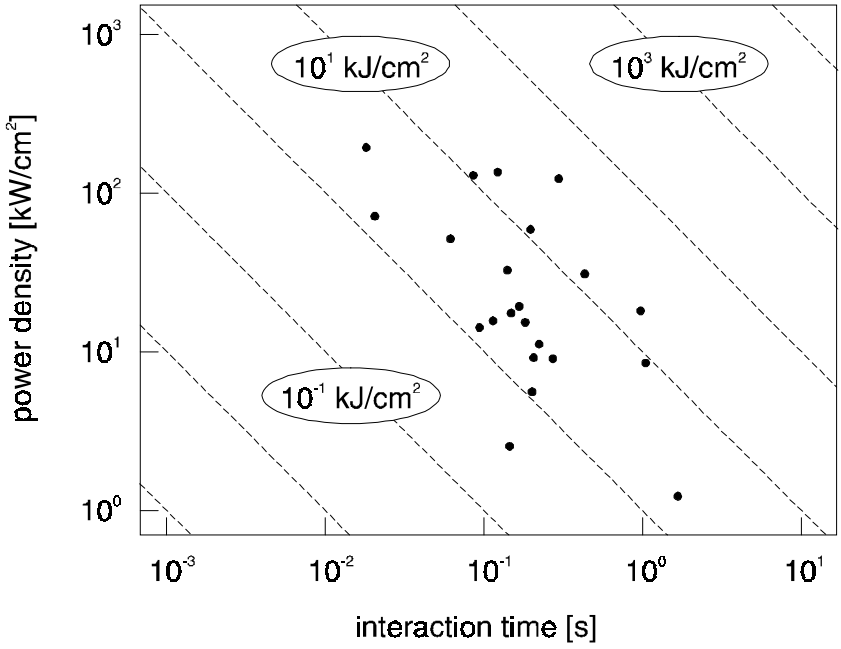

Fig. 2.12 Some values of the specific energy as reported in the literature for laser cladding of cobalt based coatings on low alloy steel. Each dot represents a different parameter setting.

Experimental design

The factorial design method is one of the methods that can be used for a systematically performed parameter evaluation. It was introduced by Box [1978] and Johnson [1977]. It is a multi parameter analysis method which is most useful for applications in which a process depends on numerous parameters. In such applications it is hardly possible to draw conclusions from graphs and tables that are achieved with ordinary one-at-a-time experiments, especially when taking into account that interactions and higher order effects between parameters can exist.

The parameters, also called factors, are varied in a systematical way from a low value to a high level (figure 2.13). In this example each parameter is evaluated

on three levels. For each possible parameter combination an experiment is performed and the process response is measured.

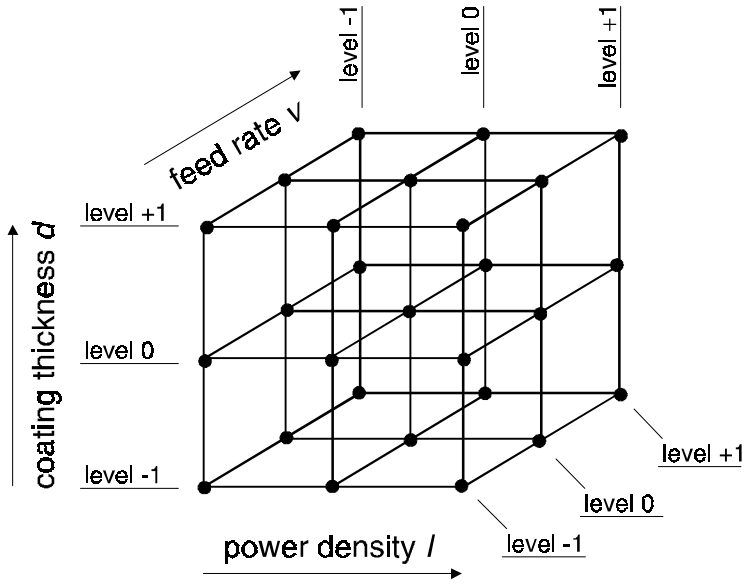

Fig. 2.13 Set-up for a three parameter factorial experiment with all parameters at three levels.

The factorial design method is more efficient than an ordinary one-at-a-time variation of parameters, because it requires less experiments to achieve the same accuracy. For example, the simplest possible factorial experiment is one with two factors that are both evaluated on two levels. In a factorial design experiment, the set-up requires four experiments. A one-at-a-time variation requires six experiments in order to obtain the same level of accuracy.
The factorial analysis gives a statistical significance to the observed relationships, which not only allows the withdrawal of insignificant process parameters from further experiments, but also allows a sensitivity analysis of the process [Box, 1978].
The calculated relationships between factors are only valid between the lower and the higher level of the parameters. Many processes in nature show an exponential course, which can not be revealed by this method. However, in a small interval such a curve can be approximated by a straight line or a second degree polynomial.
Van Sprang [1992] and Eiholzer [1985] applied this method to laser cladding with preplaced powder. They varied the laser power density (I), the feed rate of the workpiece (v) and the coating thickness (d). Thereupon, they studied the response of clad layer properties to these variations. Van Sprang evaluated all three factors on three levels for which he performed 27 experiments. The

achieved results of his analysis (table 2.4) are shown in table 2.5. These values can be used to compose a process window of machining parameters.

Tab. 2.4 Input parameters for factorial design analysis of laser cladding.

Level	power density [kW/cm^2]	feed rate [mm/s]	coating thickness [mm]
-1	18	2	0.4
0	23	4	0.6
1	28	6	0.8

Tab. 2.5 Process responds as achieved with a three level factorial experiment for three factors. All factors scaled between -1 and 1. Base material: C45; Cladding material: Metco 18C.

Property	parameter function
hardness H [Hv 0.2]	$H = 680 - 338\ I + 452\ v \pm 55$
heat affected zone HAZ [mm]	$HAZ = 0.76 + 0.25\ I - 0.43\ v - 0.30\ d \pm 0.05$
dilution DIL [%]	$DIL = 35.8 + 39.0\ I - 21.0\ v - 76.0\ d \pm 4.0$
absorption A [%]	$A = 28.9 - 3.2\ I + 0.7\ v - 0.5\ v^2 + 0.8\ d + 0.8\ v\ d + 0.3\ d \pm 1.1$

As one can see in table 2.5, the average micro hardness in the clad layer is 680 Hv. The hardness is reduced by either an increase of the power density or a reduction of the feed rate. This agrees with the findings of others (table 2.3) and can be explained by the reduced cooling rate. The feed rate has a larger impact on the hardness than the power density.
In this case, only the linear effects of the factors on the hardness, the heat affected zone and the dilution were significant. Interactions and second order effects are important for the measured absorption only.

2.7.2 Physical models

An alternative to the process analysis with experimental methods is to develop models which are based on physical laws. Models that are based on physical laws contribute to a better insight in the process. Experiments must be performed to verify the assumptions on which the model is based and to adapt the

parameters in it. A good model supports the necessary experimental research for the development of new applications.

Few models for laser cladding have been proposed. They can be distinguished into two groups. The first group of models is aimed at predicting the amount of material that can be deposited, based on the assumption that a perfect clad has no dilution with the substrate, without calculation of the temperature field in the melt [Jouvard, 1997; Lemoine, 1993, 1994 (2x), 1995; Li, 1994; Marsden, 1990]. Analytical solutions for the resulting clad geometry can be obtained because convection is not accounted for.

A typical example of such models is the work of Jouvard [1997]. As a first step he determines the laser power which is transmitted through the cloud formed by injected powder particles (P-P_{at} in figure 2.16) by application of the Beer-Lambert law. For details, one is referred to chapter 6.2, where this law is used to calculate the temperature rise of particles during their flight through the laser beam.

The second step involves the calculation of the power required to produce a melt pool in the substrate. Combined with the power attenuation factor, the therefore required laser power can be determined (threshold 1 in figure 2.14).

If more power than this first threshold is supplied, a clad layer can be built up on the substrate. During the flight through the laser beam the particles are heated but not molten. Melting occurs when the powder reaches the melt pool that has been initiated on the substrate.

The mass flow that can be molten only depends on the laser power until the second threshold is reached. At this threshold, the particles are molten by the laser beam before they arrive in the melt pool.

The second group of models is aimed at describing the main phenomena that occur during laser cladding. Models belonging to this group [Hoadley, 1992; Ollier, 1992, 1995; Picasso, 1991, 1994 (3x)] therefore calculate the temperature and velocity field in the melt and the solid substrate, the shape of the gas-liquid interface and, of course, the clad geometry. The temperature and velocity fields in the melt are important, because they determine the redistribution of elements and the cooling rates. Together, they are responsible for the attained microstructure.

One of the first attempts to explain the shape of a laser induced melt pool was made by Cline and Anthony [1977]. They were able to achieve an analytical solution for the melt pool shape, because they did not only take into account the convection in the melt, but they also neglected the presence of viscous and inertia forces and, assumed that the material properties are temperature independent.

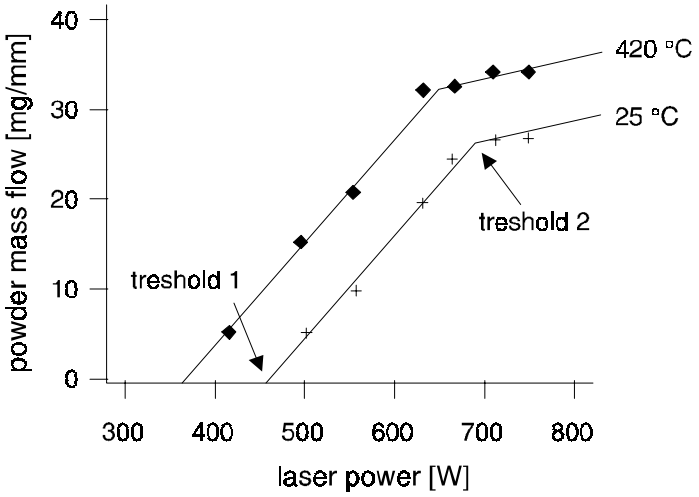

Fig. 2.14 Mass flow as a function of the laser power for two substrate temperatures [Jouvard, 1997]. Threshold 1 is the laser power required for melting the substrate. Threshold 2 is the laser power required for particle melting.

It has been shown [Picasso, 1994] that convection is important in explaining the temperature and velocity field in the melt pool. Figure 2.15 shows a cross section in the longitudinal direction of a typical melt pool without convection (left) and with convection. The shapes are quite different, indicating that the convection effects in the melt pool cannot be neglected.

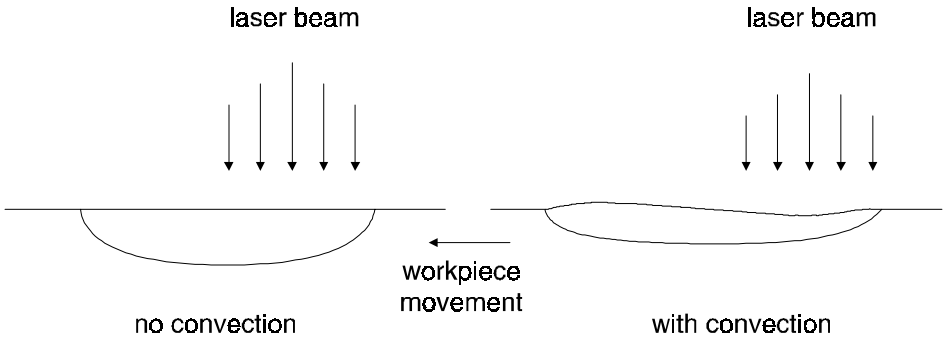

Fig. 2.15 Effect of convention on melt pool shape [Picasso, 1994] (material: Stellite 6; feed rate: 1 mm/s).

The shape of the melt is governed by convective flows which are mainly driven by surface tension gradients. Those gradients are induced by temperature differences on the surface due to absorption of energy from the laser beam. It is not possible anymore to achieve analytical solutions if all physical aspects are

incorporated in the model. Therefore, the fluid flow and the temperature profile in the melt must be calculated by numerical solution.
The temperature (T) and the velocity field in the melt are governed by three linked equations: the energy equation (Eq. 2.2) which describes the temperature field and the phase change from solid to liquid; the Navier-Stokes equation (Eq. 2.3) which describes the velocity field in the melt; and the continuity equation (Eq. 2.4).

$$\frac{\partial}{\partial t}\left(\rho H\right)+\nabla\cdot\left(\rho\,\mathbf{v}H\right)=\nabla\cdot\left(k\,\nabla\left(\rho T\right)\right)+q \qquad \textit{Eq. 2.2}$$

$$\frac{\partial}{\partial t}\left(\rho\,\mathbf{v}\right)+\left(\rho\,\mathbf{v}\nabla\right)\mathbf{v}=\rho\,g-\nabla p+\mu\,\nabla\cdot(\nabla\mathbf{v}) \qquad \textit{Eq. 2.3}$$

$$\nabla\mathbf{v}=0 \qquad \textit{Eq. 2.4}$$

with the fluid viscosity μ, a heat source q, the specific enthalpy H, the gravity field g, the pressure p, the density ρ, the time t and the thermal conductivity k. When choosing an appropriate co-ordinate system, the influence of the factor ρg is only effective in one direction. The force imposed by this factor on the fluid is called the buoyancy.
It is common practice [Basu, 1992] to simplify the Navier-Stokes equations for incompressible fluid flow by means of the Boussinesq-approximation:

$$\rho=\rho_m\left[1-\alpha\,\left(T-T_m\right)\right] \qquad \textit{Eq. 2.5}$$

with the density ρ_m at the melting temperature T_m and the thermal expansion coefficient α. The Navier-Stokes equation then reduces to:

$$\frac{\partial\,\mathbf{v}}{\partial t}+\mathbf{v}\nabla\mathbf{v}=g\alpha\left(T-T_m\right)-\frac{1}{\rho}\nabla p+\nu\,\nabla\cdot(\nabla\mathbf{v}) \qquad \textit{Eq. 2.6}$$

where ν is the kinematic viscosity (μ/ρ). The temperature and the specific enthalpy are linked by the heat capacity (c_p) and the latent heat of fusion (L_f):

$$H=\int_{T_0}^{T_m}c_p\,dT+L_f+\int_{T_m}^{T}c_p\,dT \qquad \textit{Eq. 2.7}$$

Equations 2.3, 2.4 and 2.7 must be solved simultaneously with the proper boundary conditions. The most important conditions involve the shear stress on the surface of the melt pool due to the stream of powder particles in a gas flow, the heat input from the laser beam and injected particles (figure 2.16) as well as the mass continuity law which is important because particles are added to the melt.
Both the finite element method [Ollier, 1995] and the finite volume method [Picasso, 1994] have been applied to solve these linked equations for a two dimensional clad cross-section. The finite volume method is restricted to problems in which non temperature dependent material properties are reasonable. The material properties only differ from solid to liquid state. This limitation does not exist in the finite element method. However, up to now no one has implemented this temperature dependency for laser cladding.

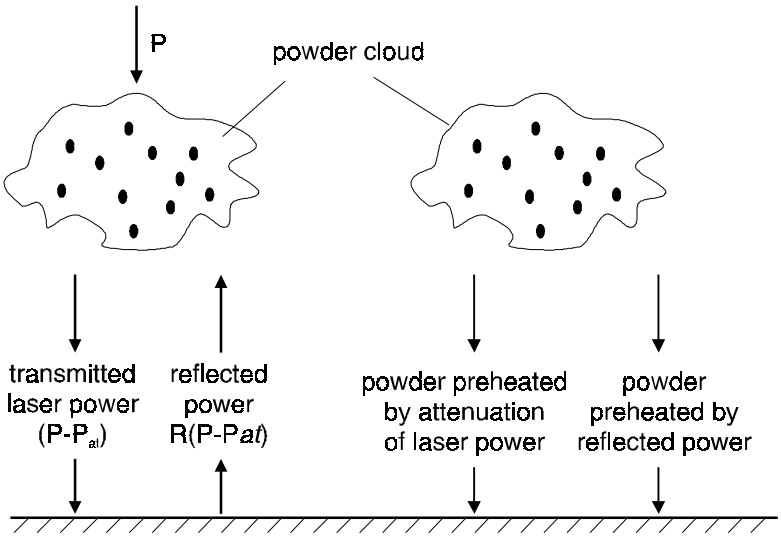

Fig. 2.16 Heat transfer to the substrate is accomplished by both laser energy and heated particles. The laser power transmitted through the powder cloud is responsible for the melting of the substrate.

Once a numerical solution of the process has been achieved, it is possible to attain process diagrams, such as figure 2.17. The left picture shows the achieved clad height as a function of the feed rate for good quality clad layers with a dilution of less than 5 % for two different power densities (top-hat laser beam). The clad height is almost inversely proportional to the feed rate of the workpiece. The required powder mass stream can then be calculated from the calculated clad dimensions and the powder efficiency.

The picture on the right shows the dilution as a function of the powder mass stream. The dilution decreases when more powder is injected in the melt pool, since more energy is required for melting the powder. As can be seen, the dilution is almost a linear function of the powder mass stream.

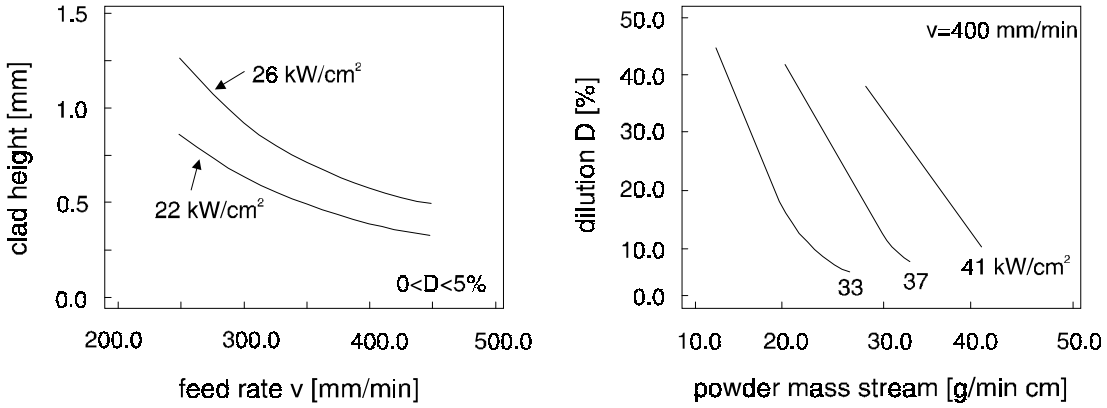

Fig. 2.17 Process diagrams of laser cladding with Stellite 6 achieved with a numerical model [Ollier, 1995].

Models allow a fast evaluation of parameter variations. In the example shown in figure 2.18, the diameter of the powder stream has been varied. The same amount of powder is injected, but the particle stream is much more confined (dotted line) than in the preferred situation (continuous line). In the preferred parameter setting the entire melt pool surface has a temperature well over the melting point. However, in the other situation the surface temperature can locally drop below the melting temperature.

2.8 Process control

In order to ensure a constant and reproducible clad quality, process control is necessary. Parameters such as substrate temperature, substrate surface condition or substrate thickness may vary during operation. Therefore, pre-set fixed operating parameters are not appropriate.

Little work on process diagnosis and control during laser cladding has been reported [Backes, 1994; Grünenwald, 1993; Li, 1988, 1989, 1990 (2x); Nowotny, 1994; Vetter, 1994; Weck, 1991].

The main point of interest in process diagnosis of laser cladding is the measurement of radiation emitted from the melt pool. For this task, several types of sensors, such as photodiodes and pyrometers are available. The radiation can

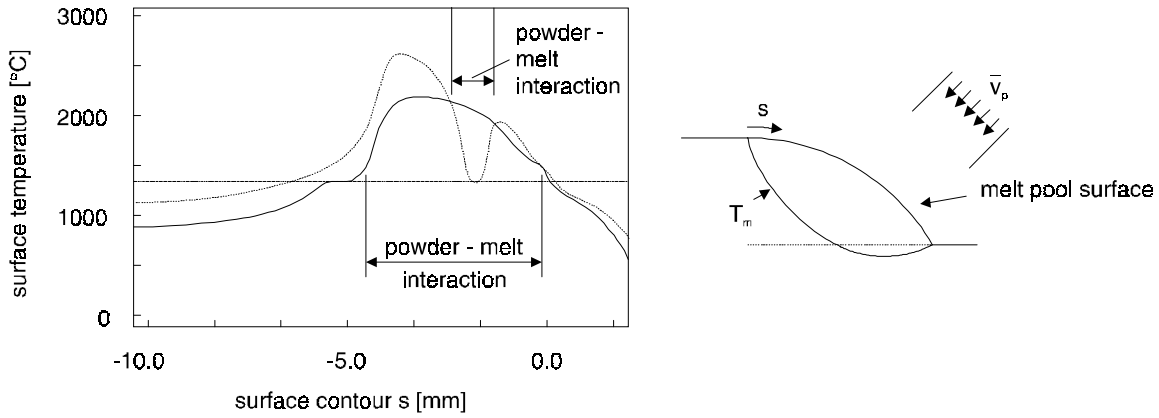

Fig. 2.18 Surface temperature along the melt pool contour s for two powder injection settings [Ollier, 1995].

be measured integrally over the entire melt as well as very locally. These measurements reveal correlations between the measured signals and process parameters such as powder injection parameters, laser power, feed rate and surface properties. Backes [1992] showed that an integral measurement of radiation emitted from the melt pool is best suited for laser cladding.
Figure 2.19 shows a temperature based PID control-loop which is typical for laser cladding [Grünenwald, 1993; Nowotny, 1996; Tönshoff, 1995; Weck, 1994]. The radiation emitted by the melt pool, and hence the temperature, is kept at a constant value by a real-time variation of the laser power. Nowotny [1996] showed that it is possible to attain with such a PID controller a clad layer with a constant thickness and composition. It was also possible to limit the dilution to only 3 %, although the substrate temperature increased from 300 to 760 °C.

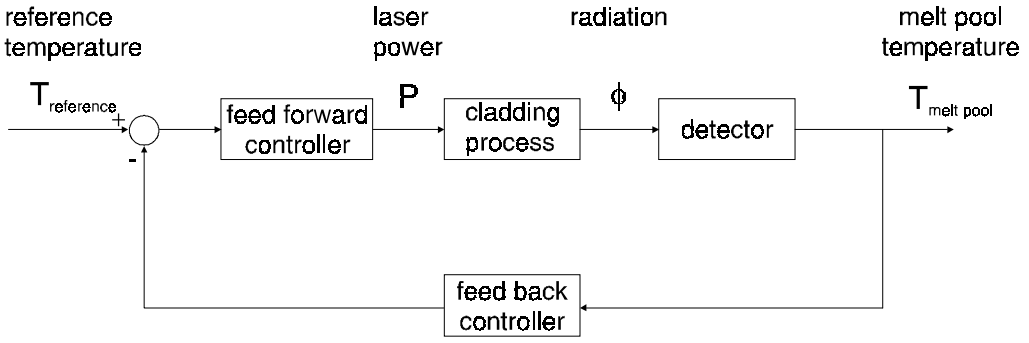

Fig. 2.19 Temperature based PID control of laser cladding.

Li [1989] developed several other sensors usable in the process control of laser cladding. The sensor signals could be used to detect the clad thickness, the level of dilution, the surface roughness and the clad profile, as well as the extent of surface oxidation. However, no applications have been reported in which these sensors are really applied.
A variation of the clad quality can also be caused by fluctuating machining parameters, such as powder feed rate, beam position and diameter, and output power. Attempts are being made to prevent fluctuations of such parameters. For instance, on-line control of powder feed rate [Carvalho, 1995; Nowotny, 1996; Weck, 1994] is becoming an industrial reality and Bianco [1994] developed a device to control the alignment of the laser beam with respect to the powder nozzle.

2.9 Optical system

The laser beam, as produced in the resonator of a laser system, must be transported and manipulated by an optical system. The laser beam must be focused into a spot with the required shape and power density on the workpiece. Both lenses and mirrors can be utilised to focus CO_2 laser beams for laser powers under 3 kW. Higher laser powers require the exclusive use of mirrors, because lenses cannot be cooled sufficiently.
In most laser cladding applications, the intensity profile as produced in the laser system, is applied. Three examples of common intensity profiles are shown in figure 2.20. The processing region is usually positioned below the focal point. This leaves a larger distance between the optical system and the workpiece, which facilitates the protection of the optical system. Large focal distances are preferred, since it reduces the sensitivity of the spot dimensions to changing beam properties and also reduces the mean power density in the focal point, which can lead to plasma formation [Beyer, 1985; Fischer, 1996; Vetter, 1994].
Although a circular laser spot is suitable for most laser cladding applications, there are cases in which another shape is preferred. For instance, a line shape is useful for treating feeder screws in plastic machinery in one single track. Such a line shape can be made by applying two cylindrical mirrors or a segmented mirror (figure 2.21) [Bruck, 1988; Fux, 1992; Gasser, 1996; Wissenbach, 1991].
The cylindrical mirrors only change the dimensions of the laser spot, but the segmented mirror also affects the spatial distribution of the power density. As a matter of fact, a segmented mirror is a one dimensional beam integrator. The

incident laser beam is separated in several beamlets which are recombined for proper overlap in the focal plane.

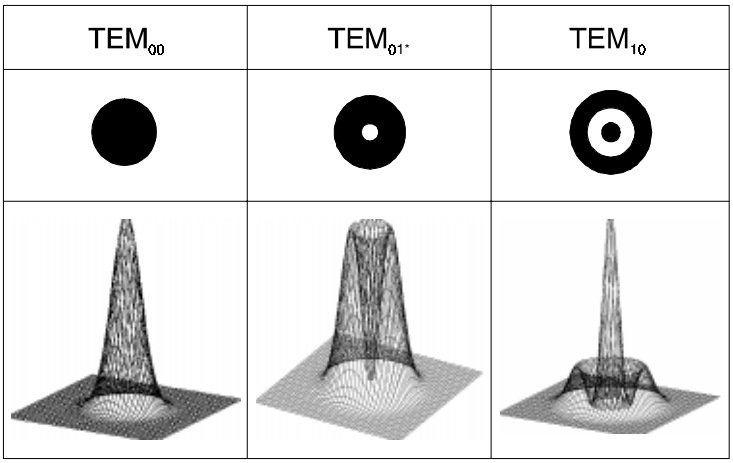

Fig. 2.20 Three examples of common circular intensity profiles.

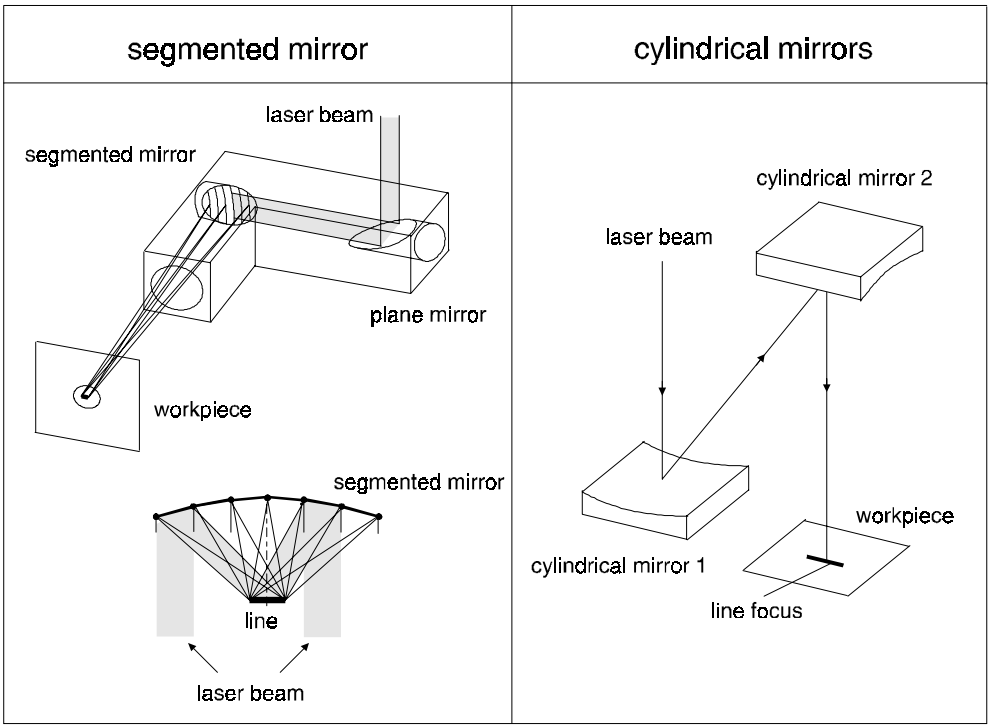

Fig. 2.21 Two possible methods for achieving a line shape on the workpiece.

A (laterally) homogeneous intensity distribution is achieved (figure 2.22). This can be favourable, as was indicated by Beckmann [1995] and König [1994]. An uniform temperature distribution over the scanned width is thus attained. This results in uniform clad properties over the width of the track.

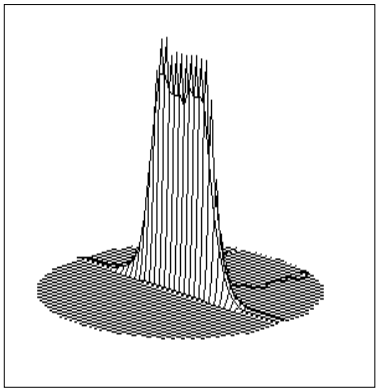

Fig. 2.22 Laterally uniform intensity profile achieved with a one dimensional beam integrator by transforming a circular mixed mode laser beam.

In laser cladding, it is also possible to use a rectangular spot with a uniform power density [Beckmann, 1990; Bianco, 1994; König, 1994]. Such a spot can be attained by means of a two dimensional beam integrator. Faceted mirrors or lenses, as well as kaleidoscope type integrators are used (figure 2.23).
An alternative to the use of integrating optics for achieving a uniform temperature profile over the width of the track is the use of scanning optics. Scanning optics [Bloehs, 1993; Bruck, 1988; Dickmann, 1995; Fux, 1992; Matthews, 1983; Nowotny, 1996; Rudlaff, 1990] add an extra degree of freedom to the process, because they allow a flexible adaptation of the spot dimensions and intensity distribution during the process. According to Nowotny [1996], the scanning frequency must be at least 60 Hz in order to attain a 'continuous' heat input in the material. Galvanometer scanners are used. Their scanning frequency (maximum 300 Hz) is adjustable and the amplitude can be controlled on-line. Now, piezo crystals are coming into practice as actuator for scanning mirrors [Römer, 1997]. The oscillating frequency of these crystals can be controlled. Frequencies of more than 1 kHz can be reached.

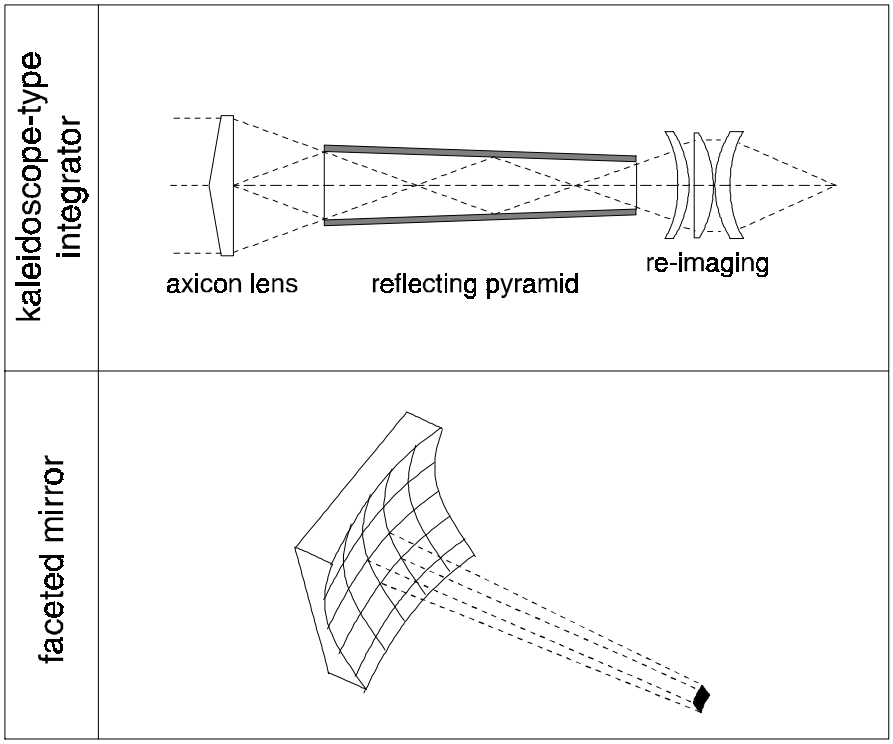

Fig. 2.23 Two possible methods for achieving a rectangular laser spot with a uniform energy distribution on the workpiece.

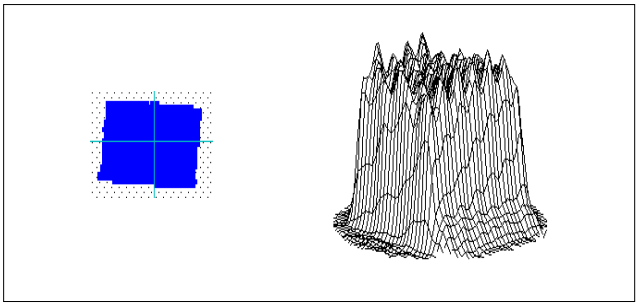

Fig. 2.24 Uniform power density distribution achieved by integrating a circular mixed mode in the kaleidoscope-type integrator.

2.10 Preview

As became clear from the presented literature research, many aspects of laser cladding have been investigated. Nevertheless, there are several aspects that require future attention in order to make laser cladding a mature technique. Current research is directed to the following fields:

- development of dedicated optical systems and material feeders;
- process modelling for optimisation of process parameters and reduction of development times;
- (control of) metallurgical aspects of laser cladding;
- development of on-line process control systems for complex shapes and development of dedicated laser cladding machines;
- development of 3-D applications by laser rapid prototyping (high accuracy, low surface roughness, reduction of stresses, integration in CAD/DAM systems);
- transfer of laboratory results to industry.

In this thesis an emphasis is laid on the transfer of laboratory results to industry. The literature search showed that, among other things, laser cladding results depend strongly on the applied laser beam intensity profile. Therefore, the effect of that parameter is studied more detailed.

A way to eliminate the effect of the laser beam properties on the cladding results is the application of dedicated optical systems that yield a laser spot on the workpiece surface that has a well defined shape and a uniform energy distribution which is independent of the applied laser source.

Apart from the laser beam properties, other machining parameters have their effect as well. By studying these effects, one can enhance the insight in the laser cladding technique. Extensive series of experiments that were performed in this respect were restricted to preplaced powder and the powder injection methods. According to the literature those are the only two realistic options.

The results of these studies are presented in the following chapters.

Chapter 3

Temperature profile on a clad surface

The formation of a shallow melt pool in the substrate is the first stage in the laser cladding with powder injection process. Injected powder particles are trapped in this melt pool and the formation of a clad layer on the substrate surface starts.

The melt pool is formed due to absorption of laser power. Not all laser energy can reach the surface due to attenuation by the powder cloud. The attenuated energy is responsible for the heating of the particles in the powder cloud. Depending on their temperature on arrival in the melt pool, they either extract or add energy to the melt pool.

The formation of a melt pool in the substrate is not only affected by the total power absorbed in the surface, but also by the intensity profile of the laser beam.

In this chapter a method is presented to calculate the temperature induced on the surface of a semi-infinite solid by an arbitrarily shaped laser source. In general, no analytical solutions for this problem can be found. Therefore, the equations describing this problem must be discretisised and solved numerically.

3.1 Numerical method for calculating the surface temperature distribution

The first stage of all laser treatments is the absorption of laser radiation in the substrate (see figure 2.2). Absorption occurs in a very thin surface layer, where the optical laser energy is converted into heat. The absorbed heat diffuses into the surrounding bulk material by conduction.
The diffusion equation for a linear heat flow in a homogeneous isotropic medium is:

$$\rho c_p \frac{\partial T}{\partial t} = k\nabla T \qquad (t > 0) \qquad \textit{Eq. 3.1}$$

The laser beam can be considered as a moving heat source with a certain power density distribution that imposes a boundary condition on the substrate surface.
The classical approach to modelling the heat flow induced by a distributed heat source moving over the surface of a semi-infinite solid, starts with the solution of the heat diffusion equation for a point source [Carslaw, 1959; Elshof, 1994]. The temperature field is connected to a Cartesian co-ordinate system moving with a velocity v along the x-axis. For time t->∞ a steady state solution is obtained for a semi-infinite body, which is valid for a point source coming from -∞:

$$T(x,y,z) = \frac{q(x,y)}{2\pi k\sqrt{x^2+y^2+z^2}} e^{\frac{-v\left(\sqrt{x^2+y^2+z^2}-x\right)}{2\kappa}} + T_0 \qquad \textit{Eq. 3.2}$$

with κ the temperature independent thermal diffusivity, *q(x,y)* the power in the point source, z the depth, y the co-ordinate along the surface perpendicular to the direction of movement and, T_0 the initial temperature.
The solution of the heat diffusion equation for the moving point source is integrated over the entire laser spot to obtain a solution for an arbitrarily shaped source. The temperature, as a result of the laser spot with boundaries x_s, x_e; y_s, y_e; z_s, z_e, is:

$$T(x,y,z)=\frac{1}{2\pi k}\int_{z_s}^{z_e}\int_{y_s}^{y_e}\int_{x_s}^{x_e}\frac{q(x',y')e^{\frac{-v\left(\sqrt{(x-x')^2+(y-y')^2+z^2}-(x-x')\right)}{2\kappa}}}{\sqrt{(x-x')^2+(y-y')^2+z^2}}dx'dy'dz'+T_0 \qquad \textit{Eq. 3.3}$$

The surface (z=0) temperature of a semi-infinite body moving past an arbitrarily shaped heat source is thus given by:

$$T(x,y,0)=\frac{1}{2\pi k}\int_{y_s}^{y_e}\int_{x_s}^{x_e}\frac{q(x',y')e^{\frac{-v\left(\sqrt{(x-x')^2+(y-y')^2}-(x-x')\right)}{2\kappa}}}{\sqrt{(x-x')^2+(y-y')^2}}dx'dy'+T_0 \qquad \textit{Eq. 3.4}$$

Analytical solutions of the type of integral in equation 3.4 are only known for some special cases [Elshof, 1994]. In general, numerical methods are needed to solve this type of integrals.
The integral was solved numerically by Bos [1993]. First, it was transformed to a series expansion on a grid with step size h. The temperature on a grid point $(x_i,y_j)=(x_0+ih,y_0+jh)$ can be written as:

$$T(x_i,y_j)=\frac{1}{2\pi k}\sum_{k=0}^{n_x}\sum_{l=0}^{n_y}K_{ijkl}^{hhhh}q_{kl}+T_0 \qquad \textit{Eq. 3.5}$$

with:

$$K_{ijkl}^{hhhh}=\int_{x_m}^{x_p}\int_{y_m}^{y_p}\frac{d(y-y')d(x-x')}{\sqrt{(x-x')^2+(y-y')^2}}e^{-\frac{v\left(\sqrt{(x-x')^2+(y-y')^2}-(x-x')\right)}{2\kappa}} \qquad \textit{Eq. 3.6}$$

An analytical expression does not exist for this surface integral and numerical calculation is very time consuming. Fortunately, Bos [1993] was able to apply an exact reduction of this surface integral to a line integral, which, apart from exponential integrals, consists of finite integrals only. Polynomial as well as rational approximations exist for the exponential integral. This integral reduction results in the following expression:

$$K_{ijkl}^{hhhh} = y_m\left[E_1\left(v(\sqrt{x_m{}^2+y_m{}^2}-x_m)\right)-E_1\left(v(\sqrt{x_p{}^2+y_m{}^2}-x_p)\right)\right]$$
$$-y_p\left[E_1\left(v(\sqrt{x_m{}^2+y_p{}^2}-x_m)\right)-E_1\left(v(\sqrt{x_p{}^2+y_p{}^2}-x_p)\right)\right]$$
$$-\int_{y_m}^{y_p}\left(\frac{e^{vx_m-v\sqrt{\xi^2+x_m{}^2}}\,\xi^2}{\sqrt{\xi^2+x_m{}^2}\left(-x_m+\sqrt{\xi^2+x_m{}^2}\right)}-\frac{e^{vx_p-v\sqrt{\xi^2+x_p{}^2}}\,\xi^2}{\sqrt{\xi^2+x_p{}^2}\left(-x_p+\sqrt{\xi^2+x_p{}^2}\right)}\right)d\xi \qquad \textit{Eq. 3.7}$$

where E_1 is an exponential integral of the form:

$$E_1(x)=\int_x^\infty \frac{e^{-t}}{t}dt \quad (x>0) \qquad \textit{Eq. 3.8}$$

Compared with a differential equation, an integral equation needs a great amount of calculation time. An integration over the entire domain is required to calculate one single point. Brandt [1984], Lubrecht [1989] and Venner [1991] developed an algorithm (multi-level multi-integration) for fast evaluation of an integral. They showed that if the kernel K has certain smoothing properties, the complexity of the evaluation of an integral can be reduced without loss of accuracy. This algorithm was subsequently applied to solve equation 3.5.
The numerical solution was checked by comparing it to the analytical solution of Ready [1971] which requires a non-moving circular laser beam with a uniform power density distribution as input to calculate the temperature in the beam centre:

$$T(z,t)=\frac{4AP}{k\pi D^2}\sqrt{4\kappa t}\left(ierfc\sqrt{\frac{z^2}{4\kappa t}}-ierfc\sqrt{\frac{z^2+\left(\frac{D}{2}\right)^2}{4\kappa t}}\right) \qquad \textit{Eq. 3.9}$$

where A is the absorptivity. A procedure to determine the value of this absorptivity is presented in appendix 2.
In order to perform this comparison, the numerical solution was flipped to yield a solution in the plane characterised by y=0. For both the numerical and the analytical solution, the depth to which a certain temperature is reached was calculated. The austenite temperature of carbon steel C45 was taken for this

purpose, because the depth to which this temperature is reached, is marked clearly by the transition from austenite to martensite.
As can be seen from figure 3.1 the numerical solution agrees very well with the analytical solution.

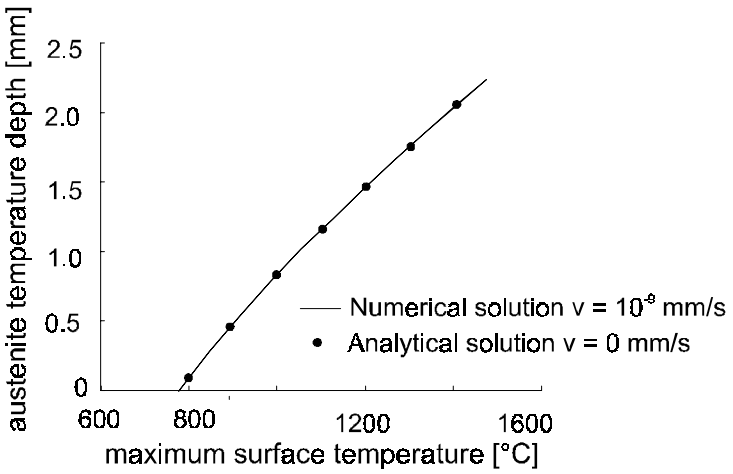

Fig. 3.1 The calculated depth at which a transition from martensite to austenite occurs is identical for the analytical and the numerical solution. Material: C45; Laser beam: circular with uniform power density.

As input, models require reliable material properties to yield accurate results. Examples of such material parameters are the thermal conductivity and the heat capacity. These parameters are temperature dependent. Since the model does not recognise this fact, an effective value was used. Based on a series of laser transformation hardening experiments the effective thermal conductivity and heat capacity was determined for several materials. The accuracy of this procedure was verified by making a comparison between the measured hardened depth in new experiments and the with the calculated values predicted hardened depth (for details one is referred to [van Wijngaarden, 1994]. The determined values are shown in table 3.1. It is clear that these values differ from the values given in handbooks.
The presented numerical method can be used to compose a process diagram that predicts the formation of a melt pool for several spot sizes. It also gives one the opportunity to study the effect of the laser beam power density distribution or the effect of the substrate thermal properties on the melt pool formation. Examples of these cases are presented in the figures 3.2-3.4.

Tab. 3.1 Thermal conductivity and specific heat for four steel substrates. The effective values were determined by means of experiments on laser transformation hardening. The other values were taken from handbooks.

	Thermal conductivity [W/mK]			specific heat [J/kg/K]		
	20 °C	average	effective	20 °C	average	effective
C45	48	35	40	460	670	615
100Cr6	35	32	36	470	670	615
X210CrW12	20	24	26	460	650	610
42CrMo4	42	34	37	460	670	615

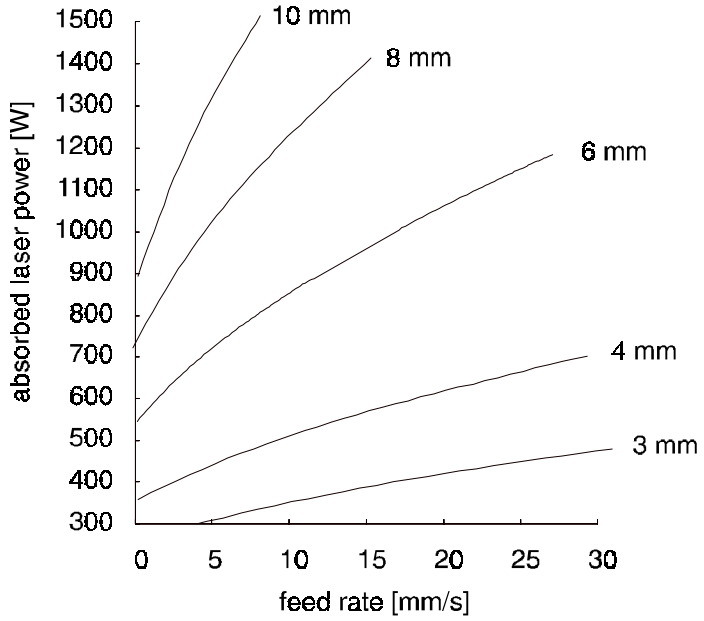

Fig. 3.2 Process diagram for formation of a melt pool with several beam diameters in a C45 workpiece achieved with a circular laser beam with a uniform power density. The lines represent the combinations of feed rate and absorbed laser power that result in the melting temperature.

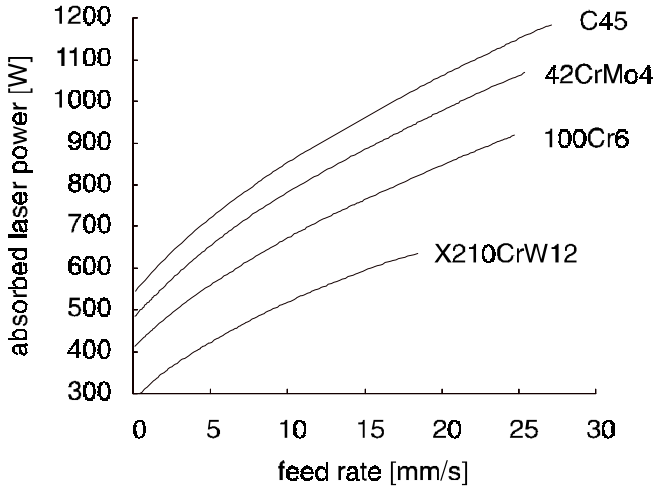

Fig. 3.3 Process diagram for formation of a melt pool in several steel substrates achieved with a circular laser beam with a uniform power density and a diameter of 6.0 mm. The lines represent combinations of feed rate and absorbed laser power that result in the melting temperature.

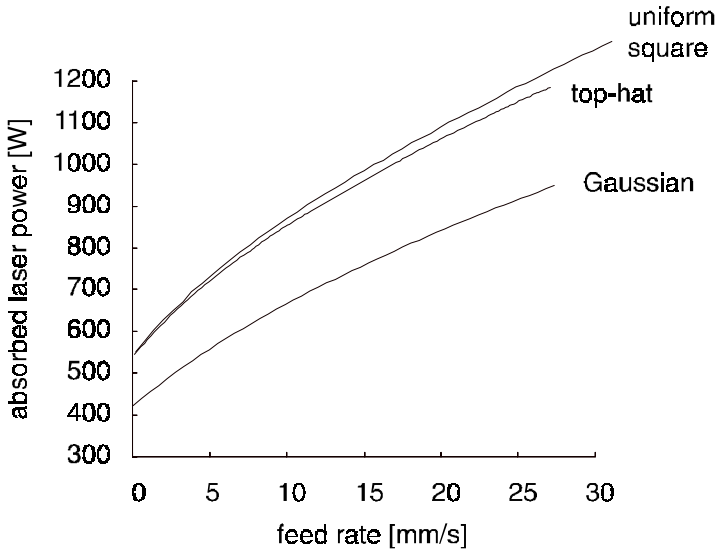

Fig. 3.4 Process diagram for formation of a melt pool in a steel C45 substrates achieved with several laser beams with a spot area of 28.3 mm^2 (spot diameter: 6.0 mm for top-hat and Gaussian beam). The lines represent the combinations of feed rate and absorbed laser power that result in the melting temperature.

The effect of the beam shape on the maximum surface temperature can be noticed clearly from figure 3.4. The developed numerical method allows a more detailed analysis of the temperature distribution over the surface. In figure 3.5

and 3.6 some examples are shown. In all four cases the same absorbed laser power has been applied and the spot area has been kept constant: 7.07 mm^2. For the circular spot shapes this area corresponds to a spot diameter of 3.0 mm. It can be noticed that the highest surface temperature in this configuration is reached with the line source. This particular line source has a laterally homogeneous intensity distribution and a Gaussian distribution in the other direction. In front view, the temperature profile is more uniform than the profiles obtained with the other beam profiles. This notion agrees with the claims made by Beckmann [1995] and König [1994].

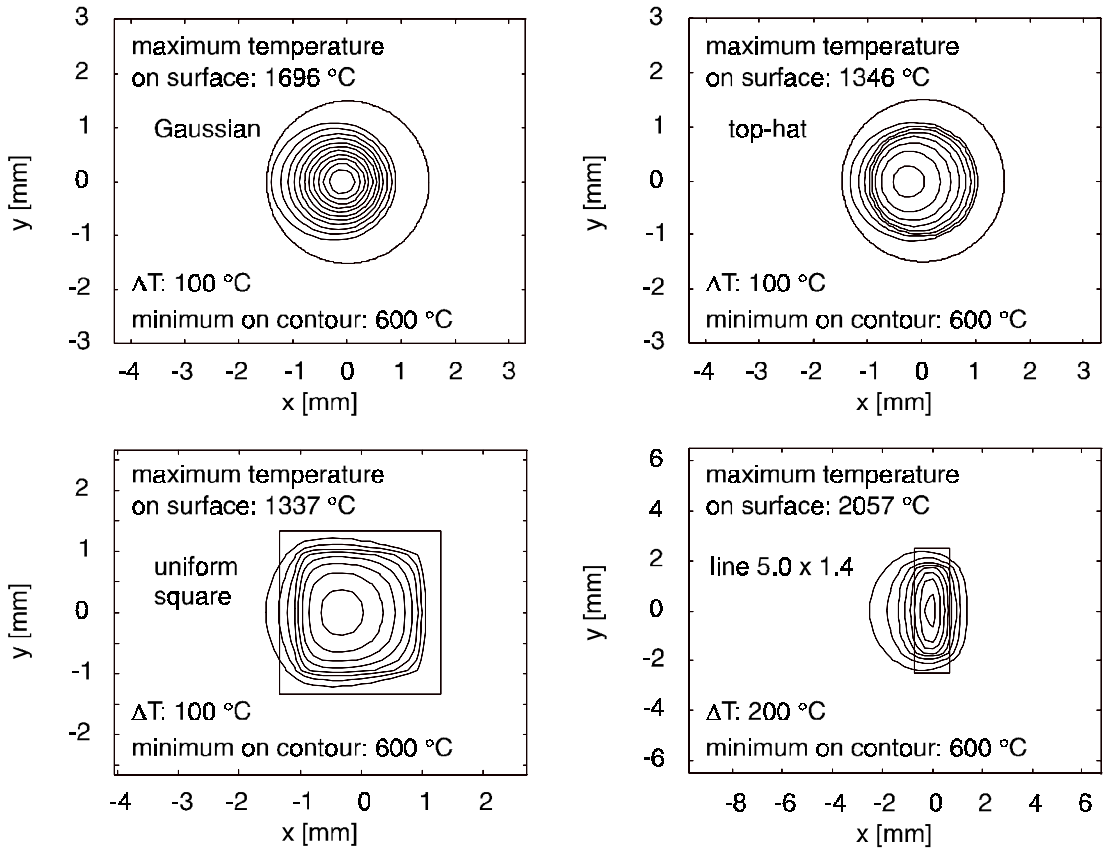

Fig. 3.5 Surface temperature distribution achieved with four intensity profiles. Material: steel C45. Laser spot area: 7.07 mm^2. Feed rate: 5 mm/s. Absorbed laser power: 300 W.

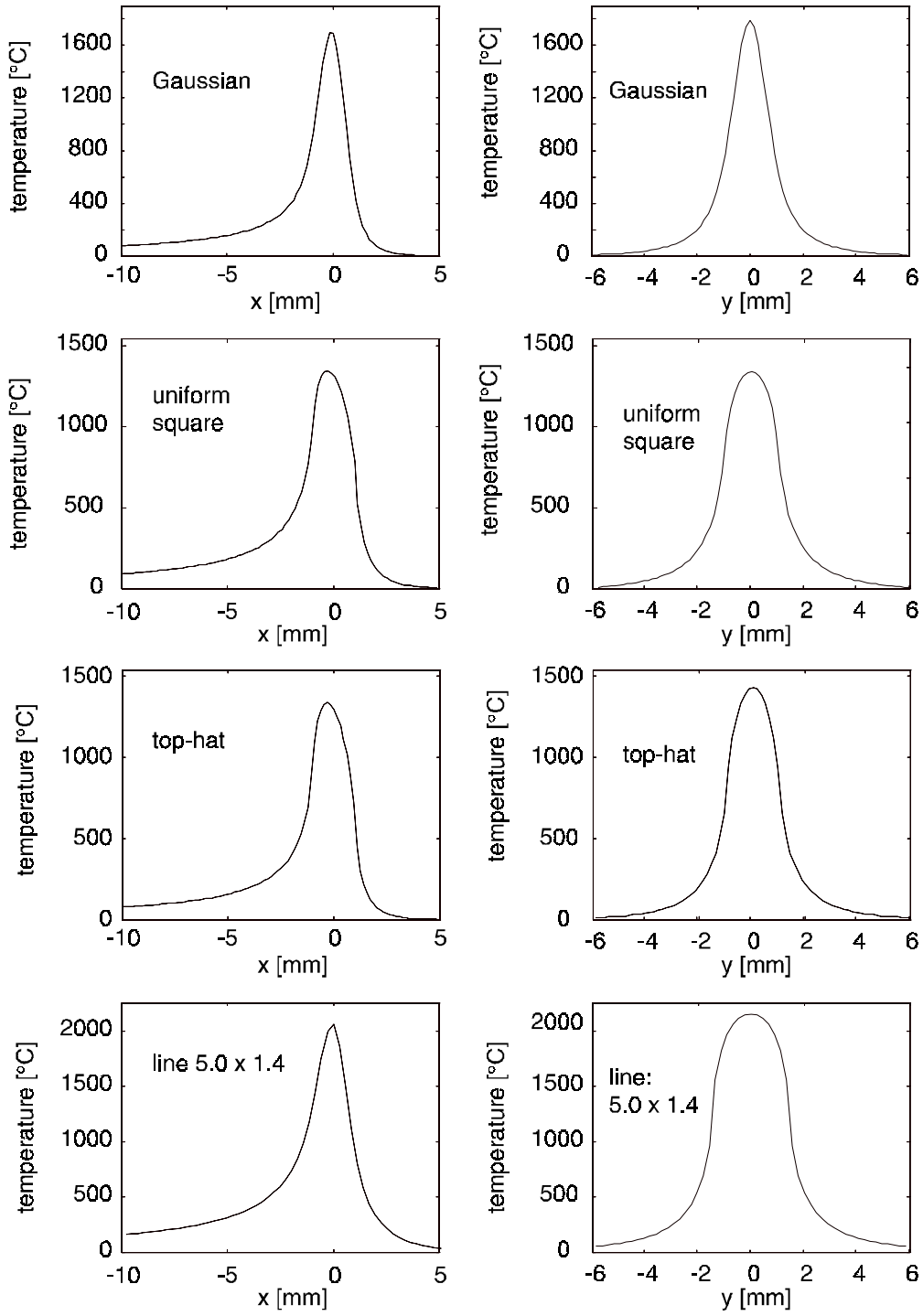

Fig. 3.6 Surface temperature profile along direction of movement and in lateral direction for four different intensity profiles. Material: steel C45. Laser spot area: 7.07 mm^2. Feed rate: 5 mm/s. Absorbed laser power: 300 W.

3.2 Discussion

The model presented in the previous section can predict the effect of an arbitrarily shaped laser beam on the surface temperature, under the assumption that the over-all absorptivity and the material properties remain constant over the effective temperature range. The model was initially intended for use in laser transformation hardening of steel. For this technique, it could accurately predict the resulting hardening depth.

Although under laser cladding conditions phase transformations and fluid flow will occur, which both are not accounted for in the model, the model proved to be useful for laser cladding as well. Due to those two mentioned factors, the model will slightly overestimate the surface temperature.

The usefulness of the model can once more be illustrated with the following example: In chapter 5 it will be concluded that good quality single track clad layers can be achieved with a more or less Gaussian laser beam if the laser power is about 1300 W (absorbed laser power: ~ 400 W, appendix 2), the feed rate is 5 mm/s and the laser spot diameter is 3 mm. In figure 3.6 the resulting surface temperature is shown for a laser power of 300 W. Compared to this power level, the power level of 400 W increases the surface temperature with about 30 % to a maximum of 2100 °C, which is a very reasonable value.

Perhaps more interesting is the opportunity to compare several basic laser beam shapes to each other. Such a comparison showed that a line integrator yields the most uniform temperature distribution over the track width. This finding agrees with the literature.

The achievement of a uniform temperature distribution in one direction, combined with the well defined spot dimensions and, the independency of the applied laser system, explains the development of such a line integrator. That subject is discussed in the following chapter.

Chapter 4

Design and development of a line integrator

The use of beam integrators that transform the initial laser intensity distribution in a homogeneous distribution in either one or two directions, offers two advantages compared to conventional optics that only focus the laser beam. First, a well defined spot size on the surface of the workpiece is attained. This spot is independent of the initial laser beam intensity distribution. Hence, beam integrators allow a reliable exchange of cladding results between different laser systems.
Secondly, a more uniform temperature distribution over the width of a laser scanned track is attained, as was shown in the previous chapter. This is favourable for achieving uniform clad properties over the width of the clad and facilitates the treatment of larger areas by the application of several adjacent tracks.
Beam integration can be achieved in several ways (see section 2.9). However, all methods are based on the same principle. The laser beam is split in a number of smaller beamlets which are recombined for proper overlap in the focal plane.
In the author's laboratory two beam integrators are available. The first one is a two dimensional beam integrator which yields a rectangular laser spot. It is suitable for application at laser powers below 3 kW, because it contains ZnSe

lenses. The second one only performs an integration in the lateral direction. This integrator yields a line shape (~ 0.7 x 8.2 mm^2). It is applicable for very high laser powers, because only reflective mirrors have been applied to fulfil the optical functions.
Both integrators are discussed in the following sections.

4.1 Two dimensional kaleidoscope-type beam integrator

The kaleidoscope type integrator, which has been originally developed for use in laser transformation hardening of steel, consists of an axicon, an oblong box with a highly reflective interior and a rectangular cross-section in which the real integration is achieved, as well as a three lens system to image the attained homogeneous energy distribution on the workpiece (figure 4.1).

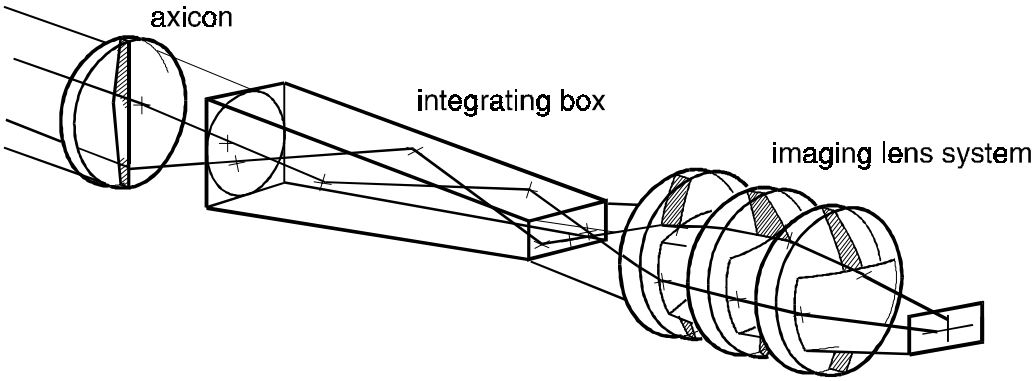

Fig. 4.1 Kaleidoscope-type two dimensional beam integrator.

A laser beam with a non homogeneous intensity distribution, that travels in an enclosed oblong chamber with reflective side walls, has after several reflections a homogeneous distribution. The number of reflections must be kept at a minimum. At each reflection a part of the energy is lost due to absorption at the reflective surface. Too many reflections would not only reduce the laser power on the exit of the integrator, but also increase the thermal load of the system.
The integrating box consists of four gold coated copper plates that together form a pyramid. The larger the tapering of the pyramid, the more internal reflections can be achieved per unit of length. The shape of the box on the exit side can be changed by adjusting the tapering of the plates.
The laser radiation is coupled into the integrating pyramid by means of an axicon. An axicon is a lens-like optical element with a cone shape on one side. This element reduces the beam diameter and, more important, disturbs the

quality of the optical imaging. This deterioration of the optical imaging is necessary to achieve a homogeneous intensity distribution with a minimal number of reflections. In the developed integrator an average of 2.5-3.5 reflections is sufficient. The length of the pyramid is 170 mm.
The imaging lens system is necessary to transpose the energy distribution from the exit of the integrating pyramid to the workpiece. The flexibility of the system is increased by applying a three lens system, which allows three fixed magnifications: 0.7, 1.0 and 1.5.
An example of the homogeneous intensity distribution that is achieved is shown in figure 4.2.

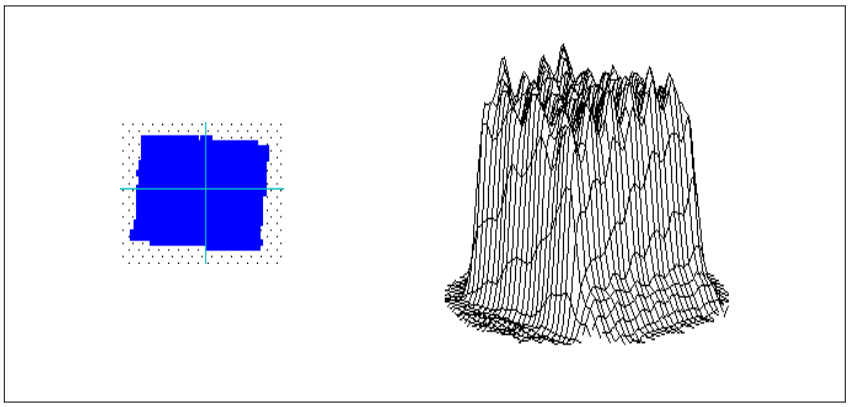

Fig. 4.2 Measured energy distribution in the spot on the workpiece.

The developed kaleidoscope-type integrator has been used successfully in laser transformation hardening of steel. For laser cladding it can not be used. First, during hardening with a highly absorptive coating, only 20-30 % of the incident energy is reflected from the workpiece surface, whereas, in case of laser cladding, this is about 70 %. The integrator can not withstand this amount of energy.
Secondly, the distance between the integrator and the workpiece is only a few centimetres. This complicates the positioning of the powder nozzle and the protection of the ZnSe lens system to spattering powder.
It was therefore decided to develop another beam integrator with a larger distance to the workpiece. This also gives the opportunity to allow the use of CO_2 laser sources with more than 3 kW.

4.2 Optical design line integrator

One of the reasons to apply beam integrators for laser cladding, is to attain a more homogeneous temperature distribution over the width of the tracks. It is sufficient to homogenise the laser beam in the lateral direction only.
The developed line integrator, which is shown schematically in figure 4.3, consists of three parts. All will be discussed in the order in which the laser radiation travels through the system.

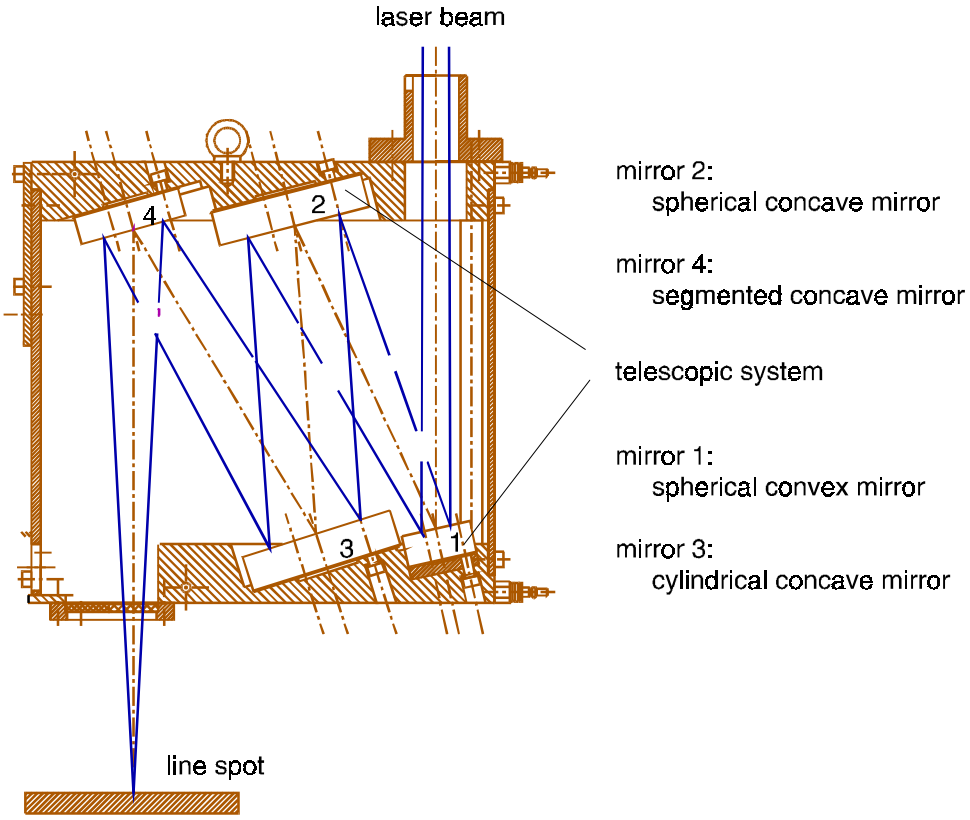

Fig. 4.3 Schematic lay-out of the line integrator.

1. Telescopic system consisting of two spherical mirrors
   The laser beam must be parallel when arriving at the faceted mirror. This is achieved by using a spherical convex mirror and a spherical concave mirror respectively. The system can be adjusted to CO_2 laser sources with a different beam divergence by changing the distance between these two mirrors.
   The second function of the telescopic system is the enlargement of the beam diameter. Firstly, higher laser powers can be utilised, because this reduces the power density on the mirrors. Secondly, the segmented mir-

ror is filled by a larger beam. Hence, more small beamlets can be made which results in a better homogeneity in the line shape.

2. Cylindrical mirror
   The parallel beam is focused in the meridional plane by means of a cylindrical mirror. The curvature of this mirror and the distance to the workpiece determine the spot length in the traverse direction.
3. Segmented mirror
   The final function, i.e. “integration” in the sagital plane is achieved by means of a segmented mirror. This mirror consists of eight segments positioned in mutually different angles. The laser beam is split into several beamlets by this mirror and recombined by overlap in the focal plane. A proper choice of the angles under which the segments are positioned, assures that a spot with a laterally homogeneous energy distribution is attained. The principle of beam integration by means of a segmented mirror is illustrated in figure 4.4.

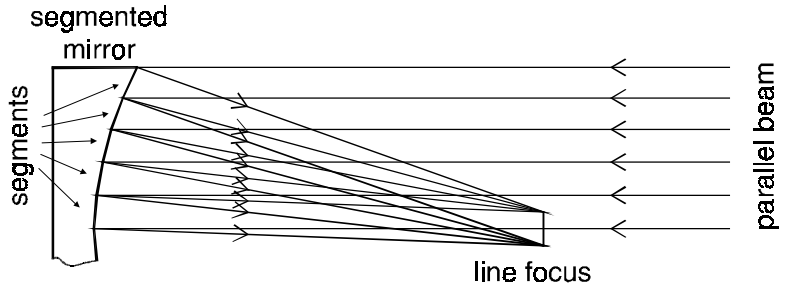

Fig. 4.4 Principle of beam integration by means of a segmented mirror. The parallel laser beam is split into beamlets by the segments and recombined in the focal plane.

The optical system was designed with the computer programme OPDESIGN. This software allows the analysis of optical systems and was developed by Beckmann [1991]. Based on the configuration of an optical system (curvature of optical elements, distance between elements, angle of incidence, wavelength of radiation, etc.) the programme calculates the path of a number of rays through the entire system. The beam shape at the exit of the optical system can be studied in the desired plane of reference.
The cylindrical mirror and the segmented mirror manipulate the beam in different planes. Hence, the spot length and width are decoupled. The goal of the optimisation of the optical system with OPDESIGN is the achievement of a line focus in the sagital plane which position agrees with the focal point in the meridional plane. The line focus has the desired shape, if the aberrations in the sagi-

tal plane form a line with the centre on the optical axis. The length of the line approximates the segment width. The analysis with OPDESIGN has resulted in the optical system which is shown in table 4.1, figure 4.5 and 4.6.

Tab. 4.1 Parameters of the developed line integrator (surface 1: convex spherical mirror; surface 2: concave spherical mirror; surface 3: concave cylindrical mirror; surface 4: segmented mirror with 8 segments).

Surface	radius [dm]	distance to next surface [dm]	tan(tilt of surface)
1	1.86209	-2.16388	-0.22170
2	6.16595	2.00000	0.18534
3	-12.5000	-> toric surface meridional curvature and radius	-0.24008
3	infinite	-> toric surface sagittal curvature and radius	
3		-2.30000	
4	- x -	3.65016	0.27732

segment no.	lower height [dm]	tangent of segment angle
0	0.00000	0.00556
1	0.07500	0.01669
2	0.14999	0.02781
3	0.22497	0.03892

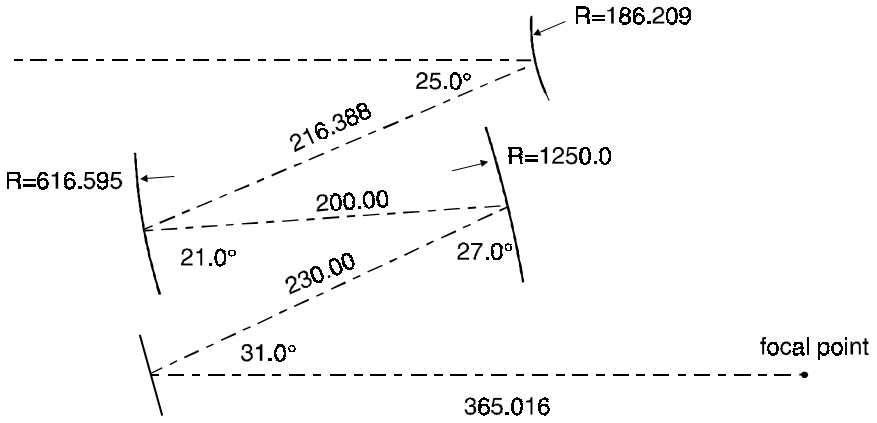

Fig. 4.5 Dimensions [mm] of the line integrator in the meridional plane.

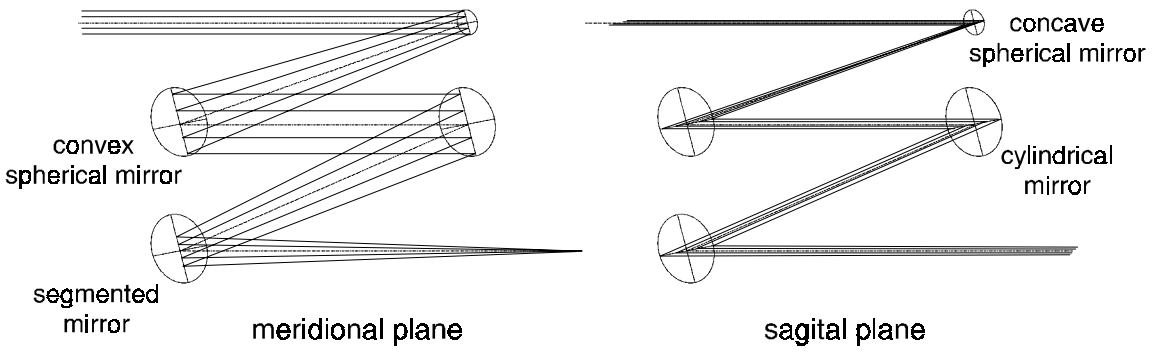

Fig. 4.6 Path of the rays in the line integrator.

The shape of the manipulated laser beam in the focal region can be seen in figure 4.7 and table 4.2. The beam converges in front of the focal point for both the meridional and the sagital directions. The focal point for the sagital direction is positioned 10 mm in front of the focal point of the meridional plane.
The dimensions of the line spot are sensitive to a variation in distance to the workpiece (figure 4.8 and table 4.2). Hence, it is possible to adjust the power density in the line spot. The smallest line spot has an area of 0.3 x 9.1 mm^2, whereas the area at a distance of 10 mm from the meridional focal point amounts to 1.1 x 7.8 mm^2.

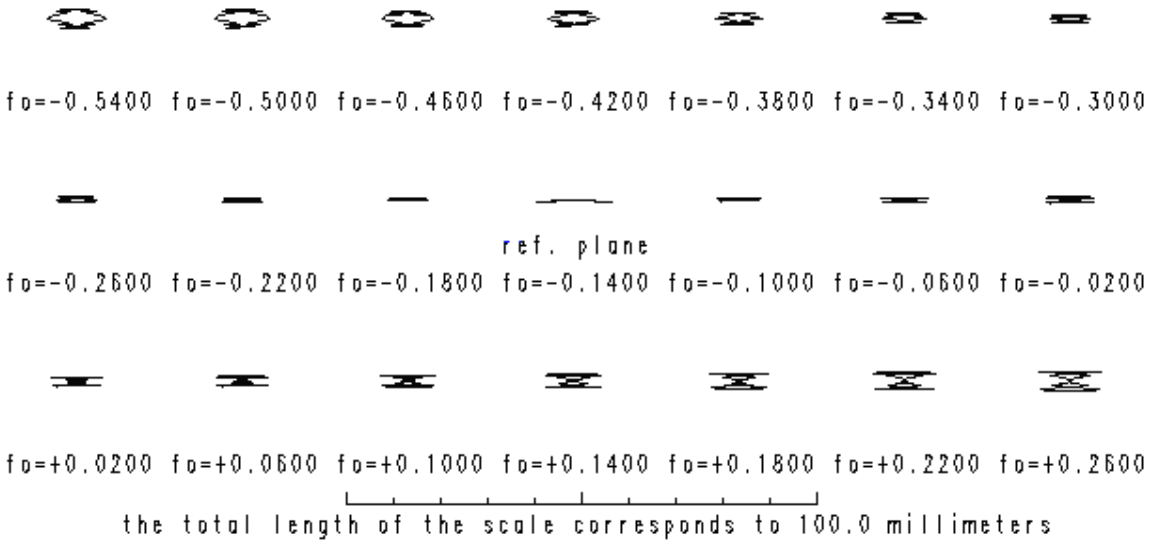

Fig. 4.7 Shape of the line source around the focal point.

Tab. 4.2 Dimensions of the line in the focal region. The focal plane off-set is relative to the focal point in the meridional plane.

focal plane off-set [mm]	meridional dimensions [mm]	sagital dimensions [mm]
-14	1.5	8.3
-10	1.1	7.8
-8	0.9	
-6	0.7	8.2
-4	0.5	
-2	0.4	8.8
0	0.3	9.1
2	0.4	9.4
4	0.5	
6	0.7	10.0

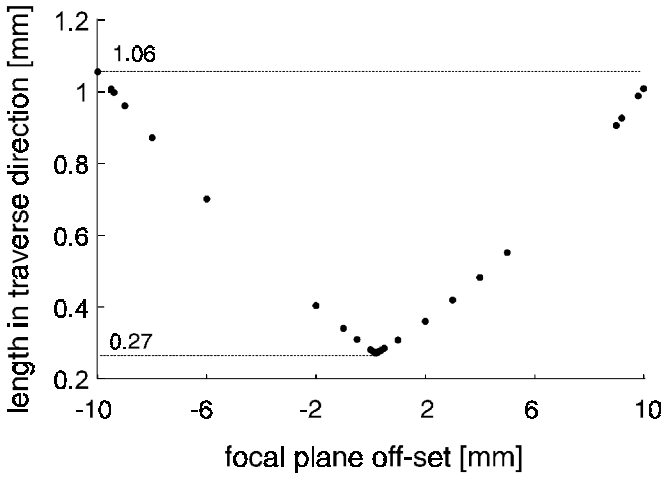

Fig. 4.8 Course of the length of the line shape in the traverse direction around the focal point in the meridional plane.

The results presented so far proceed from calculations based on ray tracing. Apparently, the energy distribution over the line width should be homogeneous. This suggestion has been verified by calculating the energy distribution in the focal plane (figure 4.9). The calculations were performed under the assumption of a Gaussian laser beam. That intensity profile is a worst case situation. Figure 4.9 shows that the attained energy distribution is rather uniform indeed between the sagital focal point and about 10 mm behind it. In the focal point the

two peaks in the energy distribution are less than 10% higher than the average value. At larger distances from the focal point the edge of the line source becomes less well defined.

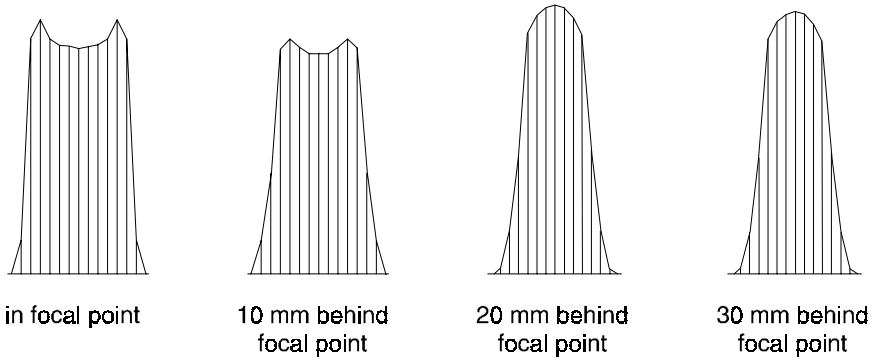

Fig. 4.9 Energy distribution along the line source in the sagital plane around in the focal point in the sagital plane (figures on different scale!).

The calculated laterally homogeneous energy distribution could be confirmed by measurements. The measured distribution is shown in figure 4.10. The peaks that can be noticed are interference patterns. The occurrence of these peaks can be prevented by the intentional introduction of small errors in the segmented mirror. Especially small changes of the angles under which the segments are positioned, are effective [Beckmann, 1995].

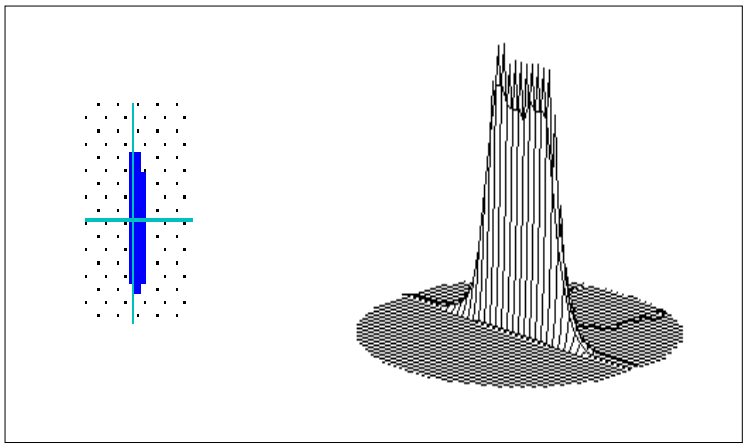

Fig. 4.10 Measured energy distribution in the line spot.

The temperature distribution that is achieved with the obtained line spot is shown in figure 4.11. These temperature distributions were calculated with the

numerical method described in chapter 3. The calculations were performed for three different line dimensions that all have a homogeneous energy distribution in the lateral direction: 0.3 x 9.1 mm^2 (smallest area), 0.6 x 8.3 mm^2 (average) and 1.1 x 7.8 mm^2 (largest area). The distribution in the other direction was assumed to be Gaussian. As can be seen, the attained temperature distribution over the line width is quite constant for all three line shapes. The temperature on the surface can be varied with a factor two by only changing the distance between integrator and workpiece.

The maximum temperatures that are attained according to figure 4.11 are quite low. Depending on the applied line configuration they vary between 1148 and 2421 °C. This is due to the low absorption of laser energy in the base material with this line integrator. When applying the laser system's maximum output power of 1800 W, surprisingly only 8 % of the supplied laser energy is effectively coupled into the irradiated material. Due to this low energy efficiency no melt pool could be formed. Therefore, this line integrator could not be used for laser cladding in the author's laboratory. The experiments on laser cladding with preplaced powder and powder injection that are discussed in the following chapters are therefore performed with ordinary optics.

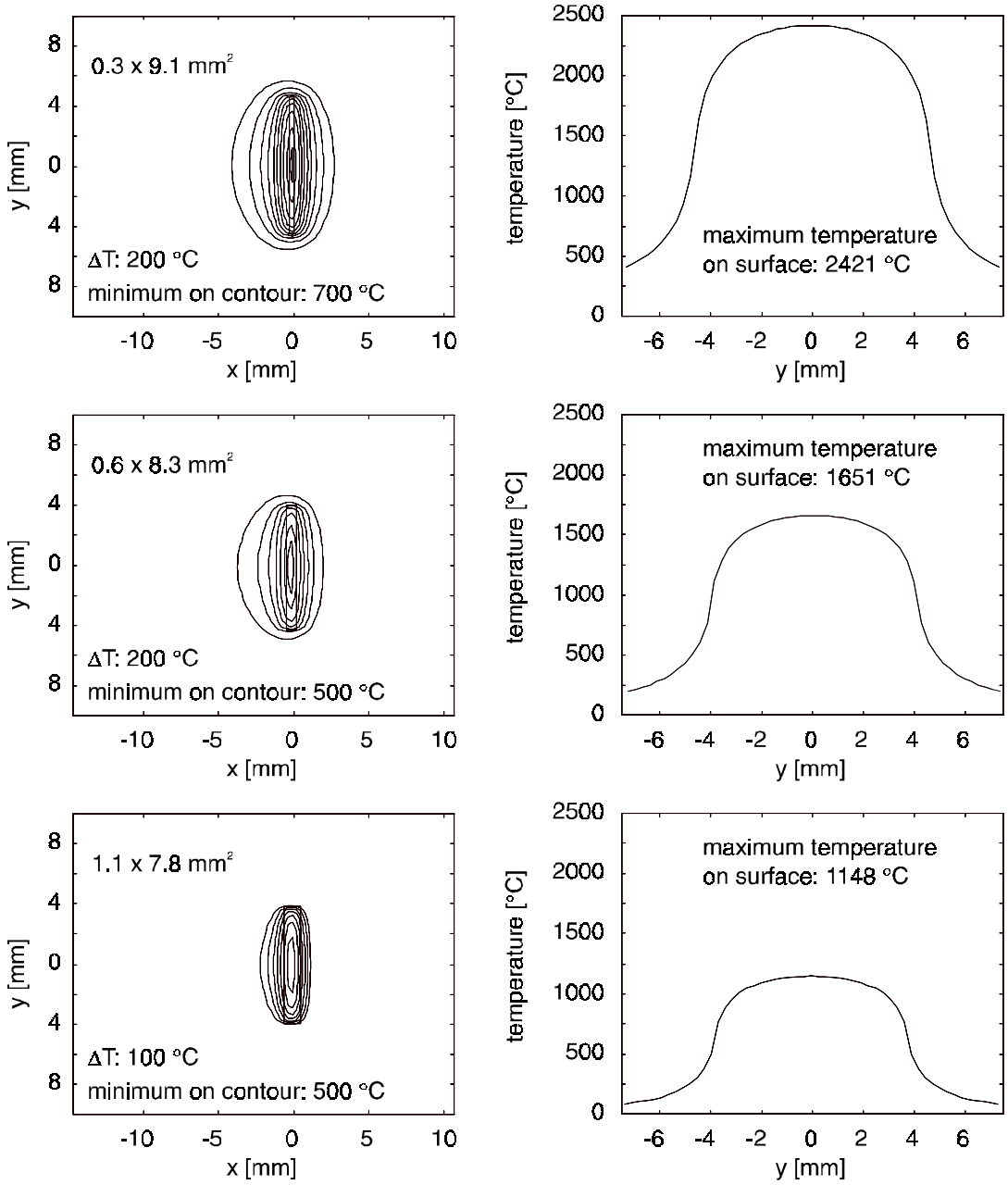

Fig. 4.11 Temperature distributions for three different line shapes. Left: temperature contours on surface; Right: temperature distribution along line width; Material: C45; Absorbed laser power: 150 W; Feed rate: 5 mm/s.

Chapter 5

Laser cladding with preplaced powder

5.1 Experimental set-up

The literature research (chapter 2) showed that laser cladding is predominantly performed for achieving wear and corrosion resistant layers on top of steel substrates that are exposed to temperatures over 200 °C. Examples are gas turbine blades, valve seats and hot working tools such as dies and inserts.
Suitable coating materials are mixtures based on cobalt, chromium and nickel.
Following this tendency, a cobalt base alloy, Metco 18C, has been applied in the experiments presented in this chapter. This material (appendix 1) is a cobalt based alloy which has a good hardness as well as an enhanced wear and corrosion resistance at elevated temperatures. Examples of applications as mentioned by the supplier of the powder are valves and valve seats in combustion engines, gas turbines blades and inserts. The maximum operating temperature can be quite high: 800 °C.
The selected base material, X32CrMoV3 3 (appendix 1), is a hot working tool steel. It is resistant to a large variation in temperature and suitable for applications such as dies and inserts.
Slots with a depth of 0.4 mm were made in samples with a thickness of 10 mm. Subsequently, the surface was degreased with ethanol. The preplaced powder

was applied as a paste. That paste consisted of a chemical binder (Nicrobraz type II), ethanol and Metco 18C. After letting the ethanol evaporate for 24 hours, a dry powder layer is attained that adheres to the base material. The use of a chemical binder prevents the powder from being blown away by the shielding gas during processing.
The goal of the experiments was to achieve good quality clad layers. In this context, a good quality clad layer means no cracks, no porosity, a good bonding to the substrate and a low dilution of coating material by the substrate.
Single track clad layers were produced. Larger areas were treated as well by applying several adjacent tracks. Several machining parameters were varied. Those parameters include the feed rate, the laser power and the initial workpiece temperature.
Argon was supplied to the processing area to prevent the clad layers from oxidation and to protect the optical system. The experimental set-up is shown in figure 5.1.
The laser beam diameter was measured by means of a Prometec UFF 100 laser beam analyser. The processing area was positioned below the focal point of the applied 95 mm ZnSe lens. The spot diameter was 3.0 mm. Energy loss due to absorption of laser energy in optical elements (deflecting mirror and ZnSe lens) was accounted for. Hence, all denoted powers are net powers on the workpiece. The laser power supplied by the Rofin Sinar 1700RF CO_2 laser was measured with an accuracy of 5%.

5.2 Experimental results

The performed experiments and their results are denoted in appendix 3. In this section some general findings are presented.

Single tracks

A variation of the laser power from 600 W to 1350 W in steps of 50 W (experiments 1-15 appendix 3) showed that a minimum power of 1150 W is required to achieve a smooth single track that is flown out over the substrate. Lower power levels result in the formation of clad layers that are not smooth, narrow or even winding. Those poor clads can be higher than the thickness of the applied coating and do not have a fusion bond to the substrate. Figure 5.2 shows that the clad height decreases with the laser power.

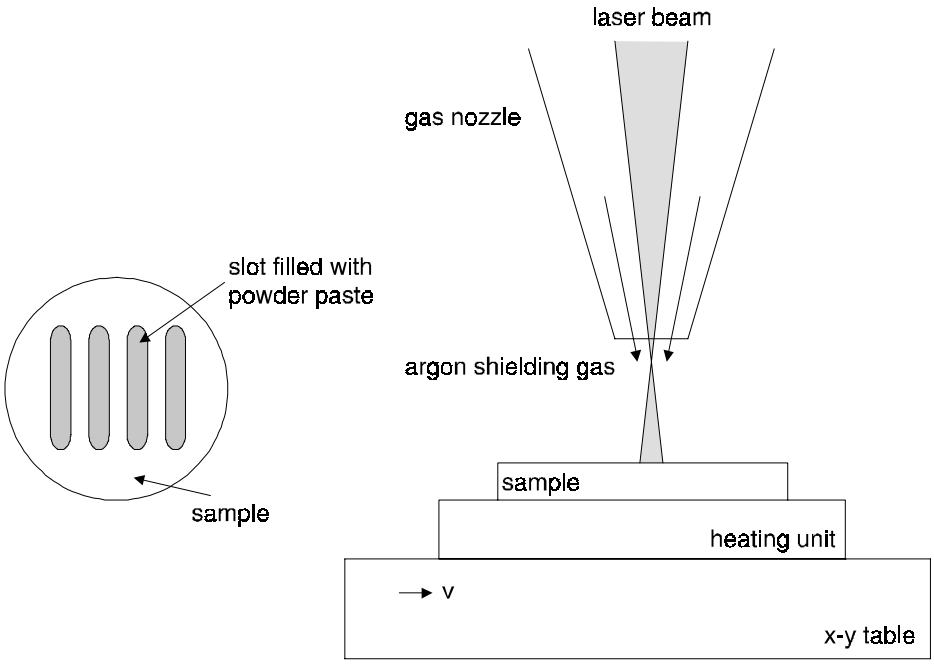

Fig. 5.1 Experimental set-up laser cladding with preplaced powder.

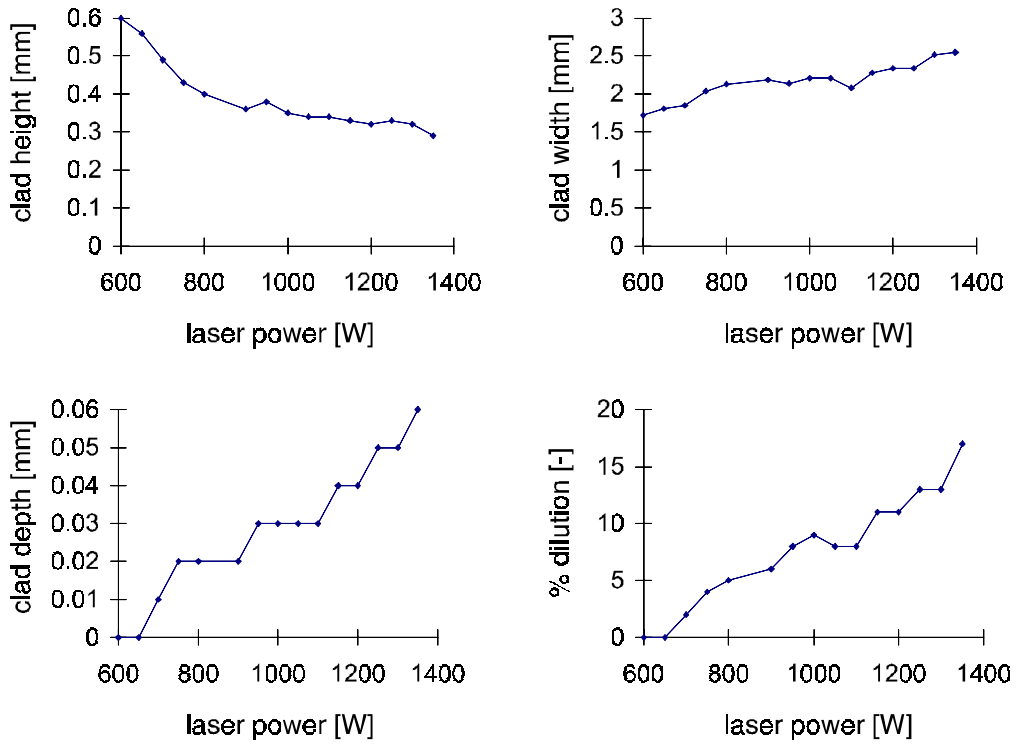

Fig. 5.2 Clad dimensions as function of the laser power.

The clad width is limited to about 2.5 mm, whereas the applied laser spot diameter was 3.0 mm. It increases with an increase of the laser power. So do the clad depth and the dilution. The minimal dilution that must be allowed to achieve smooth clad layers is about 11 %.
The effect of the feed rate on the single track clad dimensions is shown in figure 5.3. The clad height increases with the feed rate, whereas the clad width, depth and dilution decrease (experiments 16-21, appendix 3).
The clads attained at 12 and 24 mm/s are not satisfactory. As was the case with too low power levels, these clads are narrow and winding and do not have a smooth surface. In these series, the experiments performed at 8 and 6 mm/s resulted in an acceptable dilution of respectively 5 and 8 %. A further reduction of the feed rate to 4 and 3 mm/s led to a further increase of the dilution.

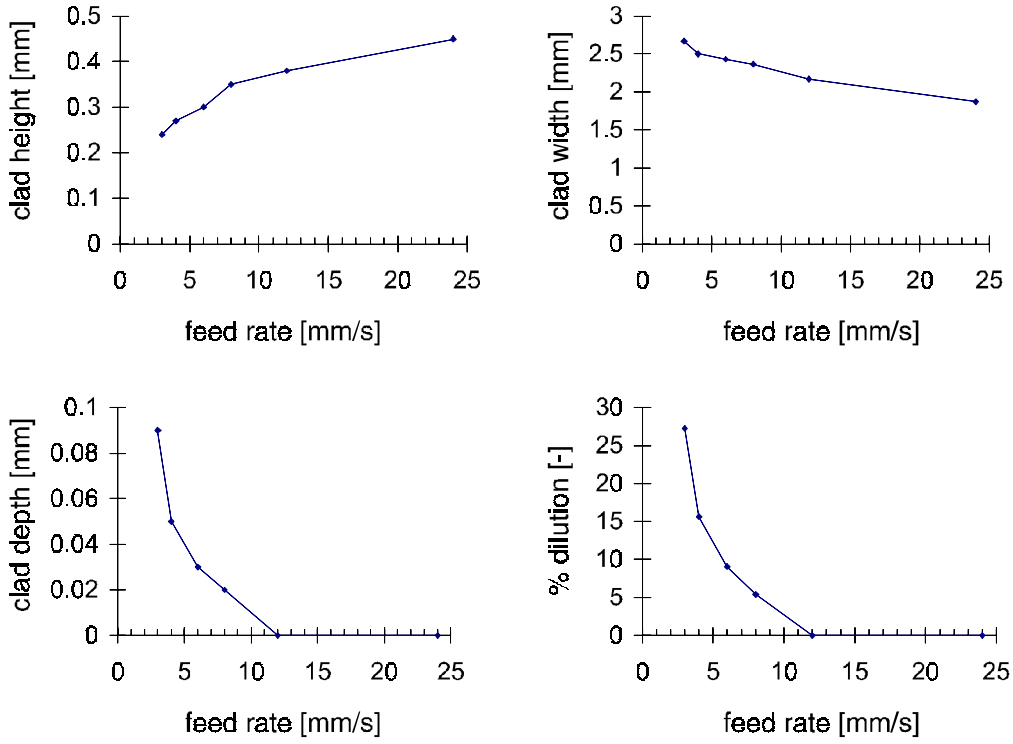

Fig. 5.3 Clad dimensions as function of the feed rate.

Figure 5.4 and 5.5 show examples of a poor clad cross-section and a good one. In the first figure the laser power was insufficient in order to melt the substrate. Only the preplaced coating could be molten. The clad layer in the other figure has been flown out over the substrate, whereas the clad depth and dilution remain small. The area that can be noticed directly below the clad is the heat af-

fected zone of the substrate. In this area the initial microstructure has been transformed to martensite. This structure is much harder (~ 800 Hv versus ~ 500 Hv in the clad) than the clad material and the initial microstructure. This can be deducted from the hardness measurement imprints.

Fig. 5.4 Example of a clad that did not flow out over the substrate.

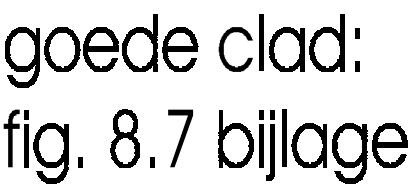

Fig. 5.5 Example of a good quality clad.

Figure 5.6 (left) shows the measured chemical composition in a good clad with a low dilution. As can be seen from this graph, the transition from the substrate to the coating material occurs within 20 µm. The cobalt content in the clad av-

erages 40 %, which agrees well with the 40.8 wt% cobalt in the coating powder Metco 18C (appendix 1). The transition from clad to substrate is shown in figure 5.6 (right).
Cracking of single track clads, produced with the material combination described here, can be prevented by a proper selection of machining parameters without preheating. If the clad flows out sufficiently over the substrate, cracking can not be observed.

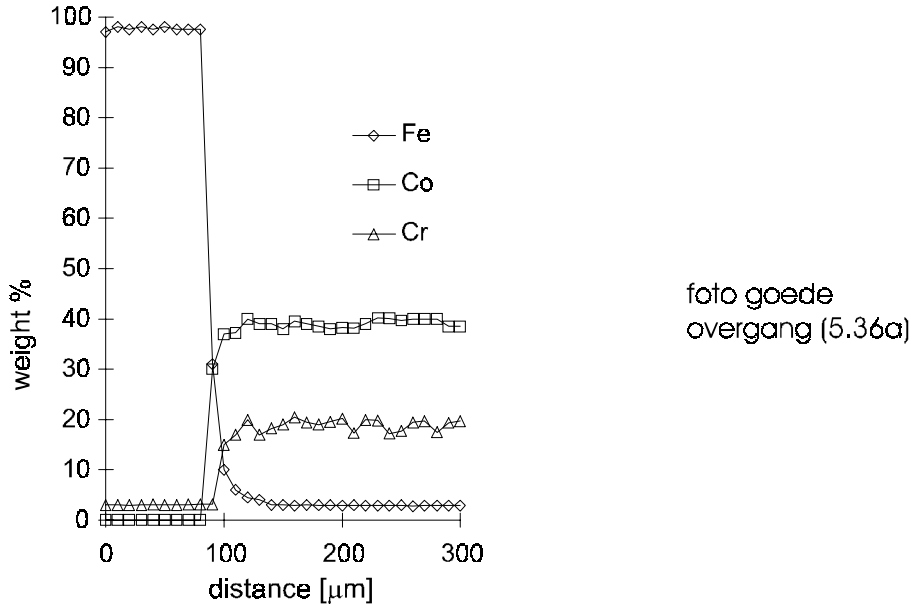

Fig. 5.6 Left: Material composition on the transition from clad layer to substrate (dilution: 4 %). Right: Corresponding picture of the transition zone.

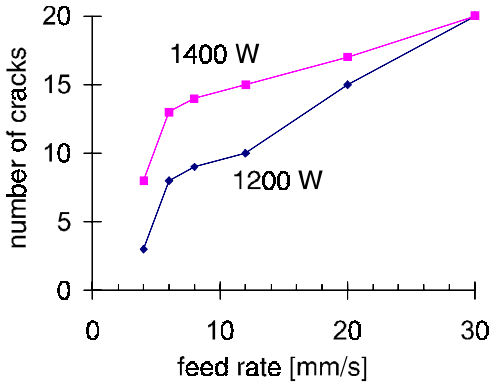

Fig. 5.7 Number of cracks in single track clads with a length of 40 mm produced on a hardened substrate for two laser powers.

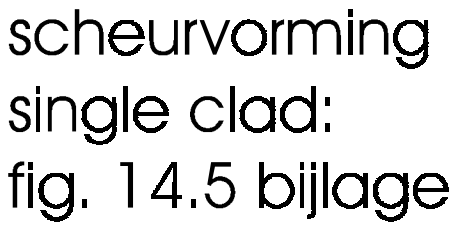

Fig. 5.8 Cracks in single track clads on a hardened substrate.

A few experiments (nr. 148-159) were performed on cladding single tracks on a hardened substrate. All these clads suffered from cracking in the transverse direction (figure 5.8). The number of cracks increases with the feed rate and the laser power (figure 5.7). Experiments on a non hardened substrate under otherwise identical conditions did not result in cracking.

Summary
Good quality single track clad layers can be obtained by making single tracks. Porosity was virtually non-existent in flown out clads, in spite of the presence of a chemical binder. Cracking is affected by the heat treatment to which the substrate has been submitted to before the laser treatment. Cracking can not be prevented when applying a hardened substrate, but can be controlled with "normal" substrates.
Good quality low dilution clads were attained with the following parameter setting:

laser power: 1200-1400 W
feed rate: 4-6 mm/s

Cladding of larger areas with overlapping tracks
Larger areas can be clad by the application of several partly overlapping tracks. The substrate is heated by each subsequent track. Therefore, the melt depth

increases with each new track. This can be prevented by a simultaneous reduction of the laser power. However, in order to attain minimum processing times, it is more practical to increase the feed rate to 12 mm/s. The poor surface quality and increased cracking tendency associated with this high feed rate, can be prevented by applying a rather large overlap between the subsequent tracks: 80 %. Furthermore, it is necessary to apply the tracks continuously in a meander shaped pattern with a maximum track length of 15 mm. The substrate remaines warm enough between each subsequent pass to reduce the cooling rates in the clad so as to limit the number of cracks. Preheating to 200 °C has proven to be helpful, although crack-free areas could not be attained. Higher preheating temperatures are not possible, because that causes evaporation of the chemical binder.
Figure 5.9 shows the cross-section of an area that was clad by means of overlapping tracks. The overlapping pattern can be recognised from the material structure in the substrate. Some deep cracks can be seen. Figure 5.10 shows the cracking pattern in several clads.

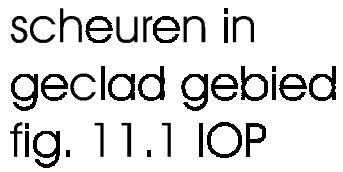

Fig. 5.10 Cracking pattern in clad areas produced by overlapping tracks.

Effect of substrate temperature and preheating
Both the coating material and a thin layer of the substrate must melt to attain a well bonded clad layer without dilution. The main part of the absorbed laser

Fig. 5.9 Clad with several cracks produced by means of overlapping tracks.

power is required for the heating of the substrate, as is shown with the following example:
A clad experiment performed with a laser power of 1300 W and a feed rate of 5 mm/s results in the formation of a clad with a width of 2.3 mm and a height of 0.3 mm. The melting of the preplaced powder requires 30 W.
The absorptivity of energy during cladding with preplaced powder averages 30 % (appendix 2). Hence, slightly less than 400 W is absorbed. This implies that in this particular case only 7.5 % of the absorbed energy is used for melting of the coating material. The remaining part of the absorbed energy contributes to the formation of a melt pool in the substrate and to the heating of the surrounding material.
The temperature of the surrounding material seems to be an important parameter in the laser cladding process. One of the requirements for achieving a good quality clad layer is the possibility for the coating material to flow over the substrate. That flowing behaviour is enhanced by a temperature increase of the substrate. One of the ways to achieve such a temperature increase is the supply of more energy to the substrate during the process.
The effect of a variation of the laser power on the flowing behaviour of the clad layer is illustrated in figure 5.11 and table 5.1 (experiment 83-87, appendix 3).
At 800 W enough laser power is available in order to melt the preplaced powder. However, the substrate did not melt. As a result of this, the coating material formed a droplet on the substrate during solidification.
At 1050 W, a thin layer of the substrate did melt. A good bonding between coating and base material was achieved and the clad layer was able to flow. At higher power levels (1300, 1500, 1800 W) this flowing behaviour was enhanced. However, this also resulted in an increase of the melting depth.

Another way to increase the temperature of the substrate is preheating. As can be seen in figure 5.12 and table 5.2, an increase of the substrate temperature results in the formation of a wider clad layer. At the same time, the clad height decreases and the melt depth increases.

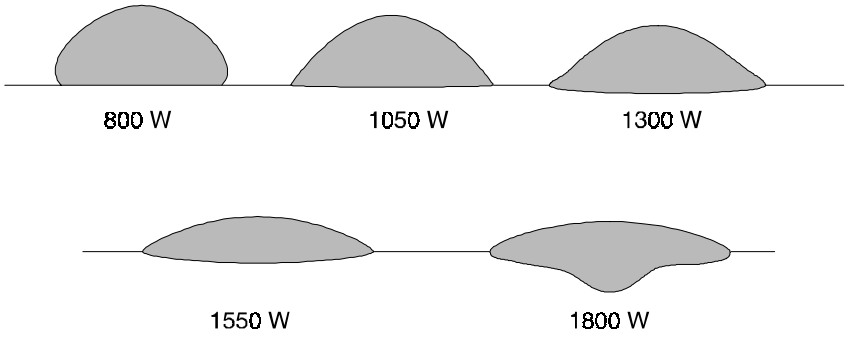

Fig. 5.11 Typical cross-sections of clad layers produced by means of the preplaced powder method (feed rate: 5 mm/s; coating thickness: 0.8 mm).

Tab. 5.1 Dimensions of the cross-sections shown in figure 5.11.

laser power [W]	**clad width** w_c [mm]	**clad height** h_c [mm]	**melt depth** d_c [mm]
800	1.89	0.94	0.00
1050	2.37	0.82	0.02
1300	2.55	0.71	0.09
1550	2.71	0.41	0.13
1800	2.82	0.35	0.47

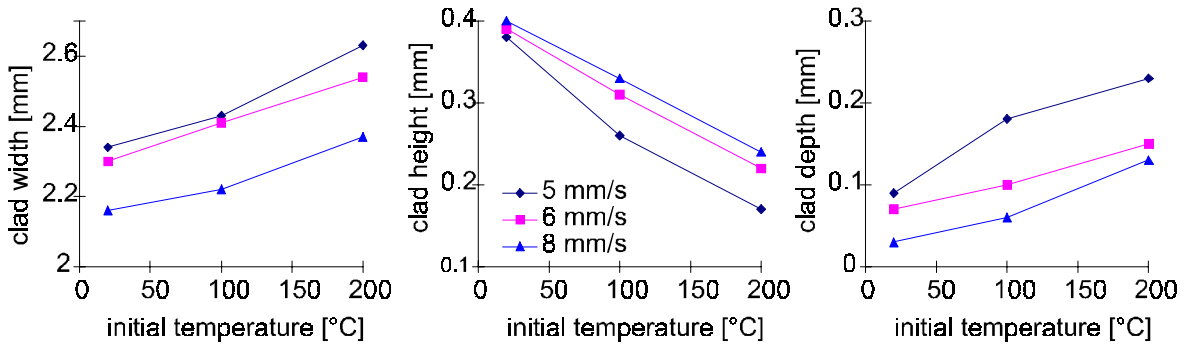

Fig. 5.12 Effect of preheating and feed rate on clad layer geometry in case of laser cladding of single tracks with preplaced powder (laser power: 1400 W).

Tab. 5.2 Effect of preheating on clad geometry and longitudinal stress in case of cladding single tracks. Laser power: 1400 W.

	initial temperature [°C]	**w_c** [mm]	**h_c** [mm]	**d_c** [mm]	**longitudinal residual stress** [MPa]
5 mm/s	20	2.34	0.38	0.09	
	100	2.43	0.26	0.18	
	200	2.63	0.17	0.23	
6 mm/s	20	2.30	0.39	0.07	
	100	2.41	0.31	0.10	
	200	2.54	0.22	0.15	
8 mm/s	20	2.16	0.40	0.03	515
	100	2.22	0.33	0.06	444
	200	2.37	0.24	0.13	380

Figure 5.12 also shows the effect of the feed rate on the clad geometry. As the feed rate increases, the energy input in the substrate is diminished. Hence, the clad width and the clad depth decrease, whereas the clad height increases.
The preheating of the samples has another, positive, effect on the clad layer quality. It reduces the cooling rate and, therefore, reduces the residual tensile stress in the clad layer as well. This reduction of the tensile stress contributes to the formation of crack-free clad layers and can improve the wear properties of the applied coating.
Table 5.2 shows this effect of preheating on the residual stress in a single track clad layer. As can be noticed, the residual stress decreases as a result of an increase of the initial substrate temperature. Higher preheating temperatures than those applied, were not possible, because of the evaporation of the chemical binder in the preplaced powder paste.
The magnitude of the residual stress is related to the number of cracks in the clad layer. Figure 5.13 shows that the tensile stress in the surface layer reduces with an increasing number of cracks by relaxation (details in appendix 3, experiments O8-O35).

Effect of dilution on clad quality

The effect of the dilution on the clad quality can be illustrated with figure 5.14. This figure shows three clad layers, each with a different clad geometry.

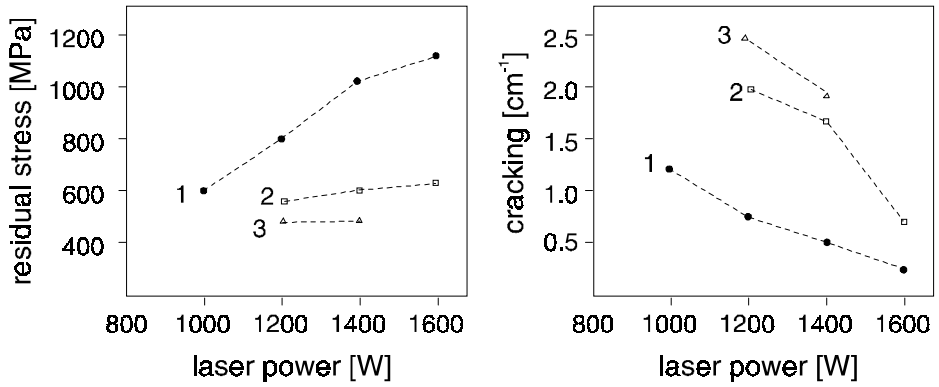

Fig. 5.13 Effect of laser power on residual stress (left) and number of cracks per cm in case of laser cladding with preplaced power with overlapping tracks (series 1: feed rate: 6 mm/s; overlap: 2.4 mm; series 2: feed rate: 8 mm/s; overlap: 1.8 mm; series 3: feed rate: 12 mm/s; overlap: 1.8 mm).

Based on the geometrical approach, the dilution in these clad layers varies from less than 5 % (figure 6.14 top) to 15 % (middle) to more than 40 % (bottom). The effect of this dilution on the associated hardness distribution in the clad layer cross-section is clear. That hardness varies from about 550 to 950 to 450 Hv respectively. The hardness of 550 Hv that is achieved in the almost undiluted clad layer is in accordance with the intrinsic hardness of the applied coating material.

The enhancement of the hardness to 950 Hv, which is associated with an increased dilution of 15 %, is caused by the formation of metastable metal-carbides in the clad layer. The carbon that is required for the formation of those hard phases is supplied by the molten substrate.

A further increase of the melting depth and the dilution leads to a reduction of the hardness. The hardness is still higher than that of the substrate, but lower than the hardness in the pure coating.

This particular case shows that the presence of some dilution can have a favourable effect on the properties of the clad layer. However, it is only possible to take full advantage of such mechanisms by having a solid understanding of all metallurgical aspects involved and by being able to control the process.

It can be useful to measure the dilution by means of the chemical composition on several positions in a clad layer cross-section. This is especially true if a non-homogeneous mixing between elements from the substrate and elements from the coating material is achieved. The occurrence of such an inhomogene-

ous mixing of elements was found indeed during the cladding of an area by means of overlapping tracks (figure 5.15).

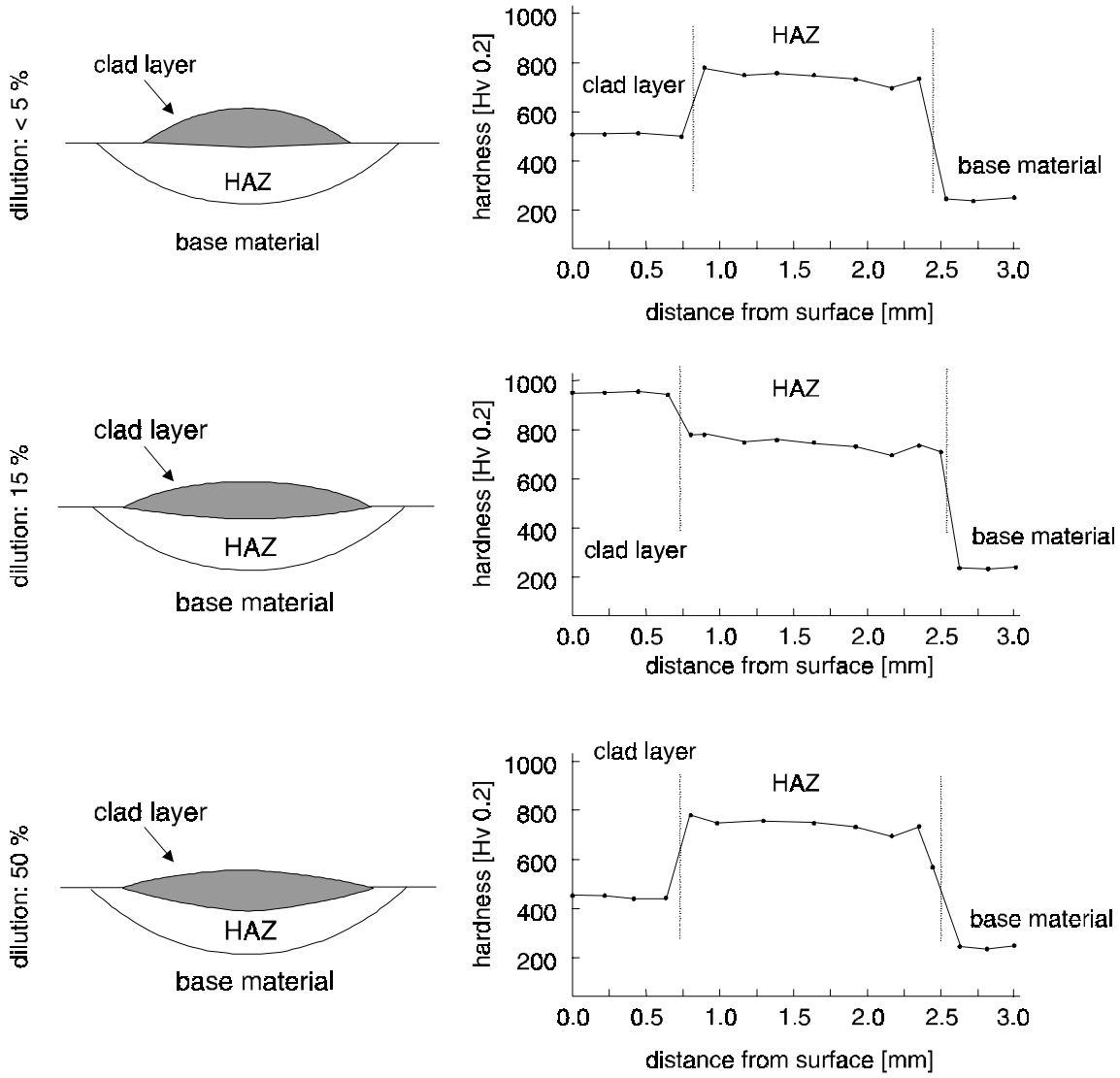

Fig. 5.14 Effect of dilution on hardness distribution in a clad layer.

The resulting clad geometry and the different zones that can be distinguished in the surface layer are shown in figure 5.15. Different material phases can be found in each zone. The composition of these phases is given in table 5.3. The microstructure of the various regions is shown in figure 5.16.

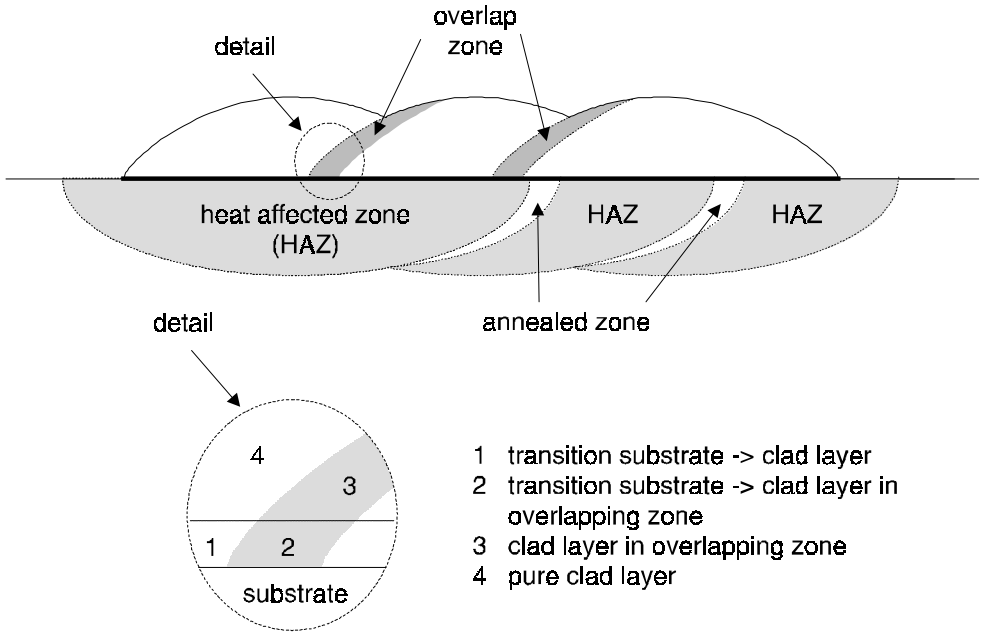

Fig. 5.15 Zones in surface layer achieved by applying several overlapping tracks by laser cladding with preplaced powder.

Tab. 5.3 Material composition of the different phases (wt %) in the clad layer.

phase	Fe	Co	Cr	Mo	Ni	Si	V
1-d	59.5	17.9	7.5	0.4	14.0	0.3	0.3
1-e	55.5	18.8	11.5	2.5	11.4	0.0	0.3
2-p	37.6	15.6	22.6	13.5	9.6	0.0	1.2
3-m	30.9	30.3	11.7	2.6	23.0	1.1	0.4
3-p	24.8	23.1	25.6	12.0	12.9	0.8	0.9
4-m	6.6	40.4	16.8	4.0	30.3	1.6	0.4
4-lp	6.4	35.4	43.4	3.1	11.5	0.0	0.2
4-rp	11.0	21.5	44.7	14.8	8.0	0.0	0.0
4-np	15.0	37.3	14.8	5.7	26.1	0.9	0.3

d: dendritic; e: eutectic; p: precipitates; m: matrix; rp: rectangular precipitates; lp: lamellar precipitates; nd: needle shaped parts

A part of the clad layer is remelted during the application of the next track. The material composition in this overlapping zone (regions 2 and 3) differs from the other parts of the clad layer (regions 1 and 4). Most remarkable is the very large ferrite content in the overlapping zone. The ferrite content in the coating mate-

rial is only 3 %. Hence, an extensive mixing with the base material in that region has occurred. The ferrite content in the metal matrix of the unaffected clad layer (region 4) is less than 7 %. Therefore, the over-all dilution is not very large. This conclusion is supported by the high cobalt content in the clad layer which almost equals the value of 40 % of an undiluted clad layer. Although the average dilution is low, the observed local regions with severe dilution can deteriorate the surface properties of the entire surface layer.

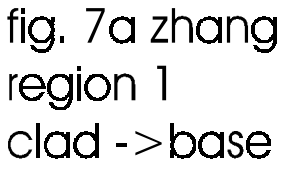

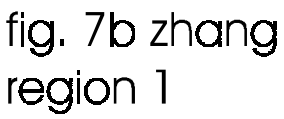

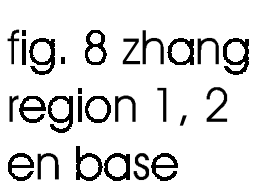

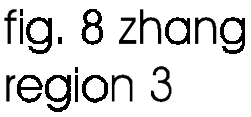

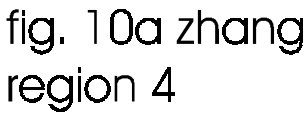

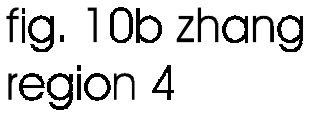

Fig. 5.16 Microstructure in the various regions. Top left: transition substrate-clad; Top right: region 1; Middle left: region 1, 2 and substrate; Middle right: region 3; Bottom left: region 4 needle phase and square precipitates; Bottom right: plate precipitates and square precipitates.

Chapter 6

Laser cladding with powder injection

6.1 Experiments

Powder Metco 18C (properties in appendix 1) was applied as cladding material. Metco 18C was selected because it was also applied in laser cladding with pre-placed powder (chapter 5). It was supplied to the melt pool by means of a powder nozzle with a diameter of 2.0 mm.
The substrate is steel X32CrMoV33 (material properties in appendix 1). It was polished and degreased.
In total 54 experiments were performed. During each experiment fifteen adjacent, partly overlapping tracks were applied with a pitch of 1.0 mm and a beam diameter of 3.0 mm. The varied process parameters are shown in table 6.1.
The combination of laser power and feed rate required to accomplish the desired specific energy level (equation 2.1) is shown in table 6.2.
The experiments (set-up in figure 6.1) were performed with argon as shielding gas for the protection of the workpiece to oxidation as well as carrier gas for the injected powder. The focal length of the applied ZnSe lens is 95 mm. The powder injection angle was measured with respect to the horizontal.

Tab. 6.1 Varied process parameters.

powder feed rate:	75 - 150 mg/s
feed rate:	3 - 5 - 7 mm/s
specific energy:	50 - 60 - 70 J/mm^2
powder injection angle:	30 - 45 - 60°

Tab. 6.2 Required laser power for obtaining a certain specific energy level with a given feed rate.

	feed rate [mm/s]		
specific energy [J/mm^2]	**3**	**5**	**7**
50	450 W	750 W	1050 W
60	540 W	900 W	1260 W
70	630 W	1050 W	1470 W

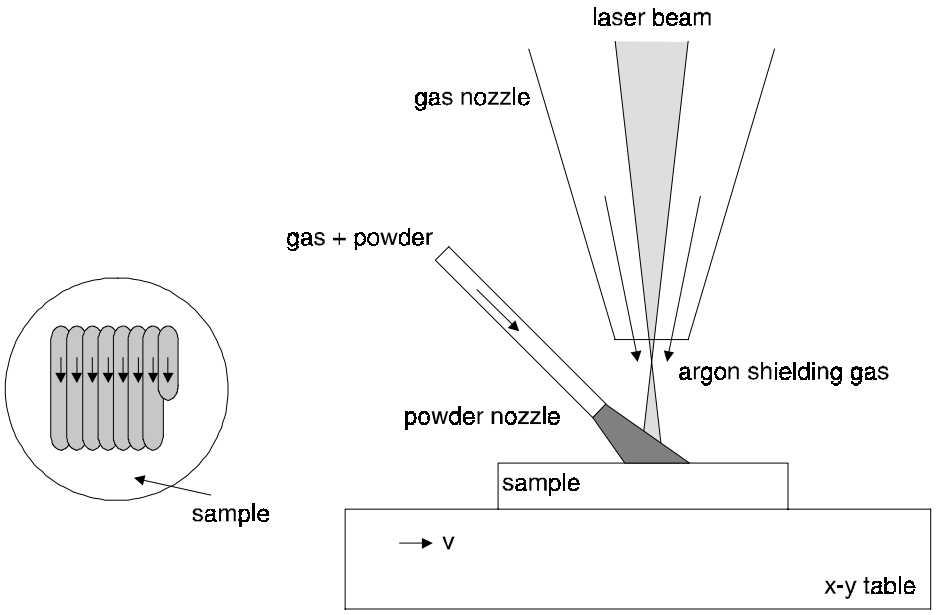

Fig. 6.1 Experimental set-up laser cladding with powder injection.

The experimental results are shown in the following tables.

The specific energy is not a good parameter to characterise the laser cladding process with. This is shown by, for instance, the experiment combination 7-16-25. These three experiments were performed with a specific energy of 70 J/mm^2. Nevertheless, the clad results are quite different due to the different combinations of laser power and feed rate and the consequently different temperature cycles. Experiment 7 (3 mm/s) yields a very thick (~ 4 mm) layer on the substrate that has no fusion bond to it and shows a lot of porosity and a capricious shape. Experiment 16 (5 mm/s) results in a good quality clad layer, whereas experiment 25 (7 mm/s) yields a thin layer (< 0.1 mm) that merely consists of molten base material.
Therefore, it was concluded that the specific energy alone is not sufficient to characterise cladding results. As a consequence, the results will be discussed by using the combination of laser power and feed rate.
The results show that the only parameter combinations that result in proper clads are laser powers of 900 and 1050 W with a feed rate of 5 mm/s and a powder feed rate of 75 mg/s (experiment 13-18). No satisfactory clads could be achieved with the higher powder feed rate of 150 mg/s. The experiments 1-12 (450-750 W) result in very thick, not bonded layers, whereas experiments 22-27 (1260-1470 W) do not yield clads at all.
Figure 6.2 shows the effect of the powder injection angle on the clad height. An increase of the powder injection angle results in higher clads, but also in a reduced surface quality. The powder injection angle must be limited to 45°.

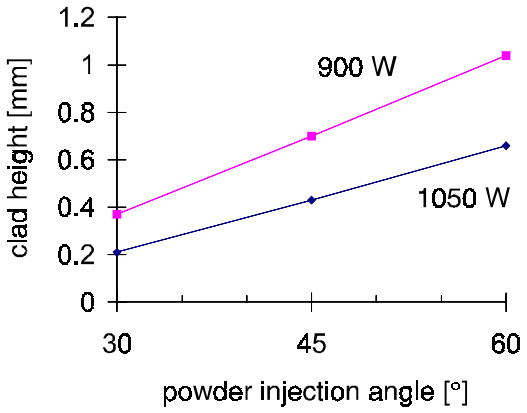

Fig. 6.2 Clad height as function of powder injection angle (feed rate: 5 mm/s; 900 W: experiment 13-14-15; 1050 W: experiment 16-17-18).

During the experiments some glowing powder particles have been noticed. Those glowing particles move away from the melt pool area. That means that

only particles that have ricocheted from the substrate (figure 6.3) are exposed to laser radiation long enough to start glowing in this particular set-up. The temperature rise that particles can experience is discussed in detail in section 6.2.

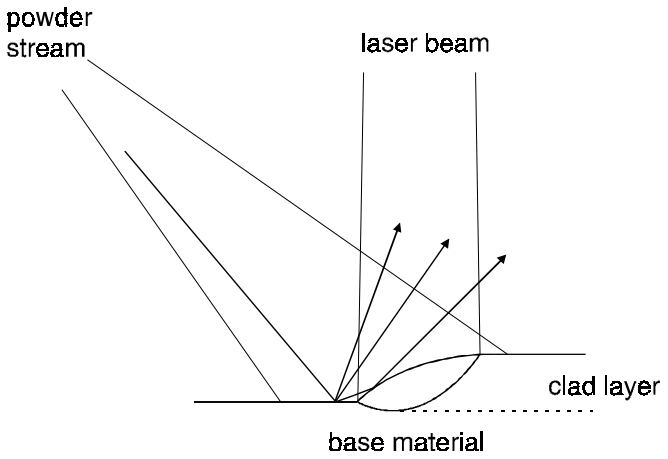

Fig. 6.3 Particles that are not caught in the melt pool ricochet on the surface.

Another phenomenon was observed during some experiments that were performed with a feed rate of 7 mm/s and a laser power of 1260 and 1470 W: the formation of a plasma. This plasma shielded the substrate from the laser beam and stopped the cladding process. Plasma formation was found to be dependent on the powder feed rate: the plasma occurs more frequently at the higher powder feed rate of 150 mg/s.
Since the formation of a plasma during laser cladding is unacceptable, this phenomenon was studied in more detail. This subject is dealt with in section 6.3.
The experiments showed the effect of the substrate temperature on the clad layer formation. Many clad layers did not start to built up immediately, but started only after a few passes of the laser beam. In that case, the laser power was too low to melt the substrate instantaneously. The first few passes of the laser beam only heat the substrate, so that after several tracks the available laser power is finally sufficient as to produce a narrow melt pool in which powder particles can be trapped.
The poor clads that were obtained with a powder feed rate of 150 mg/s all have the same typical shape (figure 6.4). The first few tracks, a relatively high lump with no bonding to the substrate was built on the substrate. These tracks pass into a layer with a constant thickness and a strong fusion bonding.

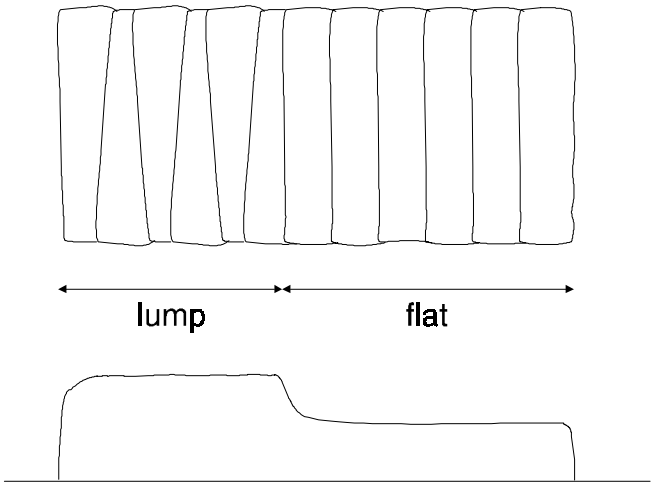

Fig. 6.4 Shape of poor quality clads. The first few tracks are higher (~ 2.5 mm) than the other tracks (~ 1.5 mm) (top: top view; bottom: cross-section in traverse direction).

6.2 Modelling of particle heating in a CO_2 laser beam

Several authors investigated the heating of powder particles on their flight through a Nd:YAG laser beam to the substrate [Jouvard, 1997; Lemoine, 1993, 1995; Marsden, 1992; Vetter, 1993, 1994]. Only Li [1995] studied this subject for CO_2 lasers. According to these papers, the most important parameters are the intensity distribution and total power of the laser beam, the velocity of the powder particles, the volume of the stream with powder particles and the concentration of the particles therein, the particle properties, the powder injection angle and, the properties of the irradiated base material.

A schematic representation of the injection of powder particles is shown in figure 6.5. Some assumptions were made:

- The powder is directed by a powder nozzle with diameter D_{pn} to the laser generated melt pool. The powder particles are transported by a gas stream to the substrate. This system of gas stream and moving particles is referred to as powder stream or powder cloud. This powder stream has a fixed angle of divergence (2ϕ). Hence, the concentration of particles (C) in the powder stream depends solely on the powder flow rate, the diameter of the powder nozzle and the distance from that nozzle (s).
- The melt pool edges in the cross-section correspond to the laser beam diameter on the substrate. The melt pool inclination is constant.
- The properties of the particles do not depend on temperature.

- The particles are spheres with a uniform size.

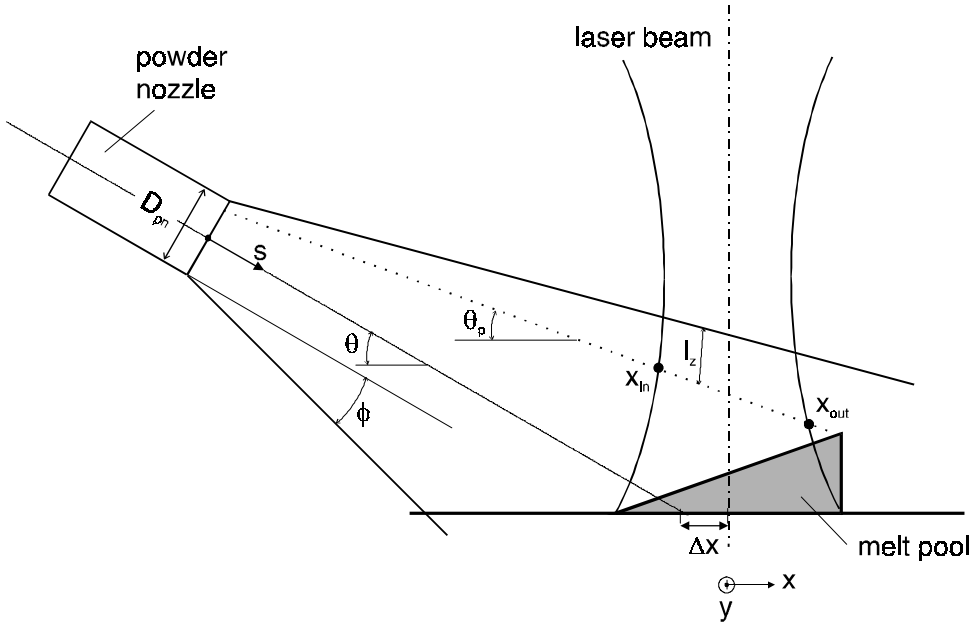

Fig. 6.5 Schematic representation of the interaction between the powder stream, the laser beam and the melt pool.

Other parameters in this figure are:

- powder injection angle θ: this is the angle with respect the horizontal along which the powder nozzle is rotated.
- *x,y,z* co-ordinate system. The origin of the system is located in the centre of the laser beam on the substrate.
- x_{in} and x_{out}: the *x* position where a particle enters (*in*) or leaves (*out*) the laser beam.
- l_z: the penetration depth of the laser light through the powder cloud to reach the powder particle concerned.
- Δx: off-set between powder stream and laser beam.

The flight path of a certain particle is shown in figure 6.5 by a dotted line. Such a particle travels some distance before it enters the laser beam. Some particles are aimed too low and touch the substrate in front of the melt pool. Other particles are aimed too high and, for that reason, miss the melt pool.

The basic consideration for calculating the temperature change of any particle is the law of energy conservation, i.e. in this particular case:

$$E_0 = E_a + E_r + E_{ra} + E_c + E_t \qquad \text{Eq. 6.1}$$

where E_0 is the incident energy on a particle, E_a is the absorbed energy, E_r is the reflected energy, E_{ra} and E_c are the energy losses due to radiation and convection and E_t is the transmitted energy through the particle. The energy loss due to radiation and convection is neglected. If the calculations indicate that the particles reach temperatures over about 1000 °C, then radiative and convective energy losses must be accounted for.
The transmitted energy can also be neglected, because the penetration depth of CO_2 laser radiation in a metal surface (~ 15 nm) is several orders smaller than the thickness of a powder particle (20-150 μm) [Wisselink, 1996]. Therefore, the energy equation (equation 6.1) reduces to:

$$E_a = E_0 - E_r = (1-R)E_0 = A\,E_0 \qquad \textit{Eq. 6.2}$$

where R and A are respectively the reflection and absorption coefficient of the particle averaged over the entire surface.
For a small time interval Δt the absorbed energy can be expressed as (figure 6.6):

$$E_a = A\,\pi\, r_p{}^2 I_z(x,y,z)\Delta t \qquad \textit{Eq. 6.3}$$

where $\pi r_p{}^2$ is the projected area of the irradiated surface of a particle with radius r_p and $I_z(x,y)$ is the power density on position (x,y) at the corresponding penetration depth l_z..

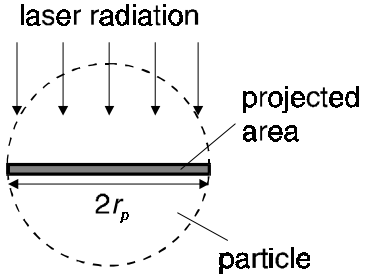

Fig. 6.6 Laser radiation is absorbed in the projected area $\pi r_p{}^2$.

It is important to note that the powder cloud attenuates the laser beam. Following the law of Beer-Lambert [Bass, 1987, Beckmann, 1989; Frenk, 1993; Lemoine, 1993, 1995; Li, 1995], the decrease of the laser intensity in a powder cloud can be described as:

$$I_z(x,y,z) = I_0(x,y,z)\, e^{-\beta l_z} \qquad \text{Eq. 6.4}$$

where β is the extinction coefficient of the powder cloud and I_0 is the intensity which has not been affected by a powder cloud.
The extinction coefficient of the powder cloud depends on the volume fraction of powder particles (f_v) in it ($0<f_v<1$). Hence:

$$\beta = \beta_0 f_v \qquad \text{Eq. 6.5}$$

where β_0 is a kind of relative extinction coefficient.
On its path through the laser beam the total energy absorbed by a particle then becomes:

$$E_a = \int_{t_{in}}^{t_{out}} A\pi r_p{}^2 I_0(x,y,z) e^{-\beta_0 f_v l_z}\, dt \qquad \text{Eq. 6.6}$$

where t_{in} and t_{out} are respectively the time of entrance in the laser beam and time of exit from the laser beam. These values can be calculated, since we have:

$$dt = \frac{dx}{v_p \cos\theta_p} \qquad \text{Eq. 6.7}$$

where v_p is the velocity of the powder particles and θ_p is the injection angle of the particle concerned. Substitution into equation 6.6, under the assumption that particles enter the laser beam at a position (x_{in},0) and leave at (x_{out},0), gives:

$$E_a = \frac{A\pi r_p{}^2}{v_p \cos\theta_p} \int_{x_{in}}^{x_{out}} I(x,y,z)\, e^{-\beta_0 f_v l_z}\, dx \qquad \text{Eq. 6.8}$$

The temperature rise of a particle [ΔT] can now be calculated, because the absorbed energy E_a must be equal to the internal energy (no melting)[1]:

$$E_a = m_p\, c_p\, \Delta T = \frac{4}{3}\pi\, r_p{}^3\, \rho\; c_p\, \Delta T \qquad \textit{Eq. 6.9}$$

where m_p is the mass of a single powder particle, ρ is the density of the powder material and c_p is the specific heat.
The temperature rise of the particle is thus:

$$\Delta T = \frac{3\,A}{4 r_p \rho\; c_p\, v_p \cos\theta_p} \int_{x_{in}}^{x_{out}} I_0(x,y,z)\, e^{-\beta_0 f_v l_z}\; dx \qquad \textit{Eq. 6.10}$$

The volume fraction f_v depends on the distance (s) from the nozzle exit:

$$f_v(s) = \frac{4\,\dot{m}_p}{\pi\,\rho\, v_p \left(D_{pn} + s\,\tan\phi\right)^2} \qquad \textit{Eq. 6.11}$$

where $\dot{m}_p$ is the powder mass flow rate.

Experimental determination of β_o:
The transmitted power was measured with the set-up shown in figure 6.7. This set-up consists of a powder injection nozzle, which directs a powder stream to the substrate. A small hole is made in this substrate, which is just large

---

[1] This equation is valid under the assumption that the temperature distribution within the particle is uniform. This condition can be fulfilled if the Biot number, which provides a measure of the temperature drop in the solid relative to the temperature difference between the surface and the environment, is much smaller than 1 [Incropera, 1990]. For a spherical powder particle, the Biot number is:

$$Bi = \frac{h\left(r_p / 3\right)}{k}$$

where h is the thermal convectivity of the environment and k is the thermal conductivity of the powder material. The Biot number of a powder particle in an Argon gas flow is approximately 60 10^{-6}, which is much lower than 1. Hence, the condition imposed by the Biot number can be fulfilled easily.

enough to let through the laser beam. Part of the laser energy is attenuated in the attenuation zone which is represented in this figure as a shaded area. The transmitted laser energy is measured with a laser power meter.
The darkly shaded area does not exist during real cladding conditions. Therefore, it must be minimised by taking a small injection angle combined with a large injection distance. No powder is allowed to bounce on the substrate in front of the hole, because the power which is absorbed by such particles is not accounted for in the equations.

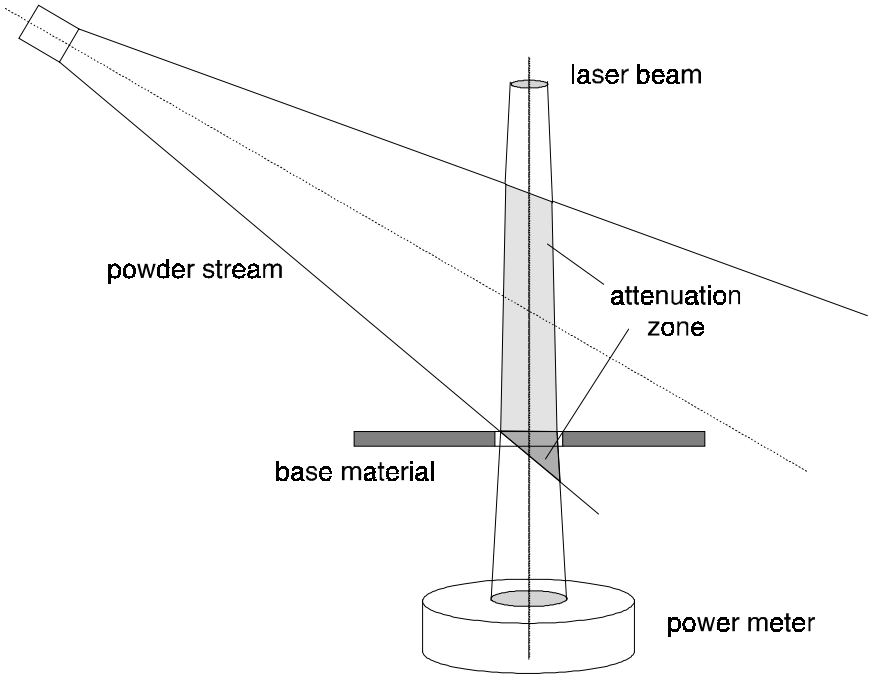

Fig. 6.7 Experimental set-up for the determination of the power attenuation by the powder stream (powder injection angle: 30°; powder injection distance: 30 mm). The darkly shaded region is the attenuation zone that must be minimised for an accurate calculation of the value of β_0.

According to Kastler[2] [1952] the absorption of laser energy in a powder cloud depends on the material in that cloud. Therefore, the absorption of the powder

[2] Kastler proposed a theory to calculate the attenuation of light in a cloud with small water droplets. This theory is based on the wave equations of light and shows an analogy with the attenuation of laser energy in powder particles. Under certain conditions ($2\pi r_p/\lambda > 100$) β_0 equals $3R/2r_p$. This condition can not be met when using CO_2 laser radiation (wavelength λ=10.6 μm). However, the wavelength of a Nd:YAG laser is ten times smaller

cloud was measured for three materials: Stellite 6 (cobalt base), Metco 15E (nickel base) and Amdry 5843 (tungsten base) (appendix 1).
The transmitted power was measured with the parameter variations shown in table 6.3.

Tab. 6.3 Parameter variation for the determination of the transmitted power.

Stellite 6	powder flow rate [mg/s] diameter laser spot [mm] laser power [W]	50 - 100 - 150 - 200 - 250 2.0 - 3.0 - 4.0 - 5.0 800 - 1300 - 1800
Metco 15 E	powder flow rate [mg/s] diameter laser spot [mm] laser power [W]	50 - 100 - 150 - 200 - 250 3.0 1300
Amdry 5843	powder flow rate [mg/s] diameter laser spot [mm] laser power [W]	50 - 100 - 150 - 200 - 250 3.0 1300

Figure 6.8 shows the power attenuation as a function of the powder flow rate for several laser powers. It shows that the laser power has no effect on the measured power attenuation. The attenuation increases linearly with the powder flow rate.
Figure 6.9 shows the power attenuation as a function of the powder flow rate for several beam diameters. The attenuation decreases when the beam diameter is enlarged and increases linearly with the powder flow rate.
Figure 6.10 shows the power attenuation for three different cladding materials. The influence of the particle size is clearly visible. The powder with the largest grains, i.e. Amdry 5843, has a power attenuation that is a factor 3.5 higher than that of Stellite 6, which has the smallest grains. The measured power attenuation of Stellite 6, Metco 15E and Amdry 5843 are in the proportion of 1 to 1.3 to 3.3. This relates closely to the inverse of their particle size.

(1.06 μm). Hence, the condition can be satisfied. Lemoine [1995] and Jouvard [1997] showed that with the thus calculated value of β_0, satisfactory results can be achieved.

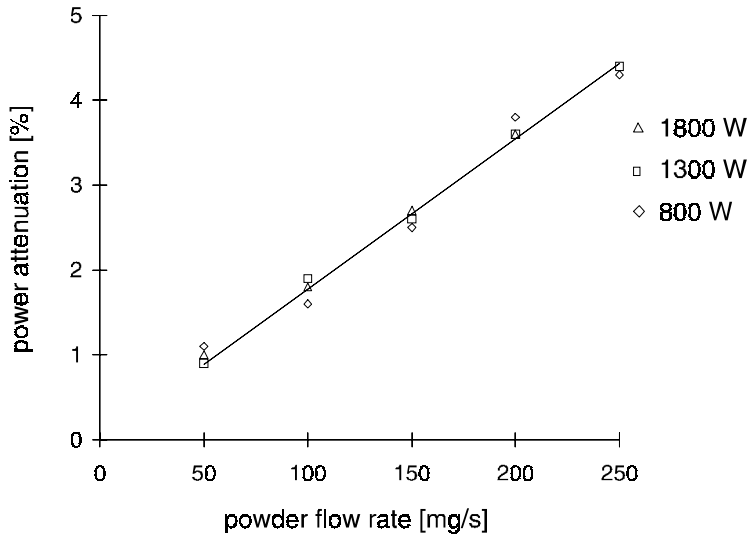

Fig. 6.8 Power attenuation as a function of the powder flow rate measured for three laser power levels (material: Stellite 6; laser beam diameter: 2.0 mm).

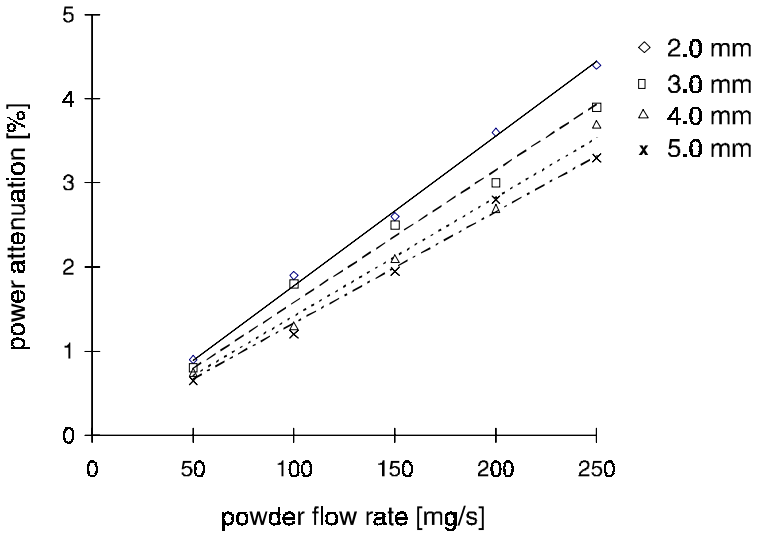

Fig. 6.9 Power attenuation as a function of the powder flow rate measured for four laser beam diameters (material: Stellite 6; laser power: 1300 W).

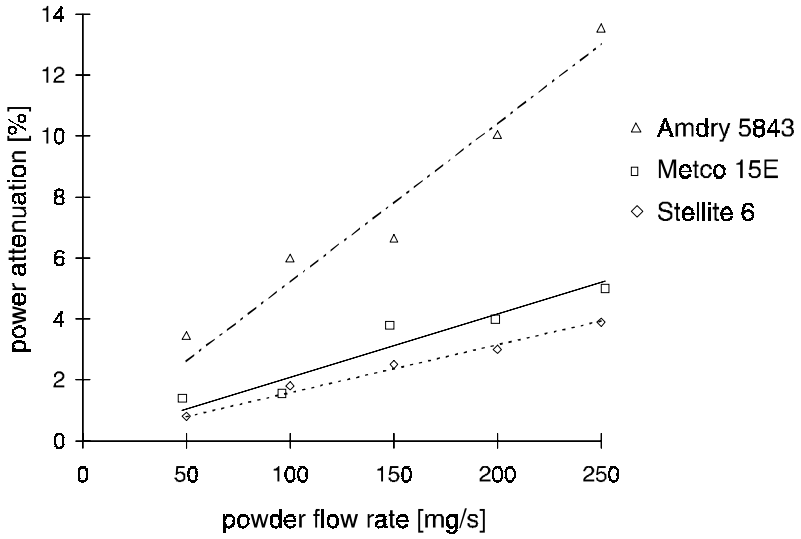

Fig. 6.10 Power attenuation as a function of the powder flow rate measured for three cladding powders (laser power: 1300 W; spot diameter: 3.0 mm).

The measured power attenuation was used to derive the value of β_0 for each material. The results are shown in table 6.4.

Tab. 6.4 Powder cloud extinction coefficient (β_0) derived from the measured power attenuation.

Material	mean particle radius [µm]	density [kg/m^3]	powder cloud extinction coefficient β_0 [mm^{-1}]
Stellite 6	48.5	8460	**363**
Metco 15E	37.5	7700	**420**
Amdry 5843	17.5	12500	**1650**

The only other author that has reported a study to the preheating of powder particles by a CO_2 laser beam [Li, 1995] used a value of 10^4 mm^{-1} for the extinction coefficient of a Stellite 6 powder cloud, which is a factor 30 larger than the value experimentally determined in this chapter. The value of Li, which is the extinction factor of CO_2 laser radiation in a solid, has been shown incorrect by calculations and by experiments. Using the value proposed by Li, less than 5 % of the laser power can reach the substrate. As a consequence, no melt pool can be formed.

Temperature of powder particles with the experimentally determined value of β_o

The temperature rise of particles was calculated for a standard configuration in the author's laboratory. These default values are shown in table 6.5.

Tab. 6.5 Default values of parameters.

coating material:	Stellite 6
focal length:	95 mm
spot diameter D:	3.0 mm
laser power P:	1500 W
beam intensity profile:	Gaussian
powder flow rate:	75 mg/s
particle speed v_p:	25 m/s
particle radius r_p:	100 µm
diameter powder nozzle D_{pn}:	2.0 mm
distance powder nozzle -> substrate:	9 mm
powder injection angle θ:	30°
angle of divergence powder stream ϕ:	10°
offset centre laser beam -> centre powder stream Δx:	0.0 mm

Figure 6.11 shows the particle temperature as a function of the position where they hit the substrate for three particle sizes. The particle temperature increases when the particle size is reduced. The top-most particles in the powder stream hit the substrate about 6 mm behind the laser spot in this configuration. Unfortunately, they do not participate to the building of the clad, although they are the particles that experience the highest temperature rise.
Figure 6.12 shows the effect of the powder velocity v_p on the particle temperature rise for a particle hitting the substrate 1.4 mm behind the laser spot centre. The powder velocity has a non-linear effect on the particle temperature. This non-linear behaviour is caused by the presence of this parameter in the denominator of equation 6.10 and enhanced by the fact that the volume fraction is also affected. Particularly at velocities below 5 m/s, a considerable temperature rise can be achieved.
Figure 6.13 shows the effect of the powder mass flow rate on the temperature rise. The mass flow rate hardly has any effect on the particle temperature in this configuration.

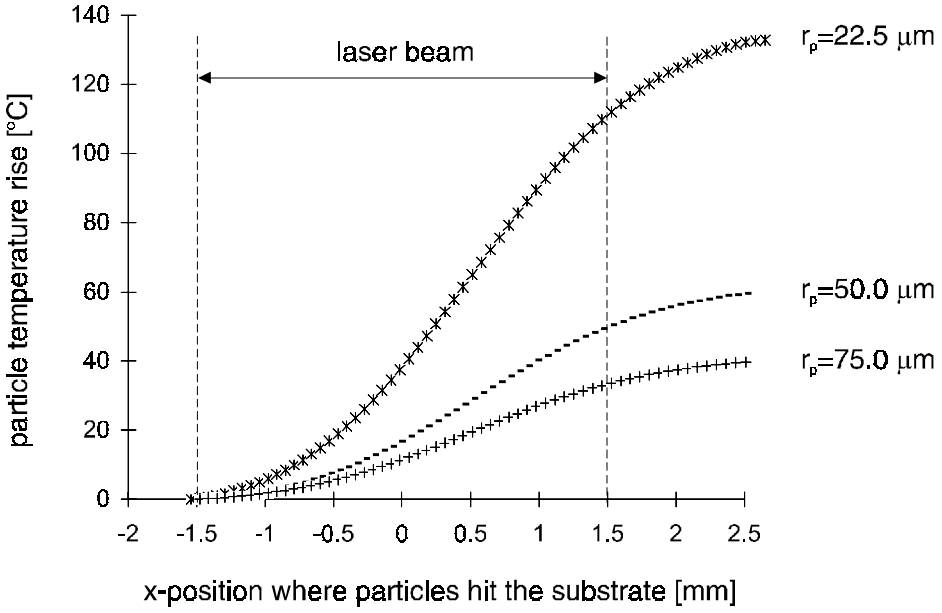

Fig. 6.11 Effect of particle size on temperature rise.

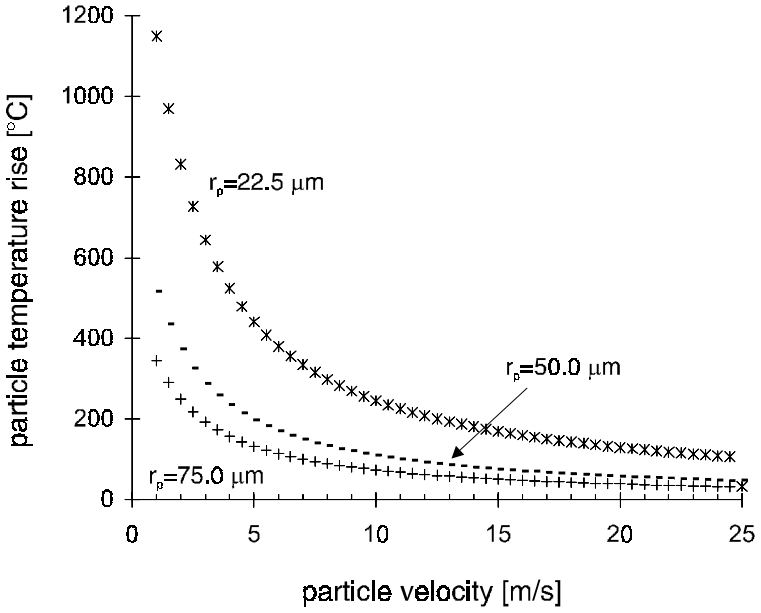

Fig. 6.12 Effect of particle velocity v_p on particle heating for a particle hitting the substrate 1.4 mm behind the laser beam centre.

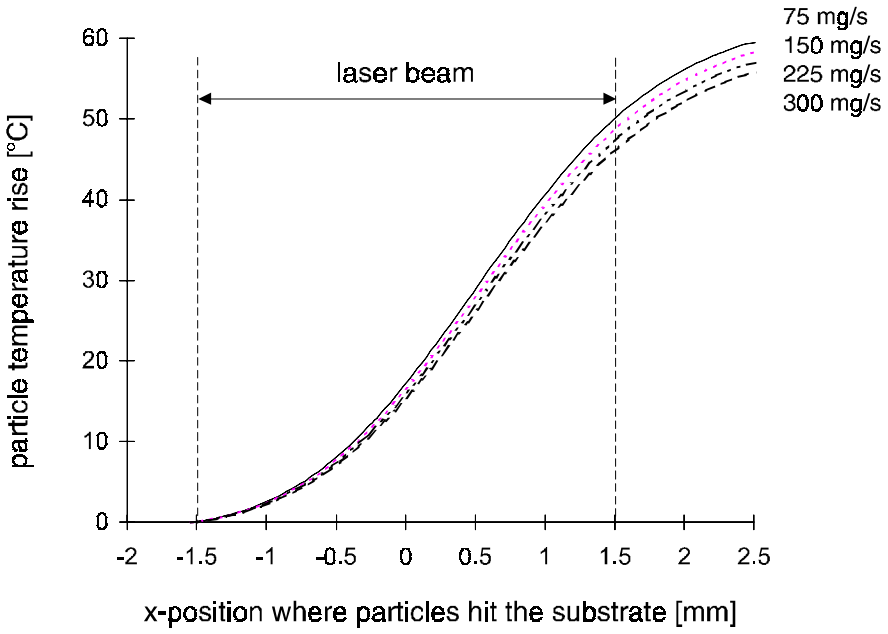

Fig. 6.13 Effect of powder mass flow rate on temperature rise.

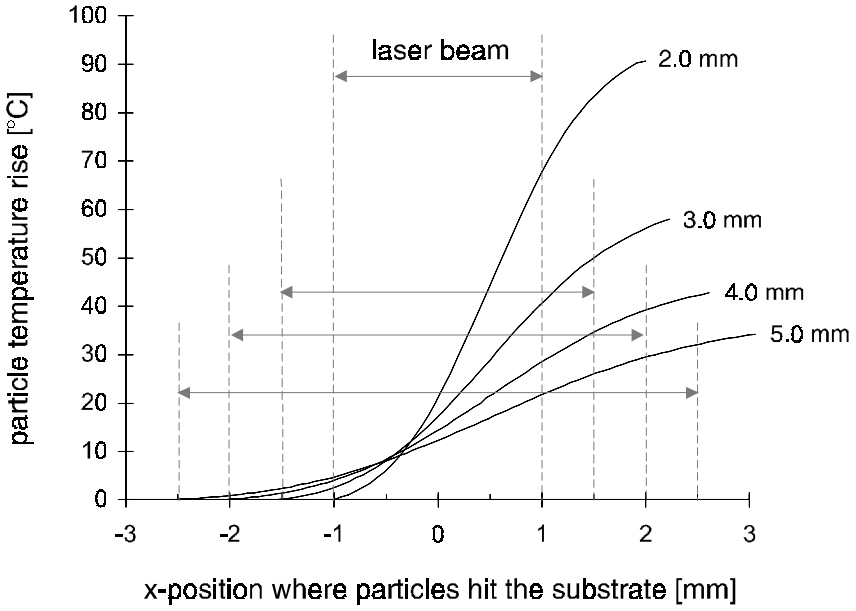

Fig. 6.14 Effect of spot diameter on particle temperature. Same power in all laser spots (1500 W).

Figure 6.14 shows the effect of the laser spot size on the particle temperature. Each of the laser spots contains the same laser power (1500 W). The particle temperature increases with a reduction of the spot diameter.

The effects of the laser power and the intensity distribution are not shown. The effect of the laser power is linear, as was already evident from equation 6.10. The effect of intensity distribution was investigated by comparing a Gaussian profile with a circular uniform distribution. The default parameters used in this simulation, yielded results that can not be distinguished from each other when plotting them in graphs.

Discussion of results

The temperature rise of particles that are transported in the carrier gas to the laser spot on the substrate is limited in the present configuration to an average of 19.9 °C. The main reasons for this low value are the high particle velocity and the large average grain size of the powder.

This low temperature rise proves that the noticed glowing particles (section 6.1) can not be particles that are injected straight from the powder nozzle to the substrate. These particles must have ricocheted from the substrate or the melt pool.

The present powder efficiency is low. Most particles are directed to a position behind the laser spot, which is a waste of precious coating material. Because of the moderate power attenuation (figure 6.10), the poor powder efficiency does not affect the cladding process itself.

Figure 6.15 shows the temperature of particles that hit the substrate for an improved configuration for three powder injection angles. The particle velocity and divergence were reduced to respectively 4 m/s and 2°. The off-set Δx was selected to ensure that the topmost particles, which are heated most, hit the substrate within the laser spot. The average temperature of particles that arrive on the substrate increases from 20 °C in the default configuration to 200 °C in this improved set-up. According to figure 6.11 this temperature rise can be enhanced substantially by reducing the average particle size.

The powder efficiency improves as well. When applying a powder injection angle of 60° an efficiency of more than 98 % can be achieved.

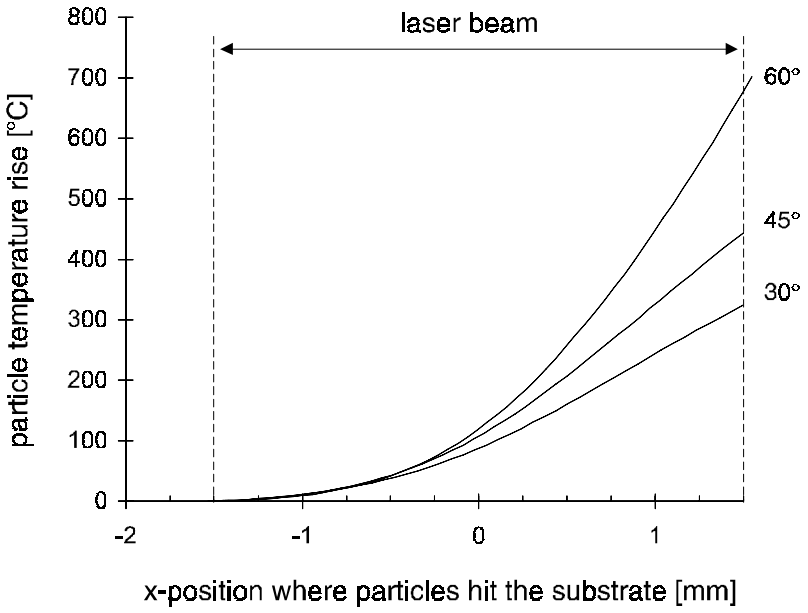

Fig. 6.15 Particle temperature for improved powder injection parameters.

6.3 Ionisation of powder particles

During the experiments described in section 6.1, the occurrence of a plasma was observed when applying laser powers of 1260 W and higher. This plasma effectively absorbs the laser radiation and shields the substrate from the laser beam. Since this stops the cladding process, plasma formation must be prevented.

Plasma formation had not been observed during laser cladding with preplaced powder. The experimental configuration was identical, as were the machining parameters. Therefore, the occurrence of a plasma must be a consequence of the injection of particles.

A laser beam intensity of 10^6-10^7 W/cm^2 is required to form a plasma in a metal vapour [Beyer, 1985]. During the experiments described in section 6.1, a laser power of at least 1260 W was necessary to achieve a plasma. The theoretical mean laser intensity in the focus is in that case $5.75 \cdot 10^6$ W/cm^2, which is in the range required for plasma formation. In practice even higher values are achieved locally, as a result of the non uniform power density distribution of the applied laser beam.

The most obvious way to prevent the formation of a plasma is not to allow particles to enter the focal area by increasing the shielding gas flow from the nozzle

(figure 6.1). Unfortunately, this is not possible because a strong gas flow disturbs the melt pool and the powder stream.
The mean power density in the focus of the laser beam can be reduced by either decreasing the laser power or by increasing the beam waist (w_{of} in figure 6.16). The first alternative cannot be considered as an option because a certain laser power level is required to melt and heat the substrate.
The second alternative can be implemented quite easily by applying a lens with a larger focal length (figure 6.16). Another advantage of a lens with a larger focal length is that the distance between the processing area and the minimum waist will increase, which, in its turn, will increase the likelihood that the shielding gas can prevent the particles from entering the focal area.
Experiments (table 6.6) showed that plasma formation could almost be completely prevented in the configuration described in section 6.1 when applying a lens with a focal length of 154 mm instead of 95 mm. The laser power could be increased to 1500 W. The use of the 154 mm lens resulted in a reduction of the average power density of 62%, bringing it down to about $2 \cdot 10^6$ W/cm^2, which is still over the critical value of 10^6 W/cm^2. Therefore, higher power levels certainly require the use of lenses with even larger focal lengths.

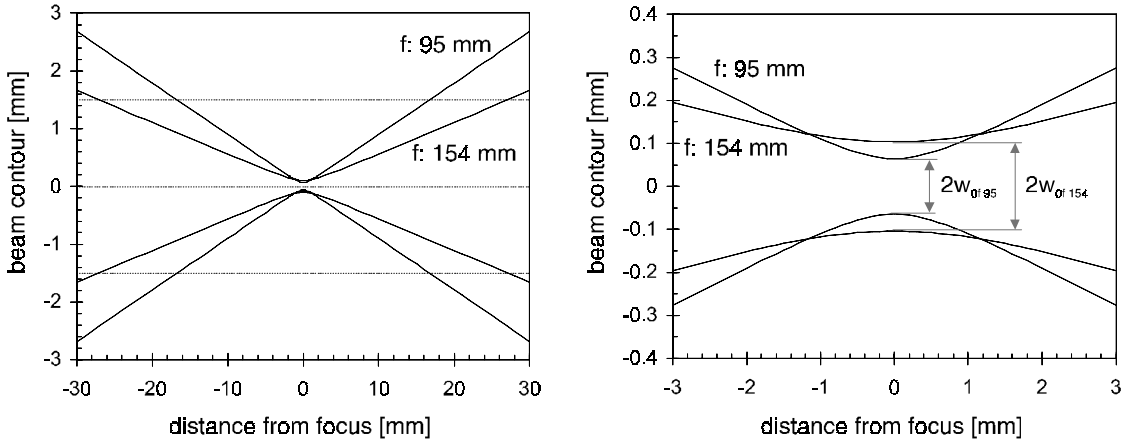

Fig. 6.16 Laser beam contour as function of the distance to the waist for lenses with a focal length of 95 and 154 mm. The smallest waist is 167 µm and 270 µm for a focal length of respectively 95 and 154 mm. The 3.0 mm beam diameter is positioned respectively 17 and 27 mm from the waist.

The experiments (table 6.6) showed that the laser power alone is not sufficient to predict the moment at which plasma formation starts. Some tracks were already interrupted after a few millimetres, whereas others under seemingly

identical process conditions could be applied successfully. Further observations showed that plasma formation in the enclosed working chamber is increased by the experimentation time and the powder mass flow rate. Apparently, a critical concentration of small particles must be reached to initiate the plasma formation.

Very small particles (< 1 μm) in the powder mixture can remain floating in the working chamber for a long time before they fall. The velocity of such particles is very low and, therefore their exposure time to the laser beam can be long. As was shown in section 6.2, the temperature rise of particles strongly depends on the inverse particle size. These three factors combined, enhance the likelihood that those particles are heated to such an extent that a metal vapour will be formed.

Tab. 6.6 Experiments on plasma formation.

plasma formation	laser power [W]	feed rate [mm/s]	plasma at track	relative powder flow rate [%]
focal length: 95 mm	1700	5	7 (of 10)	13
	1600	5	1 (of 1)	10
	1500	4	1 (of 1)	10
	1300	5	1 (of 1)	15
	1400	4	1 (of 1)	12.5
	1400	3	1 (of 1)	10
	1300	3	5 (of 10)	10
	1700	4	1 (of 1)	13
	1700	4	4 (of 10)	10
	1300	3	6 (of 10)	8
	1500	3	1 (of 1)	8
	1500	3	7 (of 15)	15
focal length: 154 mm	1500	3	2 (of 12)	12

no plasma formation	laser power [W]	feed rate [mm/s]	number of tracks	relative powder flow rate [%]
focal length: 95 mm	1300	6	1	15
	1300	5	1	10
	1300	4	1	10
	1400	4	1	10
	1400	3	1	10
	1300	3	1	10
	1300	3	1	12
	1700	4	1	13
	1300	3	1	15
	1300	3	1	20
	1300	3	10	8
	1500	3	1	15
	1500	3	12	15
focal length: 154 mm	1500	3	1	15
	1500	3	1	10
	1500	3	1	8
	1500	3	12	15
	1500	3	12	12
	1500	3	12	10
	1500	3	12	8

Chapter 7

Examples of applications

7.1 Diesel engine inlet valve

Inlet valves of diesel engines must be resistant to adhesive, abrasive and corrosive wear and, must be able to resist the impact with the valve seat (figure 7.1). The necessary material properties can only be supplied by relatively expensive materials. In order to reduce material costs, ordinary steel is covered with a dedicated surface layer that can fulfil the requirements mentioned above. Stellite 6 is a well known material for improving the surface properties of diesel engine valves (chapter 2) and has therefore been selected for the application described in this section.

Figure 7.1 shows the interaction zone between the valve and the valve seat. That is the region that must be reinforced.

The clad layer must have the following dimensions:

- clad height: > 0.3 mm;
- clad width: > 2.2 mm;
- no alteration of the surface shape.

Since the valve geometry should not be modified, a groove was made in the valves (figure 7.1 right). The experimental set-up is shown in figure 7.3.

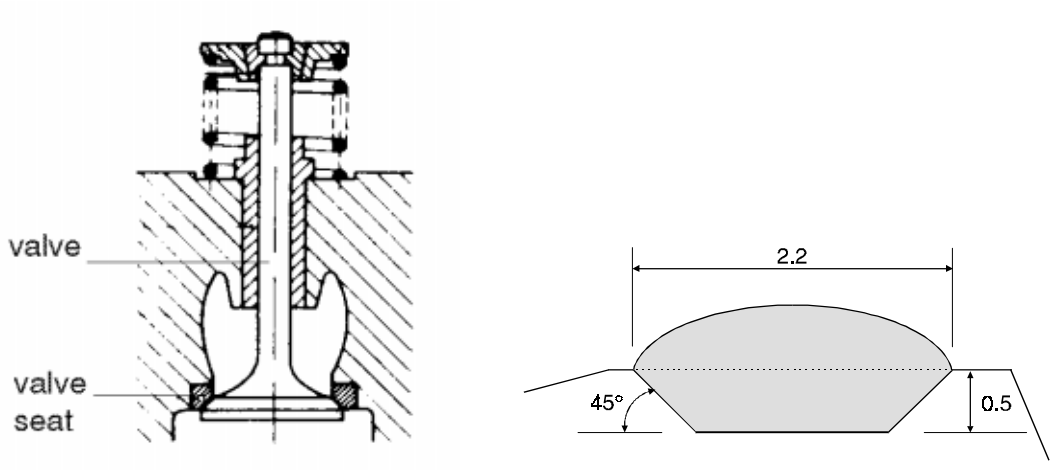

Fig. 7.1 Valve and valve seat as well as the dimensions of the clad [mm].

The following settings were used:

- feed rate: 2.0 mm/s;
- powder injection angle: 45°;
- powder mass flow rate: 4.8 mg/mm;
- powder injection distance: 10.5 mm;
- shielding gas: argon.

Two different laser intensity profiles were applied (figure 7.2).

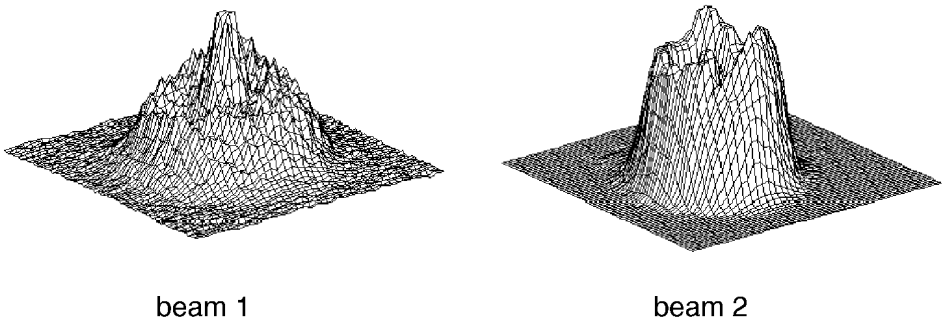

Fig. 7.2 Applied laser beam profiles.

Best cladding results were achieved with the settings shown in table 7.1. The machining parameters are different due to the different intensity profiles. The best settings for beam one were determined by performing a series of experiments.

Tab. 7.1 Machining parameters resulting in best cladding results.

	beam 1	beam 2
laser power [W]	1600	1410
spot size [mm]	3.05	2.50

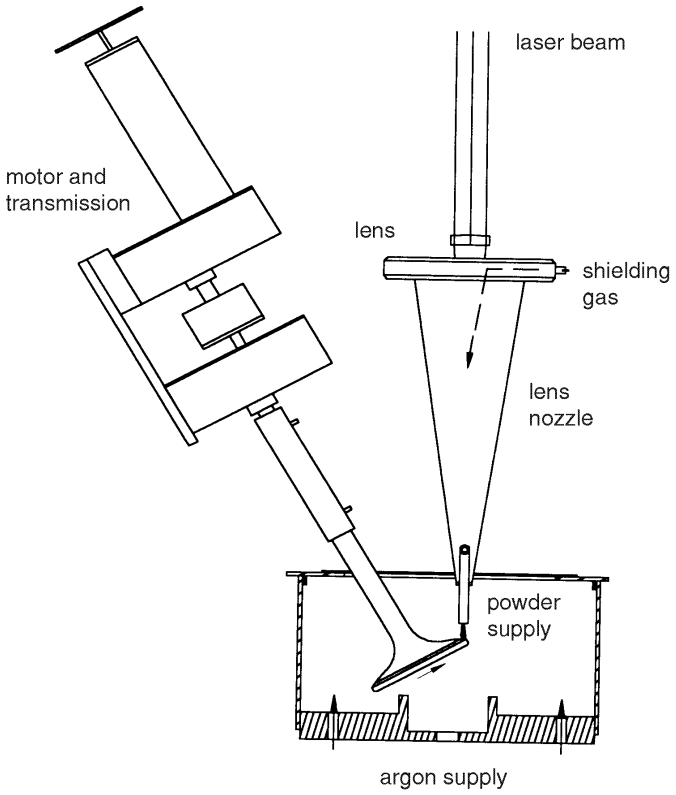

Fig. 7.3 Experimental set-up for laser cladding of an inlet valve.

However, the settings of beam 2 were determined by comparing the temperature distribution that is induced on the surface by these beam profiles (following the method described in chapter 3). With beam 1 higher temperatures are reached. The area over which a high temperature is attained is larger as well (figure 7.4). This implies that with beam 1, a deeper melt pool is formed than with beam 2, which ensures a good bonding with the base material. In order to increase the surface temperature that is attained with beam 2, a smaller

spot size with a higher power density was applied. This correction resulted in a maximum surface temperature comparable to the one achieved with beam 1. When laser beam 2 was applied with the machining parameters of beam 1, a wider clad (3.1 mm vs. 2.6 mm) with a poor quality was attained. The bonding with the base material was incomplete and a severe degree of porosity was found in the clad. As predicted by the model, the melt pool temperature was too low. However, a clad layer with the same properties as the initial one was produced when applying beam 2 with the calculated parameters.

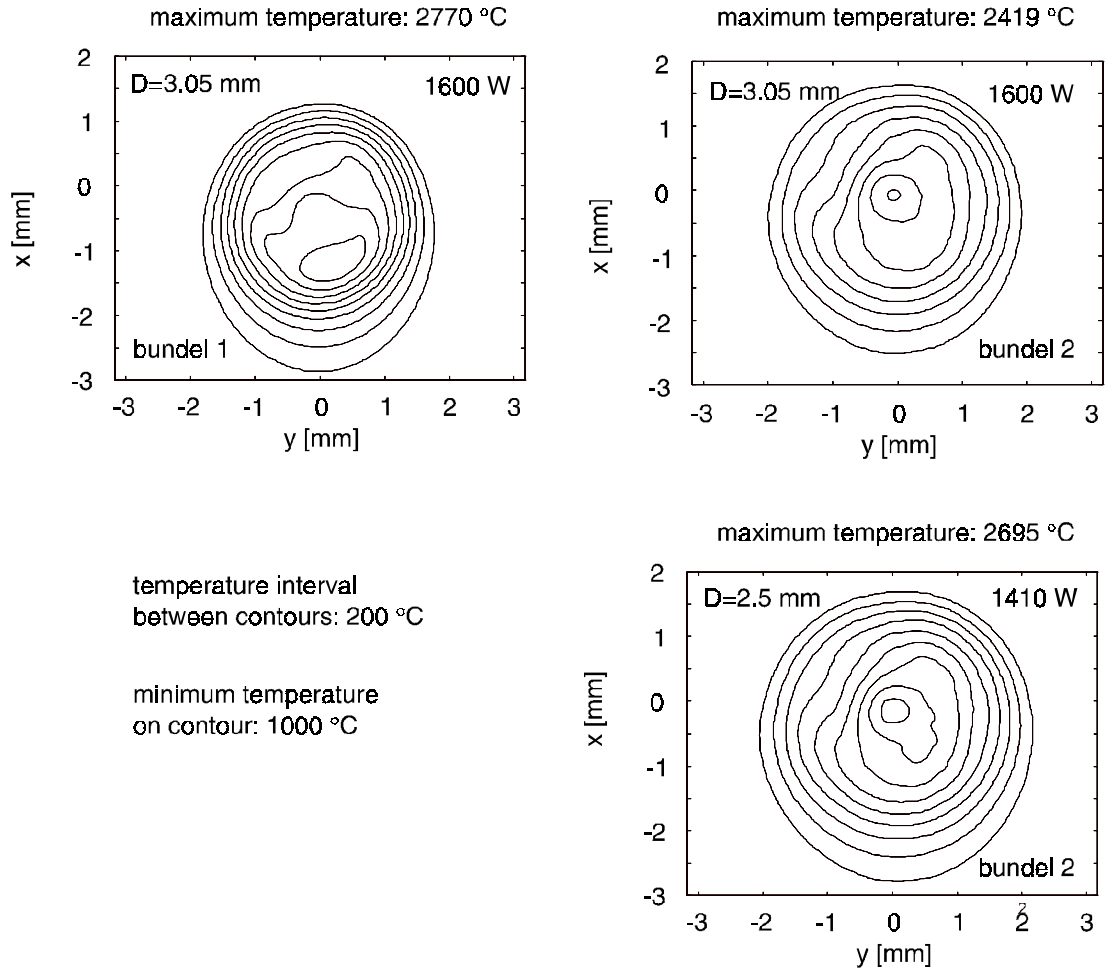

Fig. 7.4 Effect of laser beam profiles on the temperature profile on the base material (feed rate: 5 mm/s).

Results:

- clad height: 1.0 mm;
- clad width: 2.6 mm;

- dilution: < 9 %;
- hardness: 560 Hv;
- powder efficiency: 31 %;
- laser machining time: 77 seconds.

The hardness distribution over the clad cross-section (figure 7.6) is shown in figure 7.5. The hardness is uniform over the clad cross-section: between 560 and 575 Hv0.3. The hardness drops to 370 Hv0.3 at a distance of 1 mm from the top of the clad. This agrees well with the measured clad height.
The measured distribution of elements in the cross-section is shown in figure 7.7.

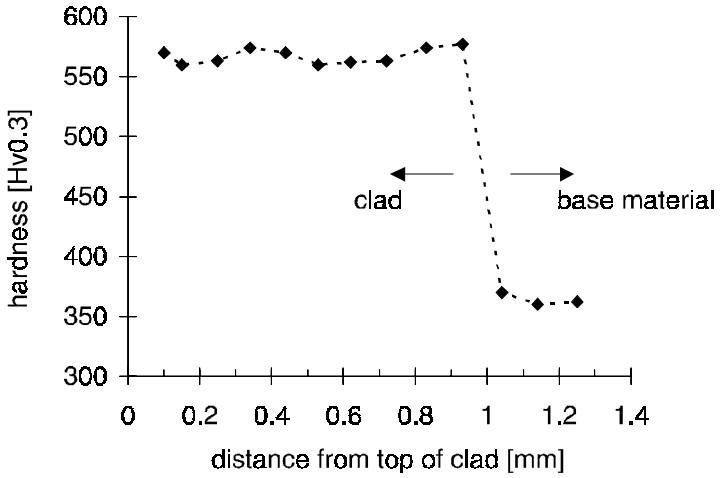

Fig. 7.5 Hardness distribution measured over the clad cross-section.

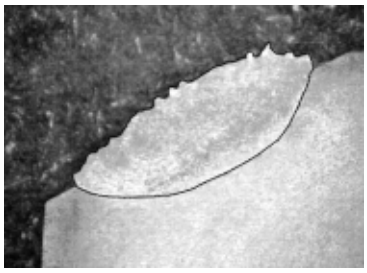

Fig. 7.6 Clad layer produced in a premade groove.

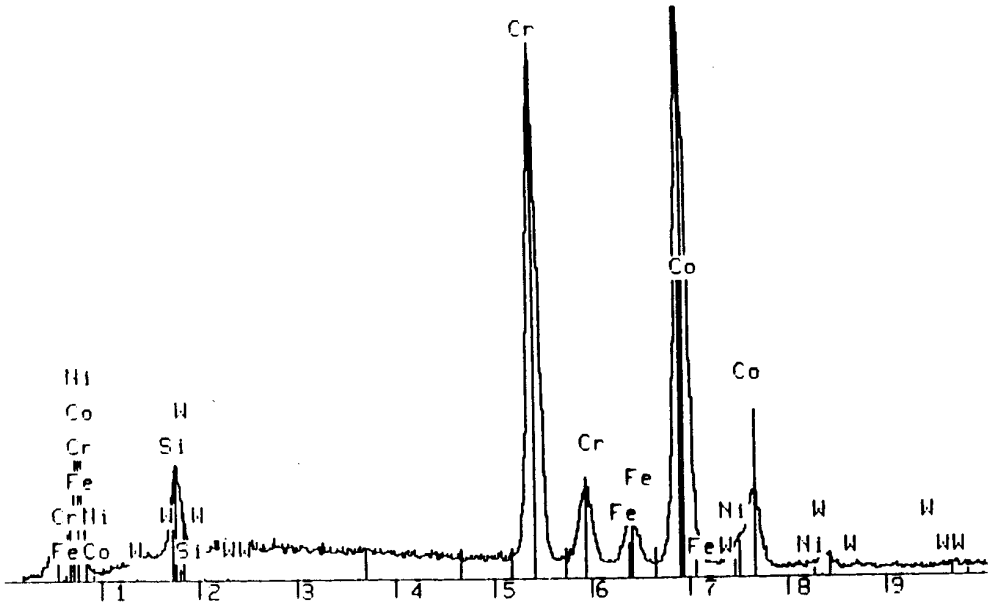

Fig. 7.7 Material composition determined by SEM measurements.

7.2 Extruder screw

Extruder screws for plastic machinery must be resistant to corrosive and mechanical wear. These requirements are normally met by nitriding the steel substrate. However, it is to be expected that this treatment will not be sufficient in the near future, because:

- high temperature resistant plastics are coming into practice;
- abrasive particles and reinforced fibres are added;
- very corrosive elements are mixed to protect the mixture from catching fire;
- plastic production rates must be increased which involves higher working pressures.

Moreover, the nitriding of screws has a major drawback. It causes severe distortion of the screw, requiring a re-alignment of the screw.

Laser cladding does not have this disadvantage because the heat input is confined to the surfaces to be treated, instead of to the entire workpiece.

Therefore, it was decided upon to investigate the possibilities of laser cladding for improving the corrosion and wear resistance of screws for plastic machinery.

The screws are produced of steel 14CrMoV69. Reparation of worn screws is performed by welding Stellite electrodes onto it. Hence, these materials were also selected for use in this laser cladding experiment.
Experiments were performed on a dummy, which dimensions are shown in figure 7.8. The pitch, which exists in a real extruder screw, is small and does not affect the cladding behaviour.
The experimental set-up and the machining parameters are shown in figure 7.9 and table 7.2.

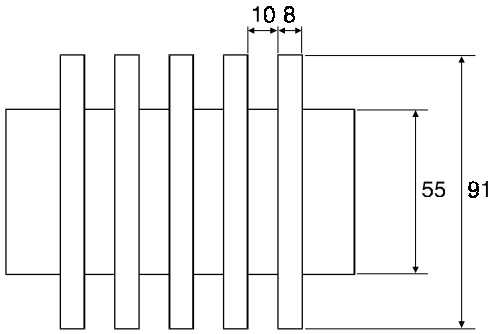

Fig. 7.8 Specimen for laser cladding on extruder screw.

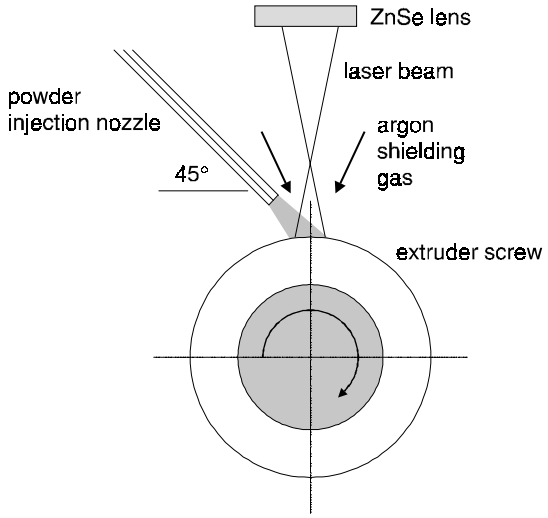

Fig. 7.9 Schematic set-up for cladding of an extruder screw.

Tab. 7.2 Parameter settings for cladding of extruder screw.

Base material:	14CrMoV69	powder mass flow:	110 mg/s
coating:	Stellite 6	track to track distance:	0.9 mm
powder nozzle diameter:	1.5 mm	laser powder:	1100 W
nozzle-workpiece distance:	9.5 mm	feed rate:	8 mm/s
powder injection angle:	45°	spot diameter:	3.0 mm
argon carrier gas:		focal length:	200 mm
- flow:	4.8 l/min	beam profile:	see app. 3
- pressure:	1.5 10^5 N/m^2		

Figure 7.10 shows the geometry of the produced clad. This clad was made by applying two layers on top of each other. The two layers were a half beam diameter displaced from each other and consist of several adjacent partly overlapping tracks. The first layer resulted in a clad thickness of about 0.6 mm. The second layer added another 0.4 mm to this.
The bonding to the base material is a strong fusion bond that shows no defects (figure 7.11). The dilution is acceptable (10 %) and no cracks and only a small degree of porosity could be observed. The hardness in the clad varies between 500 and 570 Hv, which is common for Stellite clads. Due to the application of two layers on top of each other, the hardness increase of the base material could be reduced (figure 7.12).

Fig. 7.10 Geometry of the produced clad.

Fig. 7.11 Transition from the clad to the base material.

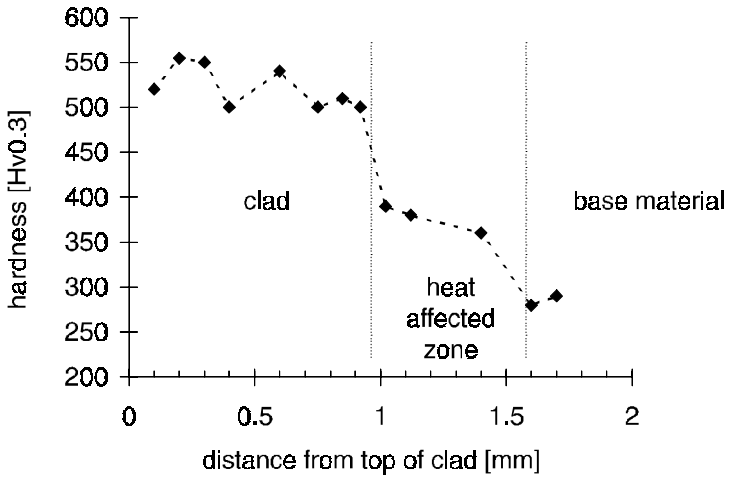

Fig. 7.12 Course of the hardness in the surface of the extruder screw.

Since the laser cladding technique in this example is meant as a reparation method, some experiments were performed on a nitrided surface as well.
These experiments also yielded clads with a good bonding to the substrate. However, cracks and gas holes were formed on the interface between the clad and the base material (figure 7.13). The nitrides directly under the interface disappeared.
It was concluded that laser cladding is a suitable technique for repairing worn extruder screws. It is essential to machine the damaged surface to below the

nitriding depth in order to prevent the formation of gas holes and cracks on the interface between clad and screw.

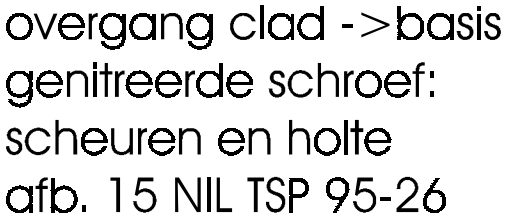

Fig. 7.13 Cracks and gas hole on the interface between substrate and clad.

Figure 7.14-7.16 show three types of porosity that were found during the experiments. The first picture shows the inter-run porosity that can be avoided by a reduction of the clad height to depth ratio. The second picture shows some rather large gas holes in the clad, as well as some defects on the interface. One of these defects is shown in the last picture.

Fig. 7.14 Inter-run porosity.

Fig. 7.15 Some rather large gas holes and interface defects.

Fig. 7.16 Defect on the interface between clad and substrate.

7.3 Wireline cylinder head

Wireline cylinders used in the petro-chemical industry are prone to corrosion. Severe corrosive wear can lead to leaking. In that case, the faces indicated as A, B and C in figure 7.17 must be repaired.

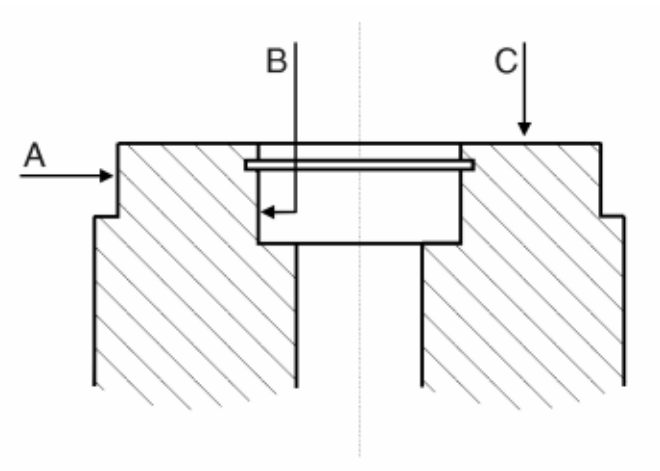

Fig. 7.17 Cross section of a wireline cylinder head.

The wireline cylinder head is made of steel AISI 4130. Powder Diamalloy 1005, which is a corrosion resistant Inconel 625 type powder, was selected as coating material.

The worn surfaces were grit blasted, machined and degreased prior to laser cladding. The cladding process itself involved the processing of the three faces as indicated in figure 7.17, as well as the edges. The two outer surfaces, i.e. the top surface and the outer diameter, were treated with a perpendicularly irradiating laser beam. For treatment of the inner surface the workpiece was positioned under an angle of 45° to the horizontal (figure 7.18).

The cladding of the edges was more complicated. To prevent the formation of a rounded clad, an auxiliary ring with the same size as the outer and inner diameter of the cylinder head, was placed on top of it. First, the outer and inner surface were clad. After machining those surfaces and removing the ring, the top surface could be treated.

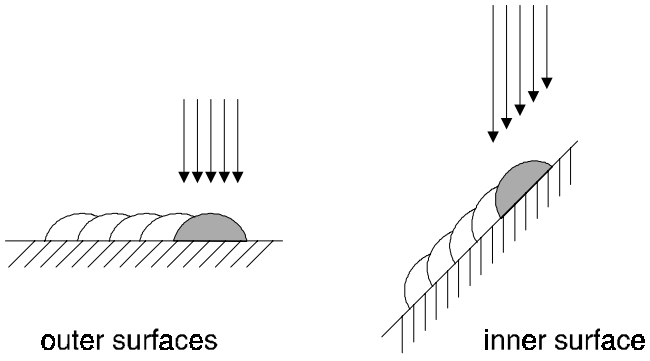

Fig. 7.18 Positioning of the surfaces with respect to the laser beam.

Laser cladding was performed with the following parameters:

Tab. 7.3 Parameter settings for cladding of a wireline cylinder head.

Laser parameters	**outer surfaces**	**inner surface**
focal length [mm]	200	200
nozzle opening [mm]	6	6
argon flow [l/min]	8	8
laser power [W]	1500	1800
spot diameter [mm]	3.0	3.0
feed rate [mm/s]	5	4
overlap between tracks [%]	40	50
powder parameters	**outer surfaces**	**inner surface**
powder feed rate [g/min]	6	7.2
argon carrier gas flow [l/min]	20	20
diameter powder nozzle [mm]	2	2
nozzle-workpiece distance [mm]	12	12
injection angle with respect to:		
- laser beam	45°	22.5°
- clad direction	90°	45°

Depending on the required clad thickness, several layers must be applied on top of each other. Each new layer increases the clad thickness with 0.4 mm.
The clads were analysed by two non-destructive methods. First, a liquid penetrant examination was performed to show possible porosity and cracks in the surface. Secondly, the workpiece was immersed in an etching Nital solution. This solution only etches the steel substrate. The applied coating will not be affected. If a dark shade can be noticed after the immersion, the substrate coverage was incomplete. However, neither of these methods showed any irregularity.
Figure 7.19 shows a micrograph of a post-machined part of the cylinder head.

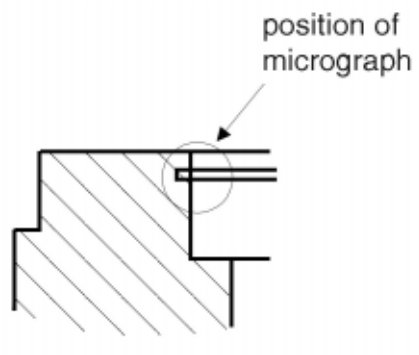

micrograph
cylinder head

Fig. 7.19 Cross-section of the post-machined cylinder head.

Figure 7.20 shows the course of the hardness as measured on the top surface. The hardness in the clad is about 250 Hv, which equals the hardness in the not heat affected zone. Unfortunately, the hardness in the heat affected zone of the base material is too high. This hardness increase is due to the formation of martensite. The formation of martensite introduces residual stresses in the workpiece. The effect on the corrosion resistance has not been known yet. Practice tests should reveal this.

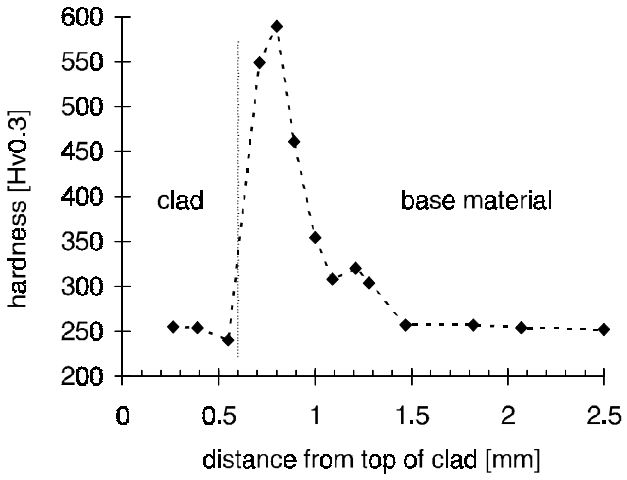

Fig. 7.20 Course of the hardness in the top surface.

Measurements of the material composition (table 7.4) in the clad showed that the dilution varies between 1 and 12 %.

Tab. 7.4 Measured chemical composition in the applied clad.

	outer surface	**top of outer edge**	**bottom of outer edge**	**outer surface**	**inner surface**	**AISI 4130**
Al	0.36	0.25	0.45	0.46	0.41	
Si	0.29	0.31	0.29	0.32	0.30	0.22
Nb	4.41	4.67	4.83	4.26	5.22	
Mo	7.53	8.29	8.47	8.22	8.39	0.19
Cr	18.71	20.57	21.89	19.39	21.59	0.92
Fe	14.95	9.83	4.86	15.37	6.01	base
Ni	53.76	56.09	59.22	51.98	58.07	0.21
C						0.31

Chapter 8

Conclusions, review and recommendations

8.1 Conclusions

The purpose of this work was to enhance the insight in mechanisms that govern the laser cladding process and to develop all kinds of tools that facilitate the experimental efforts that are required to achieve successful industrial applications. With the therewith gained knowledge, the Dutch industry should be able to apply laser cladding, as it is a strategic technique for the improvement of high quality machine parts.

Firstly, a literature research had to be performed to get an idea of the state-of-the-art. Secondly, the effect of the laser beam power density distribution of the temperature profile on the surface had to be studied. From this study, it followed that a line source with a uniform power density in the lateral direction is preferred, because this shape results in the most uniform temperature distribution. This property, combined with the advantage of having a well defined spot that does not depend on the applied laser system, led to the development of a line integrator.

The developed line integrator fulfilled the expectations in terms of power density uniformity and spot definition, but could unfortunately not be used for laser cladding experiments. The laser power available on the author's laser system was not sufficient to achieve a melt pool in the surface. Therefore, all cladding experiments had to be performed with ordinary optics. With these experiments the effect of machining parameters on the cladding behaviour had to be studied. Some interesting phenomena, such as powder preheating and the occurrence of a plasma, needed special attention.
Finally, some industrial applications had to be developed to illustrate the opportunities offered by the laser cladding technique.

The literature research showed that laser cladding is predominantly performed by powder injection, because that method is more flexible and easier to control. This conclusion was supported by the experiments described in this thesis. The literature research also revealed that laser cladding is not a mature technique yet. In order to allow the cladding of products by non-academical personnel and, an effective transfer of results from laboratory to production environment, dedicated powder injection equipment, special optical systems and accurate process control systems are required.

A numerical model was developed which allows the prediction of the surface temperature distribution that is attained with an arbitrarily shaped laser beam intensity profile. The results showed, that for laser cladding a line source with a laterally uniform energy distribution is preferred over Gaussian, top-hat or rectangular laser beam energy distributions on the surface. Such a line source results in a uniform temperature distribution over the clad width and, hence, in more uniform surface properties. The other beam profiles result in a more or less pronounced temperature peak in the centre of the track.

Therefore, a line integrator was developed. The spot dimensions can be varied between 0.3 x 9.1 mm^2 and 1.1 x 7.8 mm^2 by changing the distance between the integrator and the workpiece. The lateral energy distribution in the spot remains uniform in this entire focal range. The achieved line spot is independent of the applied laser source and has well defined dimensions. This line integrator is therefore an essential element in the laser cladding system for an effective transfer of results between different CO_2 laser systems. Unfortunately, no successful cladding experiments could be performed with this line integrator, because the available laser power of 1800 W was not enough to melt the surface.

Experiments performed on laser cladding with preplaced cobalt base powder Metco 18C on a substrate consisting of steel X32CrV3 3, showed that this method is suitable for obtaining single clad tracks. The best results were characterised by a smooth surface and a moderate dilution of 10-15 % and did not suffer from porosity or cracking. However, the parameter range in which those good results could be obtained was rather small. The laser power must be between 1200 and 1400 W and the feed rate between 4 and 6 mm/s. Lower laser powers or higher feed rates are responsible for producing continuous clad tracks. At higher power levels or lower feed rates the dilution is increased.
The maximum hardness in the clad (800 Hv) was achieved with a dilution of 15 %. This hardness is higher than the typical hardness of the applied powder (500-550 Hv), that is achieved if the dilution is limited to less than 5 %.
Preheating of the substrate to 200 °C reduced the residual stress in the clad from 515 to 380 MPa. Higher temperatures were not applicable, because the chemical binder evaporated. As a consequence, irregularly shaped tracks, or no tracks at all, were produced.
The preplaced powder method is not suitable for the cladding of larger areas by making several adjacent partly overlapping tracks. Cracking of the cladded areas could not be prevented with the applied material combination. More seriously are the occurrence of a non-uniform mixing of elements and the occurrence of a severe degree of dilution (> 20 %), which are inevitable with this method.

Laser cladding with powder injection did result in good quality clad areas without severe dilution. Powder particles are injected as a powder stream into the laser generated melt pool. The particle stream can be seen as a powder cloud that attenuates some part of the laser beam. The particles are preheated due to this attenuation during their flight through the laser beam to maximally 120 °C in the applied experimental set-up. Melting of the particles starts after they enter the melt pool. The powder efficiency was very poor. Less than 30 % of the injected powder was utilised for the building of a clad track.
Simulations performed with the model, which was developed to predict the preheating of the particles, showed that this preheating temperature can be increased easily to 700 °C and that the efficiency can be enhanced to 98 %, by improving the injection parameter settings. The powder velocity, the particle size and, of course, the laser power are very important parameters for the preheating, whereas the efficiency is affected mainly by the powder stream properties.

In the applied configuration the measured attenuation by a powder cloud consisting of particles Stellite 6 was less than 5 %. This attenuation depends on the applied powder. Other experiments applied on nickel base Metco 15E and tungsten base Amdry 5843 resulted in maximum values of respectively 5 and 14 %. Due to these low attenuation levels, the powder cloud does not affect the laser beam intensity profile.
In spite of the relatively low particle temperature, it was observed that a plasma could be formed. This plasma effectively absorbs all laser radiation and stops the process. A plasma can only be formed over a certain critical powder density level (~ $2 \cdot 10^6$ W/cm^2). In the applied configuration, this level is reached in the focal area only. Plasma formation could be prevented largely by exchanging the initially applied lens with a focal length of 95 mm with one with a focal length of 154 mm. This increased the beam waist in the focal region from 167 to 270 μm, which reduced the mean power density in the focal area.

The applicability of laser cladding was shown successfully with the development of several industrial applications.

8.2 Review

Many experiments were performed to increase the insight in mechanisms that govern the laser cladding process. At the start of this work experiments were performed in a rather empirical way. Laser cladding results were highly unpredictable. Slight variations in machining parameters could yield quite different clad layer properties. Cladding experiments reported in the literature or performed on different sites could not be reproduced. It was clear that this situation had to change to introduce the laser cladding technology successfully in the Dutch industry.
It can be concluded now that the situation has improved considerably. The model that was developed, allows the prediction of melt pool formation. That is an essential part of laser cladding. Obviously, it is not possible to achieve the desired fusion bond between the cladding material and the substrate if not both materials are molten simultaneously at some time during the process.
The model is basically an extension of the classical moving point solution of Carslaw and Jaeger. By dividing the laser spot into several discrete point sources and integrating the solution of a single point source over the entire grid, an arbitrarily shaped laser beam intensity profile can be incorporated. The accuracy of the model was validated by comparing it to the analytical solution

of Ready, which is valid for the special case of a non-moving circular laser spot which has an uniform power density distribution.
The material properties that are required by the model were derived from laser transformation hardening experiments. Those experiments are characterised by a sharp transition from the martensitic heat affected zone to the non altered ferritic structure. The depth at which this transition occurs, i.e. the hardening depth, can be measured. By varying the material properties, the model was able to predict the hardening depth accurately. As a final check, new hardening experiments were performed with different parameters. By taking the previously calculated material properties into the model, the thus achieved hardening depth could be predicted. The calculated material properties are a kind of effective value. This effective value differs rather much from the value at room temperature.
The temperature distribution that is calculated with the model is quite realistic. However, two aspects should be kept in mind. Firstly, the model assumes constant material properties. However, these properties change upon the transformation from the solid to the liquid state. Moreover, the latent heat of fusion is not incorporated. Secondly, convective flows will occur in a produced melt pool. These flows will redistribute the heat over the entire melt pool. The real temperature will therefore be lower than the calculated theoretical temperature. Nevertheless, the model gives a reasonable impression of the temperatures that occur during laser cladding.

According to the literature, a line integrator with a laterally uniform power density distribution is favourable for laser cladding. Not only does such a line integrator yield a uniform temperature distribution over the width of a clad track and therewith constant clad properties, it also supplies a well defined laser spot on the surface which properties do no longer depend on the applied laser source. The achievement of a laterally uniform temperature distribution with this line integrator could be affirmed by simulations with the model discussed It was therefore decided to develop such a line integrator. An additional requirement imposed on the integrator is that it must be adjustable to different CO_2 laser systems.
This requirement complicated the design somewhat. The final design consists of three parts. The first part is a telescope that enlarges the incoming laser beam and makes it parallel and therewith independent of the laser system in terms of divergence. The enlargement is important to be able to split the beam into several smaller beamlets.

The second part is a cylindrical mirror which focuses the beam in the direction of movement (line length). The actual line is achieved with the third part, which is a faceted mirror that splits the beam in the sagital plane and recombines it in the focal plane. The line width is mainly determined by the facet size.
This approach of decoupling the spot length and the spot width facilitates the achievement of a line spot which focal points agree with each other. It also permits a variation of the spot dimensions around its design value by changing the distance between the integrator and the workpiece. The spot dimensions can thus be varied between 0.3 x 9.1 mm^2 and 1.1 x 7.8 mm^2 without losing the uniform energy distribution on the surface in the lateral direction.
The energy distribution that was achieved with this line integrator fulfilled the expectations. It was uniform over the entire width. Only some regularly spaced interference peaks could be noticed on top of the profile. However, the integrator could not be used in the author's laboratory for laser cladding. The available laser power of 1800 W was not enough to produce a melt pool in a steel substrate. In retrospect, this was predicted already by the developed surface temperature model.

To improve the insight in other aspects of laser cladding, experiments had to be performed. According to the literature, the powder methods are the most promising cladding methods. Two methods can be distinguished: preplaced powder and powder injection. The first method is the most straightforward one: the powder is applied as a paste (mixture of binder and powder) on the substrate, so no special equipment is required. The second method requires the use of a dedicated powder delivery system and a powder nozzle to direct the powder to the desired position. This latter method is supposed to be more flexible.
The purpose of the experiments on laser cladding with preplaced powder and powder injection was to study the effect of the machining parameters on the clad results and to determine the kind of application (or geometry) which the methods are most suited for.

The experiments performed on preplaced powder revealed the existence of a lower boundary of the laser power for a given feed rate. Below this threshold value no smooth, well bonded clad layers could be formed. A further increase of the laser power resulted in an increase of the dilution. Such a working region also exists for the feed rate.

The existence of a working region can be explained easily, as will be shown with the following example. For a typical clad experiment the following experimental parameters can be used:

laser power: 1300 W
feed rate: 5 mm/s
clad thickness: 0.5 mm
laser spot size: 3.0 mm

This implies that less than 10 % of the absorbed laser power is required for the melting of the preplaced powder. The major part contributes to the heating of the substrate. This fact can be noticed during the experiments. When cladding with 800 W instead of 1300 W, the laser power is sufficient for melting of the powder. However, this molten powder only forms droplets on the surface of the substrate and does not flow out. The surface temperature remains below the critical temperature that is necessary to allow wetting by the molten powder.
The hardness in the clad layers (cobalt base Metco 18C) depended strongly on the dilution. The produced good quality clad layers had a hardness of about 800 Hv, which is much higher than the hardness of the applied powder. This is an effect of the high cooling rates and the small degree of dilution that must be accepted in order to achieve a strong fusion bond between the two materials. The hardness could be increased further by allowing more dilution. However, this does not agree with the basic principle of laser cladding.

The experimental conclusions might suggest that laser cladding depends on the applied specific energy, because that parameter relates the clad properties to the laser power and the inverse of the feed rate. Many authors found this parameter very useful indeed. However, the author of this work can not agree with this. Experiments which were performed with the same specific energy, but different combinations of laser power and feed rate, did result in quite different clad layers. This is also to be expected, because different combinations of those machining parameters result in very different cooling rates. This can be illustrated with the following example. Assuming that we need a specific energy of 50 J/mm^2 and a laser spot of 3.0 mm to achieve a good clad layer, then three possible combinations are 500 W - 3.3 mm/s, 750 W - 5 mm/s and 1000 W - 6.7 mm/s. According to the model described in this thesis, this yields the following maximum temperatures on the surface: 2300 °C, 3300 °C and 4200 °C, whereas the interaction decreases from 1.8 to 1.2 and 0.9 s. Obviously, the cooling rates will differ considerably, as will the microstructure and the residual stress.

Those cases in which the specific energy could be used to explain the cladding results, this was merely the effect of only the laser power or the feed rate and not really a combined effect of these two parameters.

Larger areas were clad by applying several adjacent, partly overlapping tracks. However, this method could not produce crack-free clad layers. Preheating of the substrate to 200 °C helped to limit the number of cracks, but could not prevent it entirely. Preheating reduces the cooling rates in the clad layers and thus limits the induced residual stress. It is to be expected that preheating to higher temperatures can prevent the formation of cracks entirely. Unfortunately, this was not possible, because the binder evaporates at temperatures above 200 °C. In the author's opinion preheating of an entire workpiece is definitely no option in laser cladding, because that would require an additional stage in the production process and, more important, would undo one of the main advantages of laser cladding, i.e. no distortion of the workpiece. The only workable alternative to reduce the cooling rates and hence the residual stress is the application of a meander shaped pattern, because this reduces the cooling of the substrate between the subsequent short tracks somewhat. If this does not work out, than another, less crack-sensitive, material combination must be applied.
The conclusion on this series of experiments is that the preplaced powder method is suitable only for producing single track clad layers.

Fortunately, it was possible to achieve good quality, crack-free clad layers by means of the powder injection method. This method apparently introduces less residual stress in the clad layers due to the different process development. The melt pool is initially formed in the substrate. The melt pool volume is increased by injection of powder particles into it. After cooling down a new surface layer is achieved on top of the initial surface. Because there exists a good contact between the melt pool and the substrate right from the start of the process, the heat flow to the cold bulk is more uniform and can be controlled more easily: A more moderate cooling rate is achieved (less internal stress) and the melting depth and dilution remains limited.
The experimental region within which good clad layers could be achieved is rather small for the applied laser set-up. The laser power must be between 900 and 1050 W when using a feed rate of 5 mm/s and a laser spot size of 3.0 mm. Lower laser power levels are not sufficient to melt the substrate. It is interesting to note that the lower limit of about 1 kW when cladding with powder injection is well below the 1.3 kW that is required for cladding with preplaced powder.

The interaction between the injected powder particles and the laser beam required some special attention. It was noticed that those particles are preheated by the laser beam and thus influence the melt pool and the beam power density on the surface. This interaction has been modelled already by several others for Nd:YAG laser beams, but only once for a CO_2 laser beam. However, in that latter article the author treated the powder stream as a solid, which does not agree with the experimental observations. It was therefore decided to model this interaction more accurately. The powder stream is treated as a cloud that attenuates laser energy. The model follows the Beer-Lambert law, which assumes that the attenuation is a function of the path length through the cloud and a certain material specific extinction coefficient. That extinction coefficient had to be derived from experiments. A typical value for this very powder dependent parameter is 363 mm^{-1} for Stellite 6. Using this value in the model revealed that the average particle temperature in the current configuration remained below 20 °C. The model showed how to improve the process efficiency: the particle speed must be reduced and the geometrical properties of the powder injection nozzle must be changed. It should be possible to achieve a powder efficiency of 98 % and to increase the powder temperature.
The only real problem that was observed during cladding with powder injection was the occurrence of a plasma that stopped the process. An analysis of this phenomenon revealed that it occurred in the focal region only and was related to very small powder particles that contaminated the working chamber. The plasma formation during laser cladding can be avoided by applying optics with which the critical value of 10^6 W/cm^2 in the focal region is not exceeded.
In general, laser cladding with powder injection proved to be a rather hassle-free technique that has certainly more potential than the preplaced powder method.

8.3 Recommendations and future research

Although laser cladding is a technique that allows the development of advanced surface layers, the present field of applications is rather conservative. The technique is merely used as an alternative to conventional methods, instead of designing new products specifically for laser cladding. The majority of applications has been based on Stellite 6, which has been known already for more than 40 years for its hardfacing quality. Other powder mixtures have definitely more potential, but are not used yet.
This aspect can be solved in two ways. Firstly, the research institutes can develop some new applications themselves and present those examples to the in-

dustry. Secondly, some tools (models) can be developed that can accurately predict the microstructure in the clad layer and the clad geometry.
In this thesis a line integrator has been discussed. It is one of the new developments that can help to improve and simplify the laser cladding technique. One of the developments in the field of spot shaping is the use of beam scanners that allow a very flexible surface treatment with local variations of the energy distribution. Although it is recognised that this spot shaping offers many opportunities, no models are available to predict the clad properties that result from it.

The next step would be the integration of the available knowledge and models in CAD/CAM systems. Based on the desired surface properties such a system should be able to select a suitable substrate-powder combination and to generate the proper machine settings.
The present powder nozzles are usually nothing more than a simple copper tube. However, the new, non circular, spot shapes require dedicated powder nozzles in order to direct the powder to the desired position.
One of the supposed advantages of laser cladding with powder injection is the on-line variation of clad layer properties, such as the dimensions and the composition. However, this opportunity is not used yet, because suitable all-inclusive commercial process control systems are not available yet. Process and quality control will become one of the most important issues in laser cladding.

Appendix 1

Material properties

All properties at room temperature:

Metco 18C	**Stellite 6**	**Metco 15 E**
Co 40.8 % Ni 27.0 % Cr 18.0 % Mo 6.0 % Si 3.5 % Fe 2.5 % B 2.0 % C 0.2 %	Co 60.2 % Cr 28.0 % W 4.84 % Ni 2.12 % Fe 2.07 % Si 1.2 % C 1.1 % Mn 0.34 % B 0.14 %	Ni 70.5 % Cr 17.0 % Si 4.0 % Fe 4.0 % B 3.5 % C 1.0 %
grain size: 53-125 µm density: 8350 kg/m^3 specific heat: 442 J/kg/K melting point: 1120 °C	grain size: 45-150 µm density: 8460 kg/m^3 specific heat: 442 J/kg/K melting point: 1340 °C thermal conductivity: 14.8 W/m/K thermal expansion: $14 \cdot 10^{-6}$ K^{-1}	grain size: 53-106 µm density: 7700 kg/m^3 melting point: 1024 °C

Amdry 5843	**C45**	**X32CrMoV33**
W 80.7 % Co 10.0 % C 5.3 % Cr 4.0 %	Fe balance Mn 0.70 % C 0.44 % Si 0.26 % Cr 0.18 %	Si 0.3 % Cr 3.0 % Mo 2.8 % Fe balance V 0.5 % C 0.3 %
grain size: 16-53 µm density: 12500 kg/m^3 melting point: 3000 °C	density: 7850 kg/m^3 specific heat: 460 J/kg/K melting point: 1450 °C thermal conductivity: 48 W/m/K thermal expansion: 13.9·10^{-6} K^{-1}	density: 7850 kg/m^3 specific heat: 460 J/kg/K melting point: 1450 °C thermal conductivity: 30 W/m/K thermal expansion: 11.1·10^{-6} K^{-1}

Appendix 2

Determination of the absorption of laser energy in the base material

The absorbed laser power is taken as an input parameter for the (in the previous section presented) numerical method. Hence, it is necessary to have a means to determine its quantity.
A calorimetric method was applied in this study. The principle of this method is shown schematically in figure A2.1. This figure shows the temperature response of a sensor placed at a certain distance from the heat input. When the heat input duration is short compared to the measurement time, the absorbed laser power (*AP*) can be calculated by extrapolating the cooling curve conditions [Bea, 1990; Borik, 1990; Tangelder, 1992):

$$AP = \frac{m c_p \Delta T_{\max}}{t_i} \qquad \textit{Eq. A2.1}$$

where t_i is the pulse duration, m is the mass of the specimen and ΔT_{max} is the maximum temperature rise, which equals T_{max}-T_0.

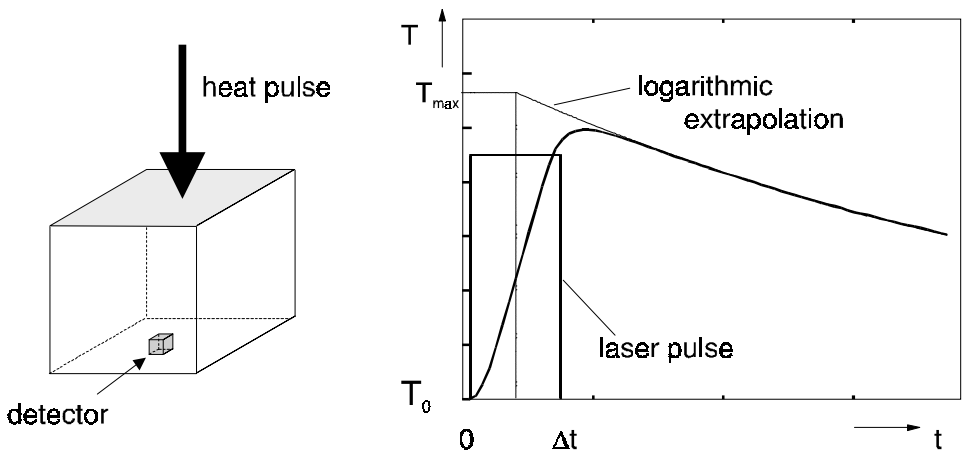

Fig. A2.1 Left: Set-up for calorimetric measurement of the absorbed laser energy. Right: response of the detector to the heat pulse.

Because the specimen exchanges heat with the surrounding air by free convection, the cooling curve must be extrapolated to $t=½\Delta t$. This time approximately marks the position on the heating curve where the effect of the heat input becomes less important than the cooling. For the extrapolation of the cooling curve, it is sufficient to perform only two measurements, as it was shown [Borik, 1990; Tangelder, 1992] that the maximum temperature rise in the material equals:

$$\Delta T_{\max} = T_{\max} - T_0 = e^{\frac{t_1 \ln(T_2 - T_0) - t_2 \ln(T_1 - T_0)}{t_1 - t_2}} \qquad \textit{Eq. A2.2}$$

A proper choice of t_1 and t_2, i.e. $t_2=2t_1$ simplifies this expression to:

$$\Delta T_{\max} = \frac{(T_1 - T_0)^2}{T_2 - T_0} \qquad \textit{Eq. A2.3}$$

The temperature of the workpiece is measured by means of one type K copper-constantane thermocouple pair. The typical sensitivity is 40.2±0.1 μV/K.
The irradiated base material (steel C45) was polished and degreased with ethyl-alcohol. The dimensions of a typical sample are 60 x 40 x 8 mm. These dimensions allow the formation of a 40 mm long track with a feed rate of 3-8 mm/s in 5-13 seconds. Such feed rates are typical for laser cladding. The drawback of

this sample size is the large thermal time constant[3] of about 80 seconds. Depending on the number of applied clad tracks, the temperature rise ranges from 2 to 30 °C.

The absorptivity was measured with and without Stellite 6 powder injection. In the first case the absorption depends mainly on the presence of a melt pool in the substrate. The absorption of laser energy in a melt pool is about 30 % (figure A2.2). Upon increasing the feed rate of the base material with respect to the laser beam, the surface temperature decreases. If a melt pool is no longer present, which is in this case at feed rates over 8 mm/s, the absorption is limited to about 10 % (figure A2.2). These values for the absorption have been confirmed by other authors [Grünenwald, 1996; Ollier, 1995; Picasso, 1994; Stern, 1990].

The measured absorptivity in the second case, i.e. with powder injection, is shown in figure A2.3. A comparison with figure A2.2 shows that the absorption during laser cladding conditions is slightly lower. This can only be contributed to the power attenuation by powder particles that are not directed in the melt pool.

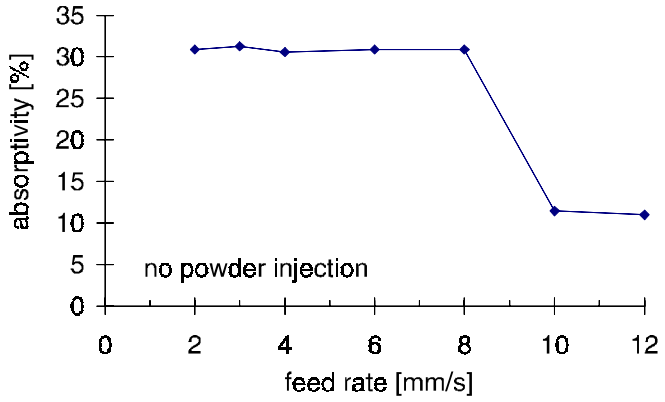

Fig. A2.2 Absorption of CO_2 laser radiation in a C45 surface. Laser power: 1350 W; spot diameter: 3.0 mm.

[3] The thermal time constant is defined as $\tau=\delta^2/4\kappa$, where δ represents the longest diffusion distance in the workpiece. After this time a homogeneous temperature distribution with a constant heat exchange to the environment is obtained and the two measurements can be made.

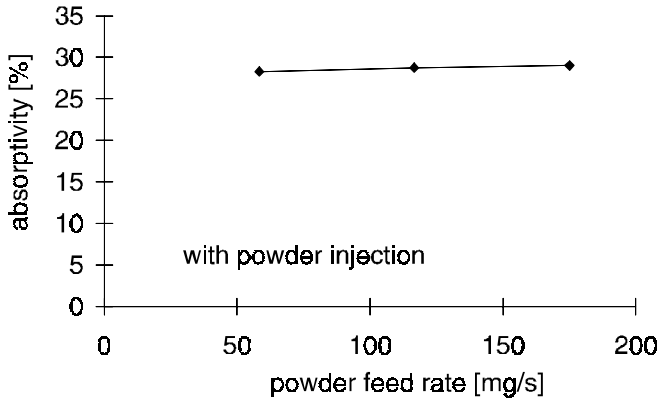

Fig. A2.3 Absorption of CO_2 laser radiation in a C45 surface under cladding conditions with a feed rate of 3 mm/s (laser power: 1350 W; spot diameter: 3.0 mm).

Appendix 3

Experiments on laser cladding with preplaced powder

coating material: Metco 18C (appendix 1)
substrate: X32CrMoV3 3 (appendix 1)
chemical binder: Nicrobraz type II
laser beam diameter: 3.0 mm (defocused) measured with Prometec UFF 100 beam analyser
laser system: Rofin Sinar 1700RF CO_2 laser with a mixed TEM_{00} and TEM_{10} intensity profile
optics: salt plate protected ZnSe lens with focal length of 95 mm
coating thickness: 0.4 mm
shielding gas: argon
power meter: Optical Engineering P-2000 (accuracy: 5%)
measurement of internal stresses by means of roentgen diffraction ($\sin^2\psi$ method).
Equipment: Rigaku Strainflex MSF-2M goniometer.

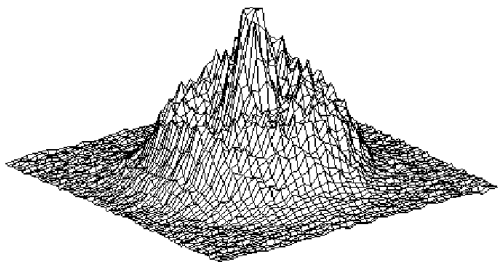

Effect of laser power and substrate temperature on residual stress and number of cracks per cm in case of laser cladding with preplaced power with overlapping tracks

10 overlapping adjacent tracks

determination of cracks: fluorescent penetrant method.

series 1: feed rate: 6 mm/s
overlap between adjacent tracks: 2.4 mm
series 2: feed rate: 8 mm/s
overlap between adjacent tracks: 1.8 mm
series 3: 12 mm/s
overlap between adjacent tracks: 1.8 mm

series	**laser power** [W]	**number of cracks** [cm^{-1}]	**longitudinal stress** [MPa]
1	1000	1.25	593
	1200	0.75	812
	1400	0.50	1023
	1600	0.25	1157
2	1200	2.00	548
	1400	1.75	602
	1600	0.75	621
3	1200	2.50	479
	1400	2.00	482

Appendix 4

Powder-substrate combinations reported in literature

base material	coating	source
FERROUS		
C40/C45	F600, C76	Burchards, 1990
	Stellite 157, F, 6, Deloro 40, 22	Gassmann, 1992
	Nicrobor 40, Deloro 60	Brenner, 1996
	Co/Ni-Al, Co/Ni-10Al, Ni-15Al/Co	Carvalho, 1995
	Stellite 6	Kreutz, 1995
	Stellite F, SF6, 1, 6, CTS 10136	Magrini, 1986
	Stellite F, SF6, 1, 6, Metco 15E, Colmonoy 5, CTS 10136	Ramous, 1989
low carbon steel	AISI 304, 316	Fouquet, 1994
C15/C20/C22	Hadfield steel	Pelletier, 1996
	mixture of ZrO_2-8%Y_2O_3 and AISI 316	Jasim, 1989
	Triballoy T-800	Amende, 1990
mild steel En1a	Al-Mn-Fe, Al-Co-Fe, Ni-Co-Fe	Steen, 1992

base material	coating	source
mild steel En3b	Stellite 6+SiC	Abbas, 1989 (2x), 1990, 1991
	AISI 316	Weerasinghe, 1983
	Stellite 6	Abbas, 1989, 1991
	Alloy 4815+SiC, Alloy 4815	Abbas, 1989
	Al-Sn10Si4Cu1 with Ni sandwich	Ellis, 1995
mild steel	Triballoy T-800	Amende, 1990
	Colmonoy 62	Lugscheider, 1990
	Ni-Cr-Nb-B, Ni-Cr-Ta-B	Lugscheider, 1990
	Ni-Cr-Fe-Si-B-Cu-Mo-C	Pelletier, 1992
	binder+WC/W_2C	
	Ni-Cr-Nb-B, Ni-Cr-Ta-B, Ni-Cr-B-Si, CoC+WC	Oberländer, 1992
	Ni-Cr-Fe-Ti	Tosto, 1994
	AISI 304	Fouquet, 1993
mild steel St 37	Stellite 6, Fe-Cr, Fe-Cr-P-C	Marsden, 1990
	F600, C76	Burchards, 1990
	Ni-Cr-B-Si	Sepold, 1989
	Ni-Cr-B-Si-Fe	Becker, 1991
	Stellite 21	König, 1994
	CuSn20+diamond	Lang, 1994
mild steel St 52	Ni-Cr-B-Si, WC/Co	Becker, 1989
	Ti (bond)+Al_2O_3/TiO_2	Lugscheider, 1994
ASTM A36	Stellite 6, 157, 156, 1, 12, 21, 158, F	Metzbower, 1986
AISI 1016	Fe-Cr-Mn-C, Cr-Mn-C	Singh, 1985
	Cr-Mn-C	Mazumder, 1986 (2x)
	Ni-Cr-Al-Hf	Singh, 1987
	Fe-Cr-Mn-C	Eiholzer, 1985; Singh, 1987
	Fe-Cr-C-W	Choi, 1994
AISI 1018 ~ A_3 steel	Fe-Cr-C-W	Komvopoulos, 1990
AISI 1020	AISI 309, Inconel 625	Bruck, 1988
	Nichrome	Ayers, 1981
	TiC+Stellite 6, Co+Stellite 6, Co+Haynes 25, $MoSi_2$+Stellite 6	Tucker, 1984
	Fe-Cr-C-W, Fe-Cr-Mn-C	Komvopoulos, 1994
	Ni-Cr-Si-B	Yang, 1988
	WC/Co	Yang, 1990
	Fe-Cr-Si-B	Yang, 1991

base material	**coating**	**source**
	Ni-Cr-Al (bond)+Al, Ni-Cr-Al (bond) +Zr	Tao, 1994
	Fe-Cr-Mo, Fe-Cr-Si_3N_4, Fe-Cr-Mo-Si_3N_4	Huang, 1995
AISI 1043/1045	WC-Co-Ni-Cr-Fe-Si-B-C, mixture Co/WC+Ni-Cr alloy	Fernandez, 1995
	composite SiC and Ni	Pei, 1995
	Ni-Cr-B-Si+TiN, Ni-Cr-B-Si +SiC	Pei, 1996
AISI 304	Stellite F, SF6, 1, 6, CTS 10136	Magrini, 1986
	Stellite 6, Colmonoy 5	Corchia, 1987
	Stellite 6	Liu, 1983
	Colmonoy 5, Metco 15E, Stellite F, SF6, 1, 6, CTS 10136	Ramous, 1989
	Stellite F, SF6	Giordano
	Ni-Cr-Co-Fe, Cenium 36, Metco 18C, 41C	Pelletier, 1993
	Cr_2O_3+pure Fe	Zhou, 1991
	Stellite 6, Eutrolloy 16262, Cenium Z20	Yellup, 1995; Li, 1992
AISI 316	Stellite F, SF6, 1, 6, CTS 10136	Magrini, 1986
	Colmonoy 5, Metco 15E, Stellite F, SF6, 1, 6, CTS 10136	Ramous, 1989
	Stellite 6	Bruck, 1988
	Metco 443 (Ni-Cr-6%Al)	Damborenea, 1994
AISI 400	Stellite 1, 6, 21, Stellite 21+Nb-C, Stellite 21+CrC, Ni-Cr-Al-Y+Al, Ni-Cr-Al-Y + Nb-C, Ni-Cr-Al-Y+CrC	Hirose, 1995
AISI 410	Stellite 6	Liu, 1983
AISI 1008	Stellite 6	Pizurova, 1993
AISI 4140	Metco 461, 202NS, Y_2O_3+ZrO_2	VandeHaar, 1988
X7Cr13 steel	TiC/Ni	Gassmann, 1992
4Cr13 stainless steel	Ni-Cr-B-Si+ZrO_2	Pei, 1996
X20Cr13	Stellite 6	Frenk, 1991
X2CrNiMo18 14	Stellite 6	Frenk, 1991, 1993
stainless steel	Stellite 6, E16001, E16019	Frenk, 1991
	graphite+BN	Sakamoto, 1995
X8CrNi18 10	Stellite 157, F, 6, Deloro 40, 20	Gassmann, 1992
20Ni4Mo steel	Ni-Cr-Fe-Si-B-C (bond)+WC	Zhu, 1993

base material	coating	source
X45CrSi9	Stellite 6, F	Küpper, 1990; Wissenbach, 1991
carbon steel	Cu/Ni	Bruck, 1987
stainless steel	Inconel 625+CrC, AISI 410	Bruck, 1988
Z10CNDV 12-2 martensitic stainless steel	Stellite F	Hernandez, 1986
RENE 80	Ni-Al-Cr-Hf	Sircar, 1988, 1989; Ribaudo, 1989
0.4C 0.6Mn steel	Wallex 6 Colmonoy 5	Monson, 1986
0.16C 1.2Mn steel	Ni-Cr-Si-B	Chen, 1989
C-Mn steel	Stellite 6, Eutrolloy 16262, Cenium Z20	Yellup, 1995
0.42C 1Cr Mo steel	Ni-base alloy	Pelletier, 1994
16MnCr5 steel	Stellite 21(bond)+WC/W_2C, Stellite 21(bond)+WC/CoNiBSi(bond)+WC/Co, NiBSi(bond)+WC/W_2C	Techel, 1995; Nowotny, 1994; Luft, 1995
90MnCrV8	Nicrobor 40, Deloro 60	Brenner, 1996
SAE 4340	Stellite 6	Riabkina-Fishman, 1996
	Co-base alloy	Fishman, 1995
SAE 4620	Ni-Al-Mo (bond)+Cr_2O_3+TiO_2	Cuetos, 1993
SAF 2205 duplex steel	Cr_2O_3+pure Fe	Zhou, 1991
steel 1.4571	LC2.3B, LC1.5A, LC0.1C	Volz, 1994
steel 1.4541 ~	LC2.3B, LC0.1C, LC15.7C. LC5.0C	Wolf, 1995
X6CrNiTi18 10	ZrO_2/Y_2O_3, Al_2O_3, Cr_2O_3, $Cr_2O_3/SiO_2/TiO_2$	Lugscheider, 1994
GGG40 cast iron	Stellite 1, 6	Wolf, 1994
	Ni-base alloy	Gasser, 1996
GGG60 cast iron	Al-bronze	Haferkamp, 1994
GG25 cast iron	Stellite 1, 6	Wolf, 1994
spheroidal cast iron	Cenium Z20, Stellite 6, Eutrolloy 16262	Yellup, 1995
	Stellite 6	Flinkfeldt, 1994
	Ni-base alloy	Pelletier, 1994
Fe-base	Ni-Cr(bond)+TiC, Ni-Cr(bond)+WC+Ni, Ni-Al-Si(bond)+TiC,	Pelletier, 1994

base material	**coating**	**source**
	Ni-Al-Si(bond)+ WC+Ni	

NON-FERROUS

Inconel 625	Al+SiC	Jasim, 1993
	Triballoy T-400	Cooper, 1989
Inconel 718	Ni-Cr-Al-Hf	Singh, 1987
Inconel 738	Ni-Cr-Al-Si-Y	Marsden, 1990
Inconel 800H	silica	Fellowes, 1990
Nicrobor 20	WC/Co	Gassmann, 1992
Ni-Cr-Al	Ni-Cr-Al+ZrO_2 (Metco 202NS),	Damborenea, 1993
	Ni-Cr-Al+ZrO_2(Metco 202NS)+	
	Y_2O_3+Y+Zr	
Ni	Al	Kar, 1989
	Fe-Cr-P-C	Marsden, 1990
	Hf	Kar, 1988; Sircar, 1989
Al 333	Ni-Al bronze (Cu-Al-Ni-Fe)	Liu, 1992
	Ni-alloy FP-5 + bond Ni-Al bronze	Liu, 1994
Al 6061	Al+SiO_2	Hosson, 1995
Al 7075	SiC	Ricciardi, 1990
Al+7%Si	Ni-Al, Al-Si	Sallamand, 1993
AlSi12	CuAl-bronze	Grünenwald, 1996
AlCu4SiMg (H15)	Stellite 6, pure Si	Li, 1992
AlMgSi	AlMgSi0,5, AlSi12	Reichelt, 1996
Al-base	Al+SiC	Hegge, 1990
Ti-6Al-4V	Triballoy T-400	Cooper, 1989
	Nimonic 80A, Inconel 100	Coquerelle, 1986
	Ti-6Al-4V+cubic BN	Lang, 1994
	Ti-6Al-4V+Cr_2O_3, Ti-6Al-4V+Cr_3C_2,	Folkes, 1994
	Ti-6Al-4V+WC, Ti-6Al-4V+Mo_2C	
Mg-base	Mg-Zr, Mg-Al	Wang, 1990
	Mg-Al	Wang, 1993
Cu-Cr-Zr (Elbrodur)	Deloro 50, PEX 23	Reichelt, 1996

base material	coating	source
Cu-Zn-Pb (brass)	Ni-base alloy	Pelletier, 1994
Cu-Sn (bronze)	Ni-base alloy	Pelletier, 1994
Cu-base	Ni-Al-Si (bond)+WC+Ni, Ni-Al-Si (bond)+TiC, Ni-Cr (bond) +TiC, Ni-Cr (bond)+WC+Ni	Pelletier, 1994
PET	Metco 101B-NS	Ayrault, 1996
PMMA	Metco 101B-NS	Ayrault, 1996
UNKNOWN MATERIAL	Mo-Cr-CrC-Ni-Si	Belmondo, 1979
	Stellite 156	Nurminen, 1983
	Stellite SF6, 158, 6, 90, Triballoy T-700, Deloro 60, Haystellite 1	Matthews, 1983
	TiC/Ni, TiC/Ni+Ni-Cr-B-Si (bond), TiC/Ni+Co-Cr-W-C (bond), WC/Co, WC/Co +Ni-Cr-B-Si (bond),	Lugscheider, 1992
	WC/Co +Co-Cr-W-C (bond)	Fux, 1992
	Co-Cr-W-Si-B-C	Smurov, 1992
	Metco 461NS (bond)+Metco 205NS	Gassmann, 1992
	Stellite 21 (bond)+ WC/Co, Stellite 21 (bond)+ WC, Stellite 21 (bond)+ WC/Ni	Hosson, 1996
	Stellite 1, 6, 20, SF20, 21 WC/Co+Ni-B-Si	Nowotny, 1994

Dankwoord

Een proefschrift kan niet tot stand komen zonder de steun en bijdrage van een heleboel anderen. Allen die hebben bijgedragen aan het welslagen van dit promotiewerk wil ik bij deze bijzonder bedanken.
Mijn dank gaat allereerst uit naar mijn collega-AIO's. Met name jullie prettige aanwezigheid en de goede sfeer heb ik erg op prijs gesteld. Chris, Frank, Gert-Willem, Herman, Paul en Roelof bedankt voor de leuke tijd en veel succes met jullie eigen werk.
Bertus en Jan zijn mij behulpzaam geweest bij het maken van proefstukken en het experimenteren. Als de onmisbare stille krachten op de achtergrond hebben zij veel gedaan voor dit project. Michel was altijd erg behulpzaam bij het materiaalkundig onderzoek. Behalve het werk was er daarbij ook altijd tijd voor de menselijke kant van het werk. Michel, sterkte met de komende veranderingen!
Veel studenten hebben tijdens hun afstuderen werk verzet voor dit project. Er werd hard gewerkt, veel opstellingen werden gebouwd en er werd vooral veel papier geproduceerd. Ik heb veel plezier aan de samenwerking met jullie beleefd.
"Een gezonde geest in een gezond lichaam" is een bekend gezegde dat voor wij zeer van toepassing is. Het uurtje hardlopen of tennissen tussen de middag was vaak hard nodig om weer fris met het werk verder te kunnen. Gelukkig voelden velen zich geroepen met mij mee te gaan. Vooral met Herman heb ik heel wat

kilometertjes in de mooie Drienerlose bossen afgelegd. Mijn toen wat mindere snelheid heeft hem heel wat spierpijn opgeleverd. Gelukkig gingen we ook wel eens tennissen. Dat ging me dan gelukkig wat beter af …
Verder dank aan Johan Meijer en prof. Beckmann. Vele discussies en suggesties leidden uiteindelijk dan toch tot dit proefschrift. De meningen liepen wel eens wat uiteen en ook de manier van aanpak was soms verschillend, maar dankzij de wederzijdse inzet is er toch een resultaat geboekt dat er gezien mag worden.
Natuurlijk ook aandacht voor het thuisfront: Iris heeft zich erg veel moeten ontzeggen voor dit proefschrift. Henk heeft vele maanden zijn geliefde computer belangeloos uitgeleend. Linda heeft het geheel doorgelezen en gecorrigeerd daar waar het Engels echt niet door de beugel kon. Brigiet, Berend, Lisette en Ronald waren zo af en toe graag bereid een dagje op Chantal te passen, zodat ik flink op kon schieten. Frank gaf het nodige advies en zorgde de laatste tijd voor een gastvrij onderkomen in Den Haag.
Tot slot, het ga jullie allen goed!

Marcel

References

[Abbas, 1989] Abbas, G., West, D.R.F., 1989, Laser Produced Composite Metal Cladding, High Power Lasers and Laser Machining Technology, Proc. SPIE, vol. 1132, pp. 232-2236

[Abbas, 1990] Abbas, G., West, D.R.F., Steen, W.M., 1990, Wear Studies of Variable Composites on Stellite-SiC Laser Clad Deposits, Key Engineering Materials Vols 46 & 47, pp. 97-102

[Abbas, 1991] Abbas, G., West, D.R.F., 1991, Laser Surface Cladding of Stellite and Stellite-SiC Composite Deposits for Enhanced Hardness and Wear, Wear, vol. 143, pp. 353-363

[Amende, 1988] Amende, W., 1988, Die Veredelung metallischer Randschichten mit dem CO_2-Hochleistungslaser, Laser und Optoelektronik, no. 2, pp. 44-47

[Amende, 1988] Amende, W., 1988, The Production of Wear-Resistant Zones on Tools by Means of the CO_2 Laser, Proc. LIM-5, pp. 119-125

[Amende, 1989] Amende, W., 1989, Oberflächenbehandlung von Werkzeugen und Motorkomponenten mit Laser, VDI-Z, vol. 131, no. 6, pp. 80-83

[Amende, 1990] Amende, W., Nowak, G., 1990, Hard Phase Particles in Laser Processed Cobalt Rich Claddings, Proc. ECLAT '90, pp. 417-428

[Anthony, 1977] Anthony, T.R., Cline, H.E., 1977, Surface Rippling Induced by Surface-Tension Gradients During Laser Surface Melting and Alloying, J. of Applied Physics, vol. 48, no. 9, pp. 3888-3894

[Arlt, 1994] Arlt, A.G., Müller, R., 1994, Technology for Wear Resistant Inside Diameter Cladding of Tubes, Proc. ECLAT '94, pp. 203-212

[Ashby, 1984] Ashby, M.F., Easterling, K.E., 1984, The Transformation Hardening of Steel Surfaces by Laser Beams - I: Hypo-Eutectod Steels, Acta Metall., vol. 32, no. 11, pp. 1935-1948

[Atamert, 1989] Atamert, S., Bhadeshia, H.K.D.H., 1989, Comparison of the Microstructures and Abrasive Wear Properties of Stellite hardfacing Alloys Deposited by Arc Welding and Laser Cladding, Metall. Trans. A, vol. 20A, no. 6, pp. 1037-1054

[Ayers, 1981] Ayers, J.D., 1981, Particulate Composite Surfaces by Laser Processing, Proc. Lasers in Metallurgy, pp. 114-125

[Ayers, 1984] Ayers, J.D., 1984, Wear Behaviour of Carbide-Injected Titanium and Aluminium Alloys, Wear, vol. 97, pp. 249-266

[Ayrault, 1996] Ayrault, S., Canonge, C., Vannes, A.B., 1996, Laser Cladding on Thermoplastic Polymers, Lasers in Engineering, vol. 5, pp. 11-22

[Backes, 1992] Backes, G. et al., 1992, Prozeßdiagnose beim Beschichten mit CO_2-Laserstrahlung, Proc. LASER 1991, pp. 249-254

[Backes, 1994] Backes, G., et al., 1994, Prozeßkontrolle und -regelung beim Beschichten, Materialbearbeitung mit CO_2-Laserstrahlen höchster Leistung, VDI, Düsseldorf, pp. 89-93

[Bass, 1987] Bass, M., 1987, Laser-Materials Interactions, Encyclopedia of Physical Science and Technology, vol. 7, pp. 129-145

[Basu, 1992] Basu, B., Date, A.W., 1992, Rapid Solidification Following Laser Melting of Pure Metals I: Study of Flow Field and Role of Convection, Int. J. Heat Mass Transfer, vol. 35, pp. 1049-1058

[Basu, 1992] Basu, B., Date, A.W., 1992, Rapid Solidification Following Laser Melting of Pure Metals II: Study of Pool and Solidification Characteristics, Int.J. Heat Mass Transf., vol. 35, pp. 1059-1067

[Bea, 1990] Bea, M., 1990, Transient Behaviour of Optical Components and Their Correction by Adaptive Optical Elements, Proc. ICALEO '90

[Becker, 1987] Becker, R., Binroth, C., Sepold, G., 1987, Laserstrahlumschmel-zen, -Beschichten und -Legieren von Oberflächen, Proc. Lasermaterialbearbeitung für den Automobilbau, pp. 93-97

[Becker, 1989] Becker, R., Sepold, G., 1989, Laserstrahl -Draht und -Spritzbeschichten, Zwei Zukünftige Beschichtungstechniken, Int. Conf. on Surface Technology

[Becker, 1991] Becker, R., et al., 1991, Laserstrahlbeschichten von NiCrBSi-Hartlegierungen durch einen Pulverförderprozeß, HTM, vol. 46, no. 2, pp. 86-90

[Beckmann, 1989] Beckmann, L.H.J.F., 1989, Materiaalbewerking met Lasers, PATO

[Beckmann, 1990] Beckmann, L.H.J.F., et al., 1990, Oppervlaktebehandelen met Lasers, Lasertransformatieharden, IOP-metalen, University of Twente, Enschede, Dept. of Mech. Eng.

[Beckmann, 1991] Beckmann, L.H.J.F., 1991, A Small Computer Program for Optical Design and Analysis Written in C, International Lens Design Conference, SPIE, vol. 1354

[Beckmann, 1995] Beckmann, L.H.J.F., Ehrlichmann, D., 1995, Optical Systems for High-Power Laser Applications: Principles and Design Aspects, Optical and Quantum Electronics, vol. 27, pp. 1407-1425

[Belmondo, 1979] Belmondo, A., Castagna, M., 1979, Wear-resistant coatings by Laser Processing, Thin Solid Films, vol. 64, pp. 249-256

[Bergmann, 1994] Bergmann, H.W., et al., 1994, Industrial Applications of Surface Treatments with High Power Lasers, Materials Science Forum, vol. 163-165, pp. 377-404

[Bergmann, 1995] Bergmann, H.W., Laser Surface Heat Treatment of Tools, Manufacturing Systems, vol. 24, no. 5, pp. 411-421

[Beyer, 1985] Beyer, E., 1985, Einfluß des Laserinduzierten Plasmas beim Schweißen mit CO_2-Lasern, Darmstadt, Ph.D. Thesis

[Bianco, 1994] Bianco, M., Rivela, C., Talentino, S., 1994, On-line Surface Treatment Feasibility of Industrial Components by Means of CO_2 Power Laser, Proc. Laser Materials Processing: Industrial and Microelectronics Applications, SPIE, vol. 2207, pp. 53-61

[Blake, 1985] Blake, A.G., Eboo, G.M., 1985, Laser Hardfacing Turbine Blades Using Dynamic Powder Feed, Laser Welding and Surface Treatment

[Blake, 1988] Blake, A.G., et al., 1988, Laser Coating Technology: A Commercial Reality, Laser Beam Surface Treating and Coating, Proc. SPIE, vol. 957, pp. 56-65

[Bloehs, 1993] Bloehs, W., Rudlaff, T., Dausinger, F., 1993, Flexible Anpassung der Intensitätsverteilung beim Laserstrahlhärten unterschied-licher Bauteilgeometrien, HTM, vol. 48, no. 1, pp. 13-19

[Bloehs, 1996] Bloehs, W., et al., 1996, Recent Progress in Laser Surface Treatment: I. Implications of Laser Wavelength, J. of Laser Applications, vol. 8, pp. 15-23

[Borik, 1990] Borik, S., Giesen, A., 1990, Finite Element Analysis of the Transient Behavior of Optical Components under Irradiation, Boulder Damage Symposium

[Bos, 1993] Bos, Moes, H., 1993, Frictional Heating of Elliptic Contacts, Proc. of the 20th Leeds-Lyon Symposium on Tribology, Lyon

[Box, 1978] Box, G.E.P., Hunter, W.G., Hunter, J.S., 1978, Statistics for Experimenters, John Wiley & Sons, New York

[Brandt, 1984] Brandt, A., 1984, Multigrid Techniques: 1984 Guide with Applications to Fluid Dynamics, GMD-studien, no. 85

[Brenner, 1996] Brenner, B. Reitzenstein, W., 1996, Laser Hardening of Turbine Blades, Industrial Laser Review, April, pp. 17-20

[Brenner, 1996] Brenner, B., et al., 1996, Induktiv unterstütztes Laserauftragschweissen - eine Hybridtechnologie überwindet Anwendungsgrenzen, Proc. ECLAT '96, pp. 469-476

[Bruck, 1987] Bruck, G.J., 1987, High Power Laser Beam Cladding, J. of Metals, vol. 39, no. 2, pp. 10-13

[Bruck, 1988] Bruck, G.J., 1988, A study of Fluxing Agents in High Power Laser Beam Cladding, LIM-5, pp. 281-299

[Bruck, 1988] Bruck, G.J., 1988, Fundamentals and Industrial Applications of High Power Laser Beam Cladding, Laser Beam Surface Treating and Coating, Proc. SPIE, vol. 957, pp. 14-28

[Burchards, 1989] Burchards, D., et al., 1989, Laserdrahtbeschichten, Mat.-Wiss. u. Werkstofftechnik, vol. 20, pp. 405-409

[Burchards, 1990] Burchards, D., et al., 1990, Laserdrahtbeschichten, Laser - Technologie und Anwendungen, pp. 307-310

[Burchards, 1992] Burchards, D., He, X., Mordike, B.L., 1992, Laseraufgetragene Verschleißschutzschichten, Proc. LASER 1991, pp. 355-359

[Cai, 1990] Cai, G., Molino, G., 1990, Comparison Between Cladding by Means of Plasma Spray and the More Recent Technologies of Plasma Transferred Arc, Plasma Semi-Transferred Arc and Laser on Traditional Filler Material and New Nickel Base Boron-Free Alloys, Proc. Laser-6, pp. 79-90

[Carslaw, 1959] Carslaw, H.C., Jaeger, J.C., 1959, Conduction of Heat in Solids, Oxford University Press

[Carvalho, 1995] Carvalho, P.A., et al., 1995, Automated Workstation for Variable Composition Laser Cladding - Its Use for Rapid Alloy Scanning, Surface and Coatings Technology, vol. 72, pp. 62-70

[Chabrol, 1987] Chabrol, C., Hernandez, J., Vannes, A.B., 1987, Determination of Internal Stresses in Laser Treated Surfaces and Cladding, Laser Treatment of Materials, pp. 91-99

[Chan, 1984] Chan, C., Mazumder, J., Chen, M.M., 1984, A Two-Dimensional Transient Model for Convection in Laser Melted Pool, Metall. Trans. A, vol. 15A, pp. 2175-2184

[Chen, 1989] Chen, X., Tao, Z., 1989, Maximum Thickness of the Laser Cladding, Key Engineering Materials Vols 46 & 47, pp. 381-386

[Choi, 1994] Choi, J., Mazumder, J., 1994, Non-equilibrium Synthesis of Fe-Cr-C-W Alloy by Laser Cladding, J. of Materials Science, vol. 29, pp. 4460-4476

[Cline, 1977] Cline, H.E., Anthony, T.R., 1977, Heat Treating and Melting Material with a Scanning Laser or Electron Beam, J. of Applied Physics, vol. 48, no. 9, pp. 3895-3900

[Cooper, 1988] Cooper, K.P., 1988, Surface Treating by Laser Melt/Particle Injection, Laser Beam Surface Treating and Coating, Proc. SPIE, vol. 957, pp. 42-53

[Cooper, 1989] Cooper, K.C., Slebodnick, P., 1989, Recent Developments in Laser Melt/Particle Injection Processing, J. of Laser Applications, October 1989, pp. 21-29

[Coquerelle, 1986] Coquerelle, G., Collin, M., Fachinetti, J.L., 1986, Laser Cladding and Alloying, Proc. LIM-3, pp. 197-205

[Corchia, 1987] Corchia, M., et al., 1987, Microstructural Aspects of Wear-Resistant Stellite and Colmonoy Coatings by Laser Processing, Wear, vol. 119, pp. 137-152

[Cuetos, 1993] Cuetos, J.M., et al., 1993, Plasma-Sprayed Coatings Treated with Lasers: Tribological Behaviour of Cr_2O_3, Wear, vol. 169, pp. 173-179

[Damborenea, 1993] Damborenea, J. de, Vázquez, A.J., 1993, Laser Cladding of High Temperature Coatings, J. of Materials Science, 1993, vol. 28, pp. 4775-4780

[Damborenea, 1994] Damborenea, J. de, Vázquez, A.J., Fernández, B., 1994, Laser-clad 316 Stainless Steel with Ni-Cr Powder Mixtures, Materials & Design, vol. 15, no. 1, pp. 41-44

[Dausinger, 1988] Dausinger, F., Rudlaff, T., 1988, Steigerung der Effizienz des Laserstrahlhärtens, Proc. ECLAT '88, pp. 88-91

[Dausinger, 1996] Dausinger, F., Hack, R., 1996, Multi-Beam Technique to Increase Power, Flexibility and Quality, Proc. ECLAT '96, pp. 19-28

[De Hosson, 1995] De Hosson, J.Th.M., 1995, Fundamental and Applied Aspects of Laser Processed Ceramic Coatings of Metals, Proc. Surface Treatment 95, pp. 1-15

[De Hosson, 1996] De Hosson, J.Th.M., Mol van Otterloo, L. de, 1996, Microstructural Features of Laser Coatings, Proc. ECLAT '96, pp. 337-348

[Dekumbis, 1989] Dekumbis, R., 1989, Oberflächenbeschichten mit Lasern, Technische Rundschau, no. 6, pp. 32-34

[Dekumbis, 1990] Dekumbis, R., 1990, Einsatz des Lasers in der Oberflächentechnik, Beschichten mit Laserstrahlen, Technischen Rundschau Sulzer, Winterthur, 1/1990

[Dekumbis, 1993] Dekumbis, R., 1993, 30 Prozent Schneller und Billiger, Sulzer Technical Review, no. 1/93, 23-25

[Dickmann, 1995] Dickmann, K., et al., 1995, Pulverbeschichtung von Werkzeugen mit Lasern, JOT, no. 12, pp. 44-47

[Ding, 1993] Ding, P., Liu, J., Shi, G., 1993, Analysis of Driving Forces for Convection in the Laser Melted Pool, Lasers in Engineering, vol. 2, pp. 75-79

[Draugelates, 1994] Draugelates, U., et al., 1994, Corrosion and Wear Protection by CO_2 Laser Beam Cladding Combined with the Hot Wire Technology, Proc. ECLAT '94, pp. 344-354

[Drenker, 1990] Drenker, A., et al., 1990, Adaptive Temperature Control in Laser Transformation Hardening, Proc. ECLAT '90, pp. 283-290

[Duhamel, 1986] Duhamel, R.F., Banas, C.M., Kosenski, R.L., 1986, Production Laser Hardfacing of Jet Engine Turbine Blades, Manufacturing Applications of Lasers, SPIE, vol. 621, pp. 31-39

[Eboo, 1983] Eboo, M., Lindemanis, A.E., 1983, Advances In Lasercladding Technology, Proc. ICALEO '83, SPIE, vol. 527, pp. 86-94

[Eigenmann, 1995] Eigenmann, B., 1995, Residual Stresses due to Thermal, Thermo-Chemical and Mechanical Surface Treatments: Generation, Deter-mination, Evaluation, Proc. Surface Treatment 95, pp. 17-25

[Eiholzer, 1985] Eiholzer, E., Cusano, C., Mazumder, J., 1985, Wear Properties of Laser Alloyed and Clad Fe-Cr-Mn-C Alloys, Proc. ICALEO '84, pp. 159-167

[Ellis, 1995] Ellis, M., et al., 1995, Processing Aspects of Laser Cladding an Aluminium Alloy onto Steel, J. of Materials Processing Technology, vol. 52, pp. 55-67

[Elshof, 1994] Elshof, H.L.F., 1994, Heat Fluxes Between Semi-Infinite Solids, Un. of Twente, Graduate Thesis, Dept. of Mech. Eng.

[Engström, 1988] Engström, H., et al., 1988, Combined Corrosion and Wear Resistance of Laser-Clad Stellite 6B, Proc. ECLAT '88, pp. 164-168

[Evers, 1993] Evers, Th., 1993, Slijtvast Lagen Aanbrengen met Laser Inductie Technologie, Metaal en Kunststof, no. 2, pp. 16-19

[Fabbro, 1990] Fabbro, R., et al., 1990, Absorption Measurements in Continuous High-Power CO_2 Laser Processing of Materials, Proc. CO_2 Lasers and Applications II, SPIE, vol. 1276, pp. 461-467

[Fellowes, 1990] Fellowes, F.C.J., Steen, W.M., Coley, K.S., 1990, Ceramic Coating for High Temperature Corrosion Resistance by Laser Processing, Key Eng. Materials Vols 46 & 47, pp. 435-446

[Fernandez, 1995] Fernandez, E., et al., 1995, Laser Surface Treatment of Al_2O_3 Coatings Plasma Sprayed, Proc. Surface Treatment 95, pp. 61-68

[Fernandez, 1995] Fernandez, E., et al., 1995, Wear Behaviour of Laser Clad WC-Co Powder, Proc. Surface Treatment 95, pp. 53-60

[Fischer, 1996] Fischer, A., Lensch, G., 1996, Technical Application of Laser Surface Treatment - Hardening, Alloying, Cladding, Proc. ECLAT '96, pp. 399-405

[Fischer, 1996] Fischer, D., et al., 1996, Mit Laser erzeugte grobkörnige Hartstoff-Dispersionsschichten auf Alumi-nium-Legierungen zum Verschleissschutz, Proc. ECLAT '96, pp. 455-460

[Fishman, 1995] Fishman, M., Sherbaum, N., Zahavi, J., 1995, Laser Cladding and Alloying for Refurbishing Worn Machine Parts and Improving their Surface Properties, SPIE, vol. 2426, pp. 181-187

[Flinkfeldt, 1994] Flinkfeldt, J.E., Pedersen, Th.F., 1994, Laser Cladding in Pre-Made Grooves: Guide-lines for Groove Design, Materials Science Forum, vols. 163-165, pp. 423-428

[Folkes, 1994] Folkes, J.A., Shibata, K., 1994, Laser Cladding of Ti-6Al-4V with Various Carbide Powders, J. of Laser Applications, vol. 6, pp. 88-94

[Fouquet, 1993] Fouquet, F., et al., 1993, Microstructural and Electrochemical Characterization of Laser Deposited 18-10 Austenitic Stainless Steel Clad Layers, J. de Physique IV, Colloque C7, pp. 991-994

[Fouquet, 1994] Fouquet, F., et al., 1994, Austenitic Stainless Steels Layers Deposited by Laser Cladding on a Mild Steel: Realization and Characterization, J. de Physique IV, Colloque C4, pp. 89-92

[Freitas, 1993] Freitas, M. de, et al., 1993, Analysis of Residual Stresses Induced by Laser Processing, Materials Science and Engineering, vol. A167, pp. 115-122

[Frenk, 1991] Frenk, A., et al., 1991, Influence of an Intermediate Layer on the Residual Stress Field in a Laser Clad, Surface and Coatings Technology, vol. 45, pp. 435-441

[Frenk, 1993] Frenk, A., Henchoz, N., Kurz, W., 1993, Laser Cladding of a Cobalt-base Alloy: Processing Parameters and Microstructure, Z. Metallkd., vol. 84, no. 12, pp. 886-892

[Frenk, 1991] Frenk, A., Hoadley, A.F.A., Wagnière, J.-D., 1991, In-Situ Technique for Measuring the Absorption During Laser Suface Remelting, Metall. Trans. B, vol. 22B, pp. 139-142

[Frenk, 1991] Frenk, A., Wagnière, J.-D., 1991, Laser Cladding with Cobalt Based Hardfacing Alloys, J. de Physique IV, vol. 1, pp. 65-68

[Frenk, 1993] Frenk, A., Kurz, W., 1993, High Speed Laser Cladding: Solidification Conditions and Microstructure of a Cobalt-Based Alloy, Materials Science and Engineering, vol. A173, pp. 339-342

[Funk, 1990] Funk, G., Müller, W., 1990, Temperaturgeregeltes Laserhärten in der Präzisionsmengenfertigung, Proc. ECLAT '90, pp. 227-236

[Fux, 1992] Fux, V., et al., 1992, Laser Cladding with Amorphous Hardfacing Alloys, Proc. ECLAT '92, pp. 387-392

[Gasser, 1996] Gasser, A., et al., 1996, Oberflächenbehandlung mit Zusatzwerkstoffen, Proc. ECLAT '96, pp. 287-298

[Gassmann, 1992] Gassmann, R., et al., 1992, Laser Cladding of Hard Particles Rich Alloy, Proc. ICALEO '92, pp. 288-300

[Gassmann, 1992] Gassmann, R., et al., 1992, Adhesion and Microstructure of Laser Cladded Coatings, Proc. ECLAT '92, pp. 405-410

[Gebhardt, 1996] Gebhardt, et al., 1996, Reconditioning of Machine and Engine Parts Using High-Power Lasers, Proc. ECLAT '96, pp. 373-381

[Gebhardt, 1996] Gebhardt, A., Petschke, U., 1996, Rapid Prototyping - Lasergestützte Revolution der Produkentwicklung, Laser Magazin, no. 1, pp. 6-9

[Geissler, 1990] Geissler, E., Bergmann, H.W., 1990, Temperature Controlled Laser Transformation Hardening, Key Engineering Materials vols. 46-47, pp. 121-132

[Giordano, 1985] Giordano, L., et al., 1985, Laser Application of Stellite Coatings on Austenitic Steels, pp. 3.23-3.27

[Giordano, 1986] Giordano, L., Ramous, E., 1986, Rapid Solidifications of Surface Layers Melted by CW Laser, Laser Surface Treatment of Metals, pp. 483-496

[Glumann, 1994] Glumann, C., et al., 1994, Zweistrahltechnik beim Schweissen und Oberflächenbehandeln - erweiterte Möglichkeiten der Prozeßgestaltung und Erhöhung der Prozeßqualität, Materialbearbeitung mit CO_2-Laserstrahlen höchster Leistung, pp. 53-65

[Gnanamuthu, 1976] Gnanamuthu, D.S., 1976, US Patent no. 3952180

[Grünenwald, 1992] Grünenwald, B., et al., 1992, Laser Cladding with a Heterogeneous Powder Mixture of WC/Co and NiCrBSi, Proc. ECLAT '92, pp. 411-416

[Grünenwald, 1992] Grünenwald, B., et al., 1992, Laser Surface Alloying of Case Hardening Steel with Tungsten Carbide and Carbon, Materials Science and Technology, July 1992, vol. 8, pp. 637-643

[Grünenwald, 1993] Grünenwald, B., Dausinger, F., Hügel, H., 1993, Laser Cladding with Composite Powders Using Pyrometric Temperature Control and Beam Combining, Proc. ISATA '93, pp. 287-294

[Grünenwald, 1996] Grünenwald, B., et al., 1996, Laserbeschichten mit CO_2- und Nd:YAG-Lasern, Proc. ECLAT '96, pp. 299-306

[Haferkamp, 1994] Haferkamp, H., et al., 1994, Application of Laser Powder Cladding and the Risk of Residual Powder, Proc. ECLAT '94, pp. 475-483

[Haferkamp, 1995] Haferkamp, H., Alvensleben, F. von, Gerken, J., 1995, Rapid Manufacturing durch Lasersintern und 3D-LaserstrahlAuftragschweißen, Laser und Optoelektronik, vol. 27, no. 3, pp. 64-69

[Haferkamp, 1995] Haferkamp, H., Bach, F.-W., Gerken, J., 1995, Laserstrahl-Legieren plasmagespritzter Molybdänschichten in Stahloberflächen zur Erhöhung des Verschleißwiederstandes, Metall, vol. 49, no. 7-8, pp. 516-522

[Haferkamp, 1996] Haferkamp, H., et al., 1996, In-Situ Untersuchung des Hartstofftransportes beim Laserstrahldispergieren mittels Hochgeschwindigkeits-Radioskopie, Metallwissenschaft und Technik, vol. 50, no. 3, pp. 185-191

[Hegge, 1990] Hegge, H.J., Boetje, J., De Hosson, J.Th.M., 1990, Oxidation Effects During Laser Cladding of Aluminium With SiC/Al Powders, J. of Materials Science, vol. 25, no. 5, pp. 2335-2338

[Hensel, 1992] Hensel, F., Binroth, C., Sepold, G., 1992, A Comparison of Powder and Wire-Fed Laser Beam Cladding, Proc. ECLAT '92, pp. 39-44

[Hernandez, 1986] Hernandez, J., et al., 1986, Laser Surface Cladding and Residual Stresses, Proc. LIM-3, pp. 181-190

[Heuvelman, 1992] Heuvelman, C.J., et al., 1992, Surface Treatment Techniques by Laser Beam Machining, Annals of the CIRP, vol. 41, pp. 657-666

[Hinse-Stern, 1992] Hinse-Stern, A., Burchards, D., 1992, Leistungsfähiges Laserdrahtbeschichtungsverfahren mit Tandemheißdrahtzufuhr, Proc. LASER 1991, pp. 349-354

[Hinse-Stern, 1992] Hinse-Stern, A., Burchards, D., Mordike, B.L., 1992, Laser Cladding with Preheated Wires, Proc. ECLAT '92, pp. 223-228

[Hirose, 1995] Hirose, A., Kobayashi, K.F., 1995, Formation of Hybrid Clad Layers by Laser Processing, ISIJ Int., vol. 35, pp. 757-763

[Hoadley, 1992] Hoadley, A.F.A, Rappaz, M., 1992, A Thermal Model of Laser Cladding by Powder Injection, Metall. Trans. B, vol. 23B, pp. 631-642

[Huang, 1995] Huang, C.-C., Tsai, W.-T., Lee, J.-T., 1995, Microstructure and Electrochemical Behavior of Laser Cladded Fe-Cr-Mo-Si-N Surface Alloys on Carbon Steel, Materials Science and Engineering, vol. A 196, pp. 243-248

[Incropera, 1990] Incropera, F.D., De Witt, D.P., 1990, Fundamentals of Heat and Mass Transfer, John Wiley & Sons, New York, 3rd ed.

[Jasim, 1989] Jasim, K.M., West, D.R.F., 1989, Laser Cladding of Carbon Steel with a Ceramic Metallic Composite, High Power Lasers and Laser Machining Technology, Proc. SPIE, vol. 1132, pp. 237-245

[Jasim, 1993] Jasim, K.M., Rawlings, R.D., West, D.R.F., 1993, Metal-Ceramic Functionally Gradient Material Produced by Laser Processing, J. of Materials Science, vol. 28, pp. 2820-2826

[Johnson, 1977] Johnson, J.L., Leone, F.C., 1977, Statistics and Experimental Design in Engineering and the Physical Sciences, John Wiley & Sons, New York, 2nd ed., vol. II

[Jouvard, 1997] Jouvard, J.-M., et al., 1997, Continuous Wave Nd:YAG Laser Cladding Modeling: A Physical Study of Track Creation During Low Power Processing, J. of Laser Applications, vol. 9, pp. 43-50

[Juch, 1994] Juch, K., 1994, Herstellung titankarbidhaltiger Verschleissschutzschichten durch Laserbestrahlung vorbeschichteter Stahloberflächen, Laser und Optoelektronik, vol. 26, no. 5, pp. 60-66

[Kar, 1988] Kar, A., Mazumder, J., 1988, One-Dimensional Finite-Medium Diffusion Model for Extended Solid Solution in Laser Cladding of Hf on Nickel, Acta Metall., vol. 36, no. 3, pp. 701-712

[Kar, 1989] Kar, A., Mazumder, J., 1989, Extended Solid Solution and Nonequilibrium Phase Diagram for Ni-Al Alloy Formed During Laser Cladding, Metall. Trans. A, vol. 20A, pp. 363-371

[Kar, 1992] Kar, A., Mazumder, J., 1992, Model for Nonequilibrium Partitioning During Rapid Solidification of Binary Concentrated Solutions, Acta Metall. et Mat., vol. 40, no. 8, pp. 1873-1881

[Kastler, 1952] Kastler, A., 1952, La Diffusion de la Lumière par les Milieux Troubles, Hermann & Cie., Paris

[Keitel, 1994] Keitel, S., et al., 1994, Oberflächenbehandeln mit dem CO_2-Hochleistungslaser im wirtschaftlichem und technologischen Vergleich zum Elektronenstrahl und zur Hochleistungslichtquelle, Materialbearbeitung mit CO_2-Laserstrahlen höchster Leistung, VDI, Düsseldorf, pp. 111-118

[Kim, 1995] Kim, T.H., et al., 1995, Calculation of CO_2 Laser Beam Absorptance as a Function of Temperature for Steels by the Numerical Method, J. of Materials Science, vol. 30, pp. 784-792

[Kindler, 1996] Kindler, H., Volz, R., Huonker, M., 1996, Ein neues Verfahren zum Laserstrahlbeschichten, Proc. ECLAT '96, pp. 447-454

[Kingslake, 1978] Kingslake, R., 1978, Lens Design Fundamentals, Academic Press, New York

[Komvopoulos, 1990] Komvopoulos, K., Nagarathnam, K., 1990, Processing and Characterization of Laser-Cladded Coating Materials, J. of Engineering Materials and Technology, vol. 112, pp. 131-143

[Komvopoulos, 1994] Komvopoulos, K., 1994, Effect of Process Parameters on the Microstructure, Geometry and Microhardness of Laser-Clad Coating Materials, Mat. Sci. Forum, vols. 163-165, pp. 417-422

[König, 1989] König, W., et al., 1989, Surface Treatment with the Laser Beam: A Discussion of Various Machining Methods, Annual Industrial Laser Handbook 1989, pp. 117-121

[König, 1992] König, W., Rozsnoki, L., Kirner, P., 1992, Laser Beam Surface Treatment - Is Wear No Longer The Bug Bear of Old, Proc. ECLAT '92, pp. 217-222

[König, 1994] König, W., Herfurth, H.-J., 1994, Einsatzpotentiale hoher Laserleistung beim Oberflächenveredeln, Materialbearbeitung mit CO_2-Laserstrahlen höchster Leistung, VDI, pp. 67-72

[König, 1994] König, W., Kirner, P.K., 1994, Laser Surface Treatments Prolongs Tool Life, Proc. Laser Materials Processing: Industrial and Microelectronics Applications, SPIE, vol. 2207, pp. 44-52

[Králová, 1994] Králová, R., 1994, Residual Stresses Induced in Steel by Laser Melting, Materials Science and Engineering, vol. A174, L51-L54

[Kreutz, 1990] Kreutz, E.W., Pirch, N., 1990, Melt Dynamics in Surface Processing with Laser Radiation: Calculations and Applications, Proc. CO_2 Lasers and Applications II, pp. 343-360

[Kreutz, 1995] Kreutz, E.W., et al., 1995, Rapid Prototyping with CO_2 Laser Radiation, Applied Surface Science, 86, pp. 310-316

[Kruth, 1995] Kruth, J.P., Ma, W., 1995, CAD/CMM Integration for Reverse Engineering, Manufacturing Systems, vol. 24, pp. 451-457

[Kuilboer, 1994] Kuilboer, R.B., et al., 1994, Laser Beam Transformation Hardening: Transferability of Machining Parameters, Annals of the CIRP, vol. 43/2/1994, pp. 585-592

[Küpper, 1990] Küpper, F., et al., 1990, Cladding of Valves with CO_2 Laser Radiation, Proc. ECLAT '90, pp. 461-467

[Kussmaul, 1996] Kussmaul, K., et al., 1996, Oberflächenveredelung von metallischen Oberflächen durch Einbringen von Zusatzwerkstoffen in Pulverform, Proc. ECLAT '96, pp. 415-417

[La Rocca, 1986] La Rocca, A.V., 1986, Developments in Laser Material Processing for the Automotive Industries, Laser Surface Treatment of Metals, pp. 521-543

[Lang, 1994] Lang, A., Waldmann, H., Bergmann, H.W., 1994, Cladding of Metallic Substrates with Diamonds and Cubic Boron Nitride, Proc. ECLAT '94, pp. 456-461

[L'Enfant, 1995] L'Enfant, H., et al., 1995, CO_2 Laser Surface Treatment in Reactive Atmosphere: Thermodiffusional Nitridation of Titanium, Proc. Surface Treatment 95, pp. 273-280

[Lemoine, 1993] Lemoine, F., et al., 1993, Modélisation de la Section de Dépôts Obtenus par Fusion d'une Poudre Métallique Projetée dans un Faisceau Laser Nd-YAG, J. de Physique III France, Octobre 1993, vol. 3, no. 10, pp. 2043-2052

[Lemoine, 1994] Lemoine, F., et al., 1994, Traitement de Surface en Continu Avec un Laser Nd:YAG Impulsionnel, J. de Physique IV, Colloque C4, Supplément au J. de Physique III, vol. 4, pp. 43-46

[Lemoine, 1994] Lemoine, F., Grevey, D.F., Vannes, A.B., 1994, Cross-section Modelling of Pulsed Nd:YAG Laser Cladding, Laser Materials Processing and Machining, Proc. SPIE, vol. 2246, pp. 37-44

[Lemoine, 1995] Lemoine, F., Grevey, D.F., Vannes, A.B., 1995, Indirect Determination of the Absorptance During Nd:YAG Laser-Matter Interaction, Lasers in Engineering, vol. 4, pp. 273-279

[Lensch, 1996] Lensch, G., Kröhnert, G., Bady, T., 1996, Hochleistungsoptiken für die Laserbearbeitung von Innenräumen, Proc. ECLAT '96, pp. 823-828

[Lepski, 1990] Lepski, D., Reitzenstein, W., 1990, Computergestützte Prozeßoptimierung bei der Laserumwandlungshärtung, Proc. ECLAT '90, pp. 183-194

[Lepski, 1990] Lepski, D., Reitzenstein, W., 1990, Prozeßoptimierung mit dem Personalcomputer bei der Laser-Oberflächenhärtung von Eisenwerkstoffen, Laser, Technologie und Anwendungen, pp. 270-278

[Lewis, 1995] Lewis, G.K., Lyons, P., 1995, Direct Laser Metal Deposition Process Fabricates Near-Net-Shape Components Rapidly, Materials Technology, vol. 10, pp. 51-54

[Li, 1988] Li, L., et al., 1988, Real-Time Expert Systems for Supervisory Control of Laser Cladding, Proc. ICALEO '87, pp. 9-16

[Li, 1989] Li, L., 1989, Intelligent Laser Cladding Control: System Design and Construction, Ph.D. Thesis

[Li, 1990] Li, L., et al., 1990, In-Process Clad Quality Monitoring Using Optical Method, Proc. ECO 3, vol. 1279, pp. 89-100

[Li, 1990] Li, L., Steen, W.M., Hibberd, R.D., 1990, Computer Aided Laser Cladding, Proc. ECLAT '90, vol. 1, pp. 355-369

[Li, 1992] Li, Y., Steen, W.M., 1992, Laser Cladding of Stellite and Silica on Aluminium Substrate, Proc. ICLOE '92, SPIE, vol. 1979, pp. 602-608

[Li, 1992] Li, Y., Steen, W.M., Sharkey, S., 1992, Laser Remelting of Plasma Sprayed Coatings on Nuclear Valves, Proc. ICLOE '92, SPIE, vol. 1979, pp. 594-601

[Li, 1994] Li, J., Yuan, L., 1994, Mathematical Method for Optimizing the Process of Heat Treatment with Powerful Lasers, Lasers in Engineering, vol. 2, pp. 239-245

[Li, 1995] Li, W.-B., et al., 1995, Modelling of the Laser Cladding Process, Preheating of the Blown Powder Material, Lasers in Engineering, vol. 4, pp. 329-341

[Liu, 1992] Liu, Y., Mazumder, J., Shibata, K., 1992, Laser Cladding of Ni-Al Bronze on Cast Al Alloy AA333, Proc. ECLAT '92, pp. 381-386

[Liu, 1994] Liu, Y., et al., 1994, Processing, Microstructure, and Properties of Laser-Clad Ni Alloy FP-5 on Al Alloy AA333, Metallurgical and Mat. Trans. B, vol. 25B, pp. 425-434

[Lubbers, 1994] Lubbers, G.W., 1994, Lasercladden op Inlaatkleppen en Nokkenstoters, Un. of Twente, Dept. of Mech. Eng., WA-371

[Lubrecht, 1989] Lubrecht, A.A., Ioannides, E., 1989, A Fast Solution of the Dry Contact Problem and the Associated Sub-Surface Stress Field, J. of Tribology, vol. 113, pp. 128-133.

[Luft, 1990] Luft, A., et al., 1990, Microstructure and Mechanical Properties of Laser Processed Steels and Cast Irons, Laser, Technologie und Anwendungen, pp. 299

[Luft, 1995] Luft, A., et al., 1995, Gefügeausbildung und Karbidauflösung beim Laserbeschichten von Stahl mit Wolframkarbidverstärkten Ni- und Co-Hartlegierungen, Prakt. Metallogr., vol. 32, pp. 235-247

[Lugscheider, 1990] Lugscheider, E., Oberländer, B.C., Meinhardt, H., 1990, Laser Cladding and Laser Surface Remelting of Nickel-base Hardfacing Alloys, Proc. ECLAT '90, pp. 555-568

[Lugscheider, 1992] Lugscheider, E., Bolender, H., Krappitz, H., 1992, Laser Cladding of Paste Bound Carbides, Proc. ECLAT '92, pp. 369-374

[Lugscheider, 1994] Lugscheider, E., et al., 1994, One-Step Powder Cladding of Oxide Ceramics on Metal Substrates with CO_2 Laser Radiation, Proc. ECLAT '94, pp. 213-218

[MacIntyre, 1983] MacIntyre, R.M., 1983, Laser Hardsurfacing of Gas Turbine Blade Shroud Interlocks, LIM-1, pp. 253-261

[Magrini, 1986] Magrini, M., Badan, B., Ramous, E., 1986, Laser Surface Cladding of Carbon and Stainless Steels, European Conference on Laser Treatment of Materials, pp. 405-411

[Marsden, 1990] Marsden, C.F., et al., 1990, Characterisation of the Laser Cladding Process, Proc. ECLAT '90, vol. 1, pp. 543-553

[Marsden, 1992] Marsden, C.F., Frenk, A., Wagnière, J.-D., 1992, Power Absorption During the Laser Cladding Process, Proc. ECLAT '92, pp. 375-380

[Matthews, 1983] Matthews, S.J., 1983, Laser Fusing of Hardfacing Alloy Powders, Lasers in Materials Processing, pp. 138-148

[Mazumder, 1986] Mazumder, J., 1986, Mathematical Modeling of Laser Surface Treatments, Laser Surface Treatment of Metals, pp. 185-199

[Mazumder, 1986] Mazumder, J., Singh, J., 1986, Laser Surface Alloying and Cladding for Corrosion and Wear, Laser Surface Treatment of Metals, pp. 297-307

[Mazumder, 1987] Mazumder, J., Kar, A., 1987, Solid Solubility in Laser Cladding, J. of Metals, vol. 39, no. 2, pp. 18-23

[Mazumder, 1991] Mazumder, J., 1991, Overview of Melt Dynamics in Laser Processing, Optical Engineering, vol. 30, no. 8, pp. 1208-1219

[Meijer, 1994] Meijer, J., et al., 1994, Laser Beam Hardening: Transferability of Machining Parameters, Proc. LANE '94, pp. 243-252

[Metzbower, 1986] Metzbower, E.A., Pierpoint, E.R., Hartman, K., 1986, Hardfacing Using a CW laser, Proc. ICALEO '86, pp. 177-184

[Meyer-Kobbe, 1990] Meyer-Kobbe, C., 1990, Anwendungen von Lasern für die Oberflächenbehandlung von metallischen Bauteilen, Maschinenmarkt, pp. 57-61

[Meyer-Kobbe, 1991] Meyer-Kobbe, C., 1991, Umschmelzen von Grauguß mit dem kw Nd:YAG Laser, Teil I: Grundlegende Ergebnisse beim Umschmelzen, Werkstoff und Innovation, vol. 4, no. 4, pp. 38-44

[Molian, 1988] Molian, P.A., 1988, Principles and Applications of Lasers for Wear-Resistant Coatings, 1st International Conference on Surface Modification Technology, pp. 237-265

[Molian, 1989] Molian, P.A., Hualan, L., 1989, Laser Cladding of Ti-6Al-4V with BN for Improved Wear Performance, Wear, vol. 130, pp. 337-352

[Monson, 1986] Monson, P.J.E., Steen, W.M., 1986, Laser Hardfacing/Cladding, European Conf. on Laser Treatment of Materials, pp. 123-132

[Monson, 1990] Monson, P.J.E., Steen, W.M., 1990, Comparison of Laser Hardfacing with Conventional Processes, Surface Engineering, vol. 6, no. 3, pp. 185-193

[Mordike, 1990] Mordike, B.L., Burchards, D., 1990, Eigenschaften Laserbehandelter Hartmetallschichten, Laser, Technologie und Anwendungen, pp. 289-294

[Mordike, 1994] Mordike, B.L., 1994, Industrial Applications of Laser Surface Treatment, Proc. ECLAT '94, pp. 173-187

[Mordike, 1995] Mordike, B.L., 1995, Surface Treatment with High Power Lasers, Lasers in Engineering, vol. 4, pp. 187-200

[Mordike, 1996] Mordike, B.L., 1996, Applications of Laser Surface Remelting, Proc. ECLAT '96, pp. 253-264

[Müller, 1996] Müller, K., Körner, C., Bergmann, H.W., 1996, Numerische Simulation der Eigenspannungen und Deformationen beim Laserstrahlrandschichthärten, HTM, vol. 51, no. 1, pp. 19-28

[Nakao, 1993] Nakao, Y., Nishimoto, K., 1993, Effects of Laser Surface Melting on Corrosion Resistance of Stainless Steel and Nickel-Base Alloy Clad Layers in Cast Bi-Metallic Pipes, ISIJ Int., vol. 33, pp. 934-940

[Nizery, 1993] Nizery, F., et al., 1993, Treatment of Overlapping Runs by CW CO_2 Laser, Laser Treatment of Materials '93, pp. 331-335

[Nowotny, 1993] Nowotny, S., et al., 1993, Geregelte Pulverzufuhr für die Laser-Oberflächenbearbeitung mit Zusatzwerkstoffen, Laser und Optoelektronik, vol. 25, no. 6, pp. 71-77

[Nowotny, 1994] Nowotny, S., et al., 1994, Influences on the Wear Resistance of Carbide Laser Claddings, Proc. ECLAT '94, pp. 252-259

[Nowotny, 1994] Nowotny, S., et al., 1994, Struktur und Verschleisseigenschaften von Hartstoffbeschichtungen, Materialbearbeitung mit CO_2-Laserstrahlen höchster Leistung, VDI, Düsseldorf, pp. 81-87

[Nowotny, 1996] Nowotny, S., et al., 1996, Systemtechnik zum Laserstrahl-Präzisionsbeschichten, ECLAT '96, pp. 383-390

[Nurminen, 1983] Nurminen, J.I., Smith, J.E., 1983, Parametric Evaluation of Laser/Clad Interactions for Hardfacing Applications, Lasers in Materials Processing, pp. 94-107

[Oberländer, 1992] Oberländer, B.C., Lugscheider, E., 1992, Comparison of Properties of Coatings Produced by Laser Cladding and Conventional Methods, Materials Science and Technology, vol. 8, pp. 657-665

[Ollier, 1992] Ollier, B., et al., 1992, Cladding with Laser Radiation: Properties and Analysis, Proc. ECLAT '92, pp. 687-692

[Ollier, 1995] Ollier, B., Pirch, N., Kreutz, E.W., 1995, Ein numerisches Modell zum Einstufigen Laserstrahlbeschichten, Laser und Optoelektronik, vol. 27, no. 1, pp. 63-70

[Pei, 1995] Pei, Y.T., et al., 1995, Microstructure of Laser-Clad SiC-(Ni Alloy) Composite Coating, Mat. Sci. and Eng. A, vol. A194, pp. 219-224

[Pei, 1996] Pei, Y.T., Ouyang, J.H., Lei, T.C., 1996, Microstructure of Bonding Zones in Laser-Clad Ni-Alloy-Based Composite Coatings Reinforced with Various Ceramic Powders, Metall. and Mat. Trans. A, vol. 27A, pp. 391-400

[Pelletier, 1992] Pelletier, J.M., et al., 1992, Improvement of Mechanical Properties of Steels by Addition of Tungsten Carbides: Laser Cladding and Laser Welding, Proc. ECLAT '92, pp. 211-216

[Pelletier, 1993] Pelletier, J.M., et al., 1993, Influence of Processing Conditions on Geometrical Features of Laser Claddings Obtained by Powder Injection, J. of Materials Science, vol. 28, pp. 5184-5188

[Pelletier, 1994] Pelletier, J.M., Sallamand, P., Criqui, B., 1994, Microstructure and Mechanical Properties of Some Metal Matrix Composites Coatings by Laser Cladding, J. de Physique IV, Colloque C4, Supplément au J. de Physique III, vol. 4, pp. 93-96

[Pelletier, 1994] Pelletier, J.M., Sallamand, P., Criqui, B., 1994, Microstructure and Mechanical Properties of Some Metal Matrix Composites Produced on Different Materials by Laser Cladding, Lasers in Engineering, vol. 3, pp. 15-27

[Pelletier, 1996] Pelletier, J.M., et al., 1996, Hadfield Steel Layers Manufactured by Laser Cladding: Mechanical and Tribological Properties, Proc. ECLAT '96, pp. 329-336

[Picasso, 1991] Picasso, M., Hoadley, A.F.A., 1991, The Influence of Convection in the Laser Cladding Process, Proc. of Numerical Methods in Thermal Problems VII, pp. 199-210

[Picasso, 1994] Picasso, M., et al., 1994, A Simple but Realistic Model for Laser Cladding, Metall. and Mat. Trans. B, vol. 25 B, pp. 281-291

[Picasso, 1994] Picasso, M., Hoadley, A.F.A., 1994, Finite Element Simulation of Laser Surface Treatments Including Convection in the Melt Pool, Int. J. of Num. Meth. for Heat and Fluid Flow, vol. 4, pp. 61-83

[Picasso, 1994] Picasso, M., Rappaz, M., 1994, Laser-Powder-Material Interactions in the Laser Cladding Process, J. de Physique IV, Colloque C4, Supplément au J. de Physique III, vol. 4, pp. 27-33

[Pilloz, 1990] Pilloz, M., et al., 1990, Study of the Parameters of Laser Coatings and Residual Stress Fields Created by These Coatings, Key Engineering Materials, Vols 46 & 47, pp. 387-414

[Pizúrová, 1993] Pizúrová, N., et al., 1993, Structure and Phase Composition of Cobalt Rich Coating Prepared by Laser Cladding on Low Carbon Steel, Materials Science and Technology, vol. 9, pp. 172-175

[Powell, 1981] Powell, J., Steen, W.M., 1981, Vibro Laser Cladding, Proc. Lasers in Metallurgy, pp. 93-104

[Pustovalov, 1993] Pustovalov, V.K., Bobuchenko, D.S., 1993, Thermal Processing in Gas-Powder Laser Cladding of Metal Materials, Int. J. of Heat and Mass Transfer, vol. 36, no. 9, pp. 2449-2456

[Ramous, 1989] Ramous, E., et al., 1989, Laser Cladding of Ceramic and Metallic Coatings on Steel, Key Engineering Materials Vols 46 & 47, pp. 425-433

[Rao, 1993] Rao, D.R.K., et al., 1993, The Effect of Laser Surface Melting on the Erosion Behaviour of a Low Alloy Steel, Surface and Coating Technology, vol. 58, pp. 85-92

[Ready, 1971] Ready, J.F., 1971, Effects of High Power Laser Radiation, Academic Press, New York

[Reichelt, 1996] Reichelt, U., Volz, R., 1996, Einsatz des 4 kW-Festkörperlasers zum Beschichten und Fügen mit pulverförmigen Zusatzwerkstoffen, Proc. ECLAT '96, pp. 365-372

[Reusch, 1995] Reusch, A., et al., 1995, Mobile Messung von Partikeleigenschaften beim Thermischen Spritzen durch Laser-Doppler-Anemometrie, Metall, vol. 49, no. 1, pp. 38-44

[Riabkina-Fishman, 1996] Riabkina-Fishman, M., Zahavi, J., 1996, Laser Alloying and Cladding for Improving Surface Properties and Refurbishing Worn Machine Parts, Lasers in Engineering, vol. 5, pp. 31-41

[Ribaudo, 1989] Ribaudo, et al., 1989, Laser Clad $Ni_{70}Al_{20}Cr_7Hf_3$ Alloys with Extended Solid Solution of Hf. Part II. Oxidation Behavior, Metall. Trans. A, vol. 20A, no. 11, pp. 2489-2497

[Ricciardi, 1990] Ricciardi, G., et al., 1990, Laser Assisted Formation of a Wear Resistant SiC-metal Composite on the Surface of a Structural Aluminium Alloy, Key Engineering Materials Vols 46 & 47, pp. 415-424

[Ritter, 1991] Ritter, U., et al., 1991, Laserbeschichten - In der Praxis bewährt, Technischen Rundschau Sulzer, Winterthur, 3/1991

[Römer, 1997] Römer, G.R.B.E., 1997, Scanning Mirrors Actuated by Piezo Crystals for Use in Laser Cladding and Alloying, University of Twente, Enschede, Internal report, Dept. of Mech.Eng.

[Römer, 1995] Römer, G.R.B.E., Meijer, J., 1995, Metal Surface Temperature Induced by Moving Laser Beams, Optical and Quantum Electronics, vol. 27, pp. 1397-1406

[Rudlaff, 1990] Rudlaff, T., Dausinger, F., 1990, Increasing the Efficiency of Laser Beam Hardening, Proc. ICALEO '90, pp. 451-458

[Rudlaff, 1990] Rudlaff, Th., Dausinger, F., 1990, Hardening with Variable Intensity Distribution, Proc. ECLAT '90, pp. 251-264

[Sakamoto, 1995] Sakamoto, T., et al., 1995, Laser Clad Lubricant Layer with Gaphite/BN, pp. 359-368

[Sallamand, 1993] Sallamand, P., Pelletier, J.M., 1993, Laser Cladding on Aluminium-Base Alloys: Microstructural Features, Materials Science and Engineering, vol. 171, pp. 263-270

[Schiere, 1995] Schiere, J., 1995, Ontwerp en Realisatie van een Pulserend Poederdoseersysteem ten Behoeve van Lasercladden, -Legeren en -Genereren, Un. of Twente, Dept. of Mech. Eng., WA-472

[Schneider, 1992] Schneider, M.F., 1992, Laser Cladding with Preplaced Powder, University of Twente, Dept. of Mech. Eng., WA-229

[Schneider, 1994] Schneider, M.F., 1994, Oppervlaktebehandelingen met Lasers: Legeren, Dispergeren en Cladden, MB Produktietechniek, vol. 60, no. 11/12, pp. 326-332

[Schneider, 1994] Schneider, M.F., 1994, Oppervlaktebewerkingen met Lasers: Transformatieharden en Omsmelten, MB Produktietechniek, vol. 60, no. 4, pp. 98-103

[Schneider, 1994] Schneider, M.F., et al., 1994, Oppervlaktebehandelen met Lasers, Lasercladden: Eindverslag, IOP-metalen, Universiteit Twente, Enschede, Dept. of Mech. Eng.

[Schneider, 1995] Schneider, M.F., 1995, Lasercladden van Extrusieschroeven, NIL, Metaalbewerken met Lasers

[Sepold, 1989] Sepold, G., Becker, R., 1989, Laser Powder Coating by Multi-Thin-Layer Technics, Proc. First International School on Laser Surface Microprocessing, SPIE, vol. 1352, pp. 125-131

[Shannon, 1992] Shannon, et al.., 1992, Photothermal Deflection Measurements for Monitoring Heat Transfer During Modulated Laser Heating of Solids, J. of Applied Physics, vol. 71, no. 1, pp. 53-63

[Singh, 1985] Singh, J., Mazumder, J., 1985, Microstructure and Wear Properties of Laser Clad Fe-Cr-Mn-C-alloys, Proc. ICALEO '85, pp. 179-185

[Singh, 1987] Singh, J., Mazumder, J., 1987, Effect of Extended Solid Solution of Hf on the Microstructure of the Laser Clad Ni-Fe-Cr-Al-Hf Alloys, Acta Metall., vol. 35, no. 8, pp. 1995-2003

[Singh, 1987] Singh, J., Mazumder, J., 1987, Microstructure and Wear Properties of Laser Clad Fe-Cr-Mn-C Alloys, Metall. Trans. A, vol. 18A, pp. 313-322

[Singh, 1987] Singh, J., et al., 1987, Laser Cladding of Ni-Cr-Al-Hf on Inconel 718 for Improved High Temperature Oxidation Resistance, High Temperature Technology, vol. 5, no. 3, pp. 131-137

[Sircar, 1988] Sircar, S., Ribaudo, C., Mazumder, J., 1988, Laser Clad Nickel Based Superal loys: Microstructure Evaluation and High Temperature Oxidation Studies, Laser Beam Surface Treating and Coating, SPIE, vol. 957, pp. 29-41

[Sircar, 1989] Sircar, S., et al., 1989, Laser Clad $Ni7_0Al_{20}Cr_7Hf_3$ Alloys with Extended Solid Solution of Hf. Part I. Microstructure Evolution, Metall. Trans. A, vol. 20A, no. 11, pp. 2267-2277

[Sircar, 1989] Sircar, S., Singh, J., Mazumder, J., 1989, Microstructure and Nonequilibrium Phase Diagram for Ni-Hf Binary Alloy Produced by Laser Cladding, Acta Metall., vol. 37, no. 4, pp. 1167-1176

[Smurov, 1992] Smurov, I., Covelli, L., 1992, Synthesis of Nitride and Carbide Compounts on Titanium by Means of a Solid State Laser Source, Proc. ECLAT '92, pp. 251-256

[Smurov, 1992] Smurov, I., et al., 1992, Pulsed Laser Treatment of Plasma-Sprayed Thermal Barrier Coatings: Effect of Pulse Duration and Energy Input, J. of Materials Science, vol. 27, pp. 4523-4530

[Steen, 1987] Steen, W.M., 1987, Laser Surface Cladding, Proc. Surtek-4, pp. 159-166

[Steen, 1987] Steen, W.M., 1987, Surface Engineering with Lasers, Applied Laser Tooling, pp. 131-181

[Steen, 1992] Steen, W.M., et al., 1992, Alloy System Analysis by Laser Cladding, Proc. ICALEO '92, pp. 278-287

[Steen, 1994] Steen, P.H., Ehrhard, P., Schüssler, A., 1994, Depth of Melt-Pool and Heat-Affected Zone in Laser Surface Treatments, Metall. and Mat. Trans. A, vol. 25A, pp. 427-435

[Steenbergen, 1993] Steenbergen, M., 1993, Ontwerp en Realisatie van een Draadtoevoersysteem voor Lasercladden, Un. of Twente, Dept. of Mech. Eng., WA-285

[Stern, 1990] Stern, G., 1990, Absorptivity of CW CO_2, CO and YAG-Lasers by Different Metallic Alloys, Proc. ECLAT '90, pp. 25

[Takeda, 1985] Takeda, T., Steen, W.M., West, D.R.F., 1985, Laser Cladding with Mixed Powder Feed, Proc. ICALEO '84, vol. 44, pp. 151-158

[Tangelder, 1992] Tangelder, R., 1992, Focuspuntverschuiving van Lenzen in Hoogvermogen Laser Systemen - een Modelverificatie, Un. of Twente, Dept. of Mech. Eng., WA-262

[Tangelder, 1992] Tangelder, R.J., Beckmann, L.H.J.F., Meijer, J., 1992, Influence of Temperature Gradients on the Performance of ZnSe-Lenses, Conf. on Lens and Optical Systems Design, SPIE, vol. 1780

[Techel, 1995] Techel, A, et al., 1995, Production of Hard Metal-like Wear Protection Coatings by CO_2 Laser Cladding, Optical and Quantum Electronics, 27, pp. 1313-1318

[Tönshoff, 1994] Tönshoff, S, Pierdominici, F., Bianco, M., 1994, Laser Cladding and Alloying of a Ni-base Superalloy on Plain Carbon Steel, J. of Materials Science, vol. 29, pp. 504-509

[Tönshoff, 1995] Tönshoff, H.K., Overmeyer, L., 1995, Process Control Systems in Laser Materials Processing, Optical and Quantum Electronics, 27, pp. 1439-1447

[Tucker, 1984] Tucker, T.R., et al., 1984, Laser-Processed Composite Metal Cladding for Slurry Erosion Resistance, Thin Solid Films, vol. 118, pp. 73-84

[van Oosten, 1993] van Oosten, A., 1993, Laser Cladding with Powder Injection, Dept. of Mech. Eng., WA-298

[van Sprang, 1992] van Sprang, I., 1992, The Use of Models for the Determination of the Machining Parameters of Laser Hardening and Laser Cladding, Enschede, Ph.D. Thesis

[van Wijngaarden, 1994] van Wijngaarden, C., 1994, Procesdiagrammen voor het Lasertransformtieharden van Staal, Un. of Twente, Dept. of Mech. Eng., WA-362

[VandeHaar, 1988] VandeHaar, et al., 1988, Effect of Process Variables on the Laser Cladding of Zirconia, Proc. ICALEO '87, pp. 189-193

[Vasauskas, 1996] Vasauskas, V., et al., 1996, Investigation of Surface Layers Properties in Laser Cladding, Proc. ECLAT '96, pp. 391-398

[Venner, 1991] Venner, C.H., 1991, Multilevel Solutions of the EHL Line and Point Contact Problems, Ph.D. Thesis, Enschede

[Vetter, 1993] Vetter, P.A., et al., 1993, Characterization of Laser-Material Interaction During Laser Cladding, pp. 185-194

[Vetter, 1994] Vetter, P.-A., Engel, T., Fontaine, J., 1994, Laser Cladding: The Relevant Parameters for Process Control, Proc. Laser Materials Processing: Industrial and Microelectronics Applications, SPIE, vol. 2207, pp. 452-462

[Volz, 1994] Volz, R., Maisenhälder, F., 1994, Beschichten von Stahl- und Kupfersubstraten mit CO_2-Hochleistungslasern nach der Einstufigen Prozeßführung, Materialbearbeitung mit CO_2-Laserstrahlen höchster Leistung, VDI, Düsseldorf, pp. 73-79

[Wang, 1990] Wang, A.A., Sircar, S., Mazumder, J., 1990, Laser Cladding of MG-Al Alloys, Proc. ICALEO '90, vol. 71, pp. 502-512

[Wang, 1993] Wang, A.A., Sircar, S., Mazumder, J., 1993, Laser Cladding of Mg-Al Alloys, J. of Materials Science, vol. 28, pp. 5113-5122

[Wang, 1994] Wang, T., et al., 1994, Ceramic Coating and Laser Treatment, Proc. Laser Materials Processing: Industrial and Microelectronics Applications, SPIE, vol. 2207, pp. 824-829

[Webber, 1987] Webber, T., 1987, Advances in the Applications of Laser Cladding of Multi-Dimensional Part Geometries, Lasers in Motion for Industrial Applications, vol. 744, pp. 137-143

[Webber, 1991] Webber, T., 1991, Application of a Hardface Coating with CO_2 and CW Nd:YAG Lasers, Laser Materials Processing, Proc. ICALEO '91, pp. 380-388

[Weck, 1994] Weck, M., Schön, J., 1994, Integration prozeßspecifischer Sensoren und Aktoren in das Strahlführungssystem - Arbeitskopf mit Wechselobjektiv für das Oberflächenveredeln,

Materialbearbei-tung mit CO_2-Laserstrahlen höchster Leistung, pp. 105-110

[Weerasinghe, 1983] Weerasinghe, V.M., Steen, W.M., 1983, Laser Cladding by Powder Injection, Proc. Lasers in Manufacturing, pp. 125-132

[Weerasinghe, 1983] Weerasinghe, V.M., Steen, W.M., 1983, Laser Cladding with Pneumatic Powder Delivery, Lasers in Materials Processing, pp. 166-174

[Weerasinghe, 1984] Weerasinghe, V.M., 1984, Laser Cladding of Flat Plates, Ph.D. Thesis

[Weerasinghe, 1987] Weerasinghe, V.M., Steen, W.M., 1987, Laser Cladding with Pneumatic Powder Delivery, Applied Laser Tooling, pp. 183-211

[Willerscheid, 1990] Willerscheid, H., 1990, Prozeßüberwachung und Konzepte zur Prozeßoptimierung des Laserstrahlhärtens, Ph.D. Thesis

[Wisselink, 1996] Wisselink, F.W.A., 1996, Use of the Plume Initiation Time in Laser Milling, Enschede, Ph.D. Thesis

[Wissenbach, 1991] Wissenbach, K., et al., 1991, Surface Treatment of Car Engine Components with Laser Radiation, Proc. ISATA '91, pp. 333-341

[Wolf, 1994] Wolf, S., et al., 1994, Laserstrahlbeschichten nach der Einstufigen Prozeßführung am Beispiel "Beschichten von Gußeisen", Laser und Optoelektronik, vol. 26, no. 4, pp. 63-67

[Wolf, 1995] Wolf, S., Volz, R., 1995, Einzatz des Laserstrahlbeschichtens beim Bau von Kunststoffverarbeitungsmaschinen, Laser und Optoelektronik, vol. 27, no. 2, pp. 47-53

[Yang, 1988] Yang, X.C., et al., 1988, Microstructure and Performance of Laser Cladding NiCrSiB Alloy, Proc. ICALEO '87, pp. 209-220

[Yang, 1990] Yang, X.-C., Zhen, T.-X., Zhang, N.-K., 1990, Laser Cladding of WC-Co Powder, Proc. ICALEO '90, pp. 520-524

[Yang, 1991] Yang, X.-C., Zheng, T.-X., Zhang, N.-K., 1991, Research on Convection and Mass Transport in Laser Cladding: FeCrSiB Alloy, Proc. ICALEO '91, pp. 445-452

[Yellup, 1995] Yellup, J.M., 1995, Laser Cladding Using the Powder Blowing Technique, Surface and Coatings Technology, 71, pp, 121-128

[Zambon, 1993] Zambon, A, Ramous, E., 1993, Laser Beam Energy Absorption Enhancement by Means of Coatings, Lasers in Engineering, vol. 2, pp. 163-167

[Zhang, 1994] Zhang, N., Ekambaranathan, G., Willemse, P.F., 1994, Residual Stresses and Cracking in a Laser-Deposited Co-Cr-Ni-Mo Alloy on Steel, Proc. LANE '94, pp. 317-324

[Zhou, 1991] Zhou, X.B., De Hosson, J.Th.M., 1991, Dependance of Surface Residual Stress on Laser Power and Laser Scan Velocity, Scripta Metall. et Mat., vol. 25, pp. 2007-2010

[Zhou, 1991] Zhou, X.B., De Hosson, J.Th.M., 1991, Spinel/Metal Interfaces in Laser Coated Steels: A Transmission Electron Microscopy Study, Acta Metall. et Mat., vol. 39, no. 10, pp. 2267-2273

[Zhu, 1993] Zhu, B., et al., 1993, Coarse Cemented WC Particle Ceramic-Metal Composite Coatings Produced by Laser Cladding, Wear, vol. 170, pp. 161-166